Moesin orchestrates the reorganisation of the actin cortex and shape changes during mitotic progression in an epithelium

Nélio Tiago Lacerda Rodrigues

A thesis submitted to University College London
for the degree of Doctor of Philosophy
2014

Supervised by Professor Buzz Baum

MRC Laboratory for Molecular Cell Biology
University College London

Declaration

I, Nélio Tiago Lacerda Rodrigues, confirm that the work presented in this thesis is my own. Where information has been obtained from other sources, I confirm that this has been indicated in the thesis.

Signed_____

Acknowledgements

First, I would like to thank my supervisor, Buzz Baum, for his constant advice and support, for our stimulating discussions, for making me enjoy science and for always making me go that extra mile.

Next I need to thank all members of the Baum lab that I worked with throughout the last *few* years. A big thank you to all past members – Eliana, André, Marina, Marios, Jenny, Oscar, Remi, Michael, Julien, Mario, Arturo and Nick. Also, my gratitude to the lab members that have been and still are, as I write these words, putting up with my moods, impatience and sloppy humour – Scott, Andrea, Helen, Jigna, Charlotte, Tom, Maxine, Christina, Ginger, Nunu, Pelin, Naomi and Katarzyna. Lastly, I am especially grateful, and indebted, to Pato and Sergey for all their work and for helping me make the last years so fruitful.

I also need to thank everyone at the LMCB for making this such a great institution. It has been an immense pleasure to complete my PhD here and it will be difficult to find a place that handles test tubes and cocktails as well as this institute.

I am incredibly grateful to my family for helping me come this far. Also, I want to thank all my friends for their support and for the fun we have.

To Robert, my endless gratitude. You are the best thing one could ever wish for in a lifetime. Thank for your time and patience. Thank you for your eternal love. And thank you for the memories I carry, and those I have yet to collect, by your side.

Abstract

Animal cells endure dramatic actin-dependent changes in shape as they progress through mitosis – they round up at mitotic entry, elongate at anaphase and split into two at cytokinesis. In this thesis I explore the role of Moesin, an actin-membrane crosslinker and the sole ERM protein expressed in *Drosophila*, in orchestrating rearrangements of the actin cortex and morphological changes in epithelial cells undergoing mitosis. To perform my studies I used the fly notum and sensory organ precursor (SOP) cells therein as a model system.

In this thesis I show that Moesin is required for the stabilisation of the actomyosin cortex at metaphase. This mechanism is dependent upon phosphorylation of Moesin by the Slik kinase, which activates the ERM protein. Reduced levels of Moesin or Slik lead to myosin-II-driven cortical instabilities. Cortical stabilisation in mitotic SOP cells ensures the efficient accumulation of fate determinants at the plasma membrane.

At mitotic exit, a pool of active, phosphorylated Moesin is lost from the cell poles, thereby triggering polar relaxation and initiating anaphase cell elongation. These two events precede furrow formation, are independent of centrosome or astral microtubules-derived signals, and are induced by proximity of the segregating chromosomes to the cell poles. I show that a pool of kinetochore-localised PP1-87B phosphatase and its regulatory subunit Sds22 inactivate cortical Moesin and elicit the dismantling of the actomyosin cortex at mid-anaphase. Cells with reduced amounts of PP1-87B or Sds22 fail to clear Moesin and actin from the anaphase poles. Importantly, these defects in polar relaxation are mimicked by the expression of a constitutively active form of Moesin in fly tissues. Finally, I demonstrate that delocalisation of PP1/Sds22 from the kinetochores via KNL1 depletion abolishes polar blebbing at anaphase and impairs cell elongation.

My work shows how the dynamic regulation of Moesin activation and localisation controls shape changes in cells undergoing mitosis. Moreover, it sheds light on a novel mechanism of polar relaxation at anaphase, in which a kinetochore-derived signal instructs the cell cortex to become polarised, thereby initiating cytokinesis.

Table of contents

Table of Figures

Abbreviations

A-P	Anterior-Posterior axis
APC/C	Anaphase-promoting complex/cyclosome
APF	After Puparium Formation
aPKC	Atypical Protein Kinase C
CDK1	Cyclin-dependent Kinase 1
Cnn	Centrosomin
CPC	Chromosome Passenger Complex
E3KARP	NHE3 Kinase A Regulatory Protein
EBP50	ERM Binding Protein 50
ERM	Ezrin, Radixin, Moesin
GAP	GTPase-activating protein
GEF	Guanine nucleotide exchange factor
GMA	GFP-tagged Moesin actin-binding domain
ICAM-2	Intercellular adhesion molecule 2
KMN	KNL-1/Mis12 complex/Ndc80 complex
MKLP1	Mitotic kinesin-like protein 1
MKLP2	Mitotic kinesin-like protein 2
MLCK	Myosin light-chain kinase
MRCK	Myotonic dystrophy-related Cdc42-binding kinase
MRLC	Myosin regulatory light chain
NEB	Nuclear Envelope Breakdown
PCP	Planar Cell Polarity
PIP2	Phosphatidylinositol 4,5-bisphosphate
PKC	Protein kinase C
Plk1	Polo-like kinase 1
PON	Partner of Numb
PRC1	Protein Regulator of Cytokinesis 1
S/T-P	Serine/Threonine-Proline motif
SAC	Spindle Assembly Checkpoint
SOP	Sensory Organ Precursor
UAS	Upstream Activating Sequence

Chapter 1

Introduction

This introductory chapter provides an overview of Moesin and its partners within the actin cortex, the function of the actomyosin cortex in driving changes in mitotic cell shape, and the mechanisms used to couple changes in shape to mitotic entry and exit. The chapter also provides an overview of the model system that I have used as a simple tool with which to address the roles of Moesin and its phospho-regulators – the Slik kinase and the PP1-87B/Sds22 phosphatase complex – in mitotic rounding, metaphase cortical stability and anaphase polar relaxation.

1.1 ERM proteins: organisers of the cell cortex

The actin cytoskeleton is a highly dynamic network of actin filaments and a large plethora of associated proteins. It is well established that the actin cytoskeleton plays key roles in cellular and developmental processes. Importantly, the association of actin filaments with the plasma membrane is crucial in the organisation and maintenance of specialised subcellular domains, like adherens junctions and microvilli (Louvet-Vallee, 2000, Fehon et al., 2010). Many decades of research have implicated Ezrin, Radixin and Moesin, collectively known as ERMs, as organisers of these membrane domains. ERMs provide regulated linkage between transmembrane proteins, phospholipids, adaptor proteins and actin filaments (Fievet et al., 2007, Fehon et al., 2010). Not only do ERM proteins provide structural support in the maintenance of membrane domains, but they also function in other mechanisms of cellular physiology, such as signal transduction (McClatchey and Fehon, 2009).

1.1.1 Overview of ERM organisation and evolutionary conservation

Ezrin, Radixin and Moesin were first characterised in human cells over two decades ago. Ezrin was the first to be identified and was initially implicated in the regulation of acid secretion in parietal cells (Hanzel et al., 1991). Radixin was first visualised in human liver cells, where it appeared to localise to the adherens junctions and cytokinetic furrow (Tsukita and Hieda, 1989, Sato et al., 1991). Moesin was characterised as a protein that binds heparin and glycosaminoglycan (Lankes et al., 1988). A few years after the identification of Ezrin, Radixin and Moesin, the *Neurofibromatosis 2* tumour-suppressor gene was identified, and its product, Merlin, was found to have a high degree of sequence similarity to the ERM family (Rouleau et al., 1993, Trofatter et al., 1993).

ERM proteins are composed of two major domains: a membrane-associated domain in the N-terminus (N-ERMAD) and a C-terminal ERM-association domain (C-ERMAD), which can bind to N-ERMAD (Bretscher et al., 2002, Polesello and Payre, 2004). The N-ERMAD domain is also called FERM, since its ~300-amino acid long sequence is found in the protein band 4.1 (FERM

for four.one protein, ezrin, radixin, moesin) (Louvet-Vallee, 2000). In fact, this domain is conserved across multicellular species and is present in multiple membrane-linked proteins (Chishti et al., 1998). The C-ERMAD contains a binding site for F-actin (the last ~34 amino acids in Ezrin (Turunen et al., 1994)). The region between the FERM domain and C-ERMAD is believed to have high propensity to form an α-helical coiled-coil (Li et al., 2007).

In vertebrates, ERM proteins are encoded by three paralogous genes (Bretscher et al., 2002, Polesello and Payre, 2004). Studies have shown that ERMs exhibit tissue-specific expression patterns: Ezrin appears to be mostly abundant in epithelial cells; Moesin is mostly expressed in endothelial cells; and Radixin is mostly present in hepatocytes. The high degree of structural conservation among ERMs indicates that they might have redundant functions. Indeed, mice deficient in ezrin or moesin are viable and do not present major developmental defects (Doi et al., 1999, Saotome et al., 2004). The same is true for mice where radixin is inactivated (Kikuchi et al., 2002). While it is likely that ERMs have overlapping functions, several studies have implicated individual ERMs in various physiological contexts, such as villar organisation in the gut (Saotome et al., 2004, Casaletto et al., 2011), lymphocyte homeostasis (Hirata et al., 2012, Nomachi et al., 2013) and maintenance of cochlear stereocilia (Kitajiri et al., 2004). To better understand the redundancy and diversity of ERM functions, researchers have turned their attention to lower metazoans, such as *Drosophila melanogaster*, which express a single ERM gene.

1.1.2 Regulation of ERM function

1.1.2.1 ERMs are negatively regulated by an intramolecular association

Several lines of evidence indicate that ERMs are regulated by an auto-inhibitory association between the FERM and C-ERMAD domains. Early evidence came from a study showing that ERM proteins can form homotypic and heterotypic associations with each other (Gary and Bretscher, 1993). Subsequent studies demonstrated that the majority of cytoplasmic Ezrin exist as monomers, in which FERM and C-ERMAD domains interact with each other (Bretscher et al., 1995, Gary and Bretscher, 1995). In this ‘closed’ conformation, the binding sites for F-actin and other proteins are masked. Therefore, it was proposed that full

activation requires disruption of the intramolecular association (Gary and Bretscher, 1995, Reczek and Bretscher, 1998). It is believed that the α-helical domain between the N-terminal and C-terminal domains can also participate in intramolecular associations that inhibit protein function (Li et al., 2007).

1.1.2.2 ERMs are activated by PIP2 binding and phosphorylation

One of the first studies on the regulation of ERMs demonstrated that enhanced phosphorylation of human Moesin at the Thr558 residue (situated in the C-ERMAD) was crucial for its function during platelet activation (Nakamura et al., 1995). Later reports showed that the equivalent threonine residue in Ezrin and Radixin, as well in the Drosophila Moesin, is also phosphorylated, leading to protein activation (Fig. 1.1) (Matsui et al., 1998, Polesello et al., 2002, Hipfner et al., 2004). Importantly, activation of ERMs also depends on their interaction with PIP2 (Fig. 1.1), which binds to the FERM domain and helps induce conformational changes (Niggli et al., 1995, Fievet et al., 2004, Blin et al., 2008, Roch et al., 2010).

Many kinases in vertebrate systems are thought to phosphorylate ERMs on the regulatory C-terminal threonine. These include the Rho-associated kinase (Jeon et al., 2002, Hebert et al., 2008), MRCK (Nakamura et al., 2000), PKC (Ren et al., 2009a), Nck-interacting kinase (Baumgartner et al., 2006), Jun N-terminal kinase (Pan et al., 2013) and STK10 (Belkina et al., 2009).

Various studies have proposed additional mechanisms of ERM activation, which encompass the phosphorylation of residues other than the conserved C-ERMAD threonine (Krieg and Hunter, 1992, Yang and Hinds, 2003).

1.1.2.3 Direct and indirect association of ERMs with the plasma membrane

The FERM domain of ERMs can interact directly with transmembrane proteins (Fig. 1.1), including the adhesion molecules CD44 and ICAM2 (Yonemura et al., 1998, Yang and Hinds, 2003). It is also known that ERMs can associate with the membrane indirectly through association with scaffolding proteins (Fig. 1.1), such as the PDZ-containing proteins EBP50 and E3KARP (Reczek and Bretscher, 1998, Yun et al., 1998). Importantly, it has been proposed that interaction of these proteins with ERMs through the FERM domain helps reduce the affinity of this region for the C-ERMAD (Terawaki et al., 2006).

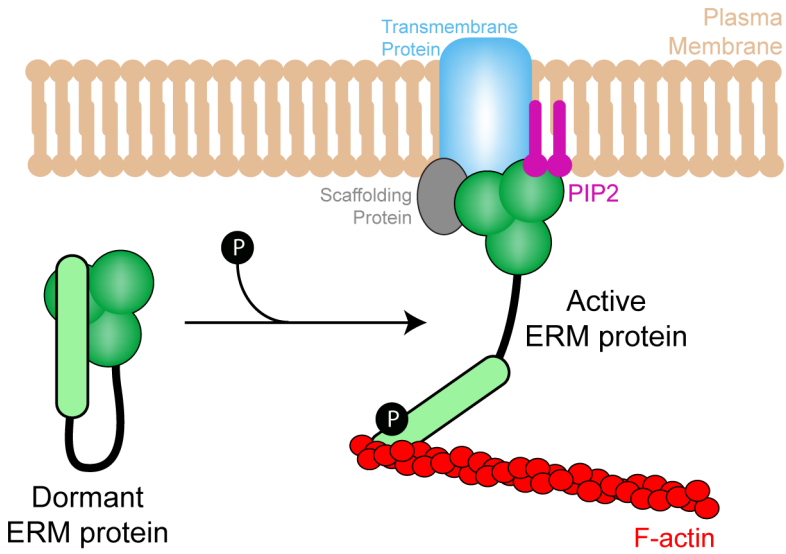

Figure 1.1 – Model for ERM activation.

ERM proteins are activated through PIP2 binding and phosphorylation of the conserved threonine located in the C-ERMAD (depicted in light green), which decreases the affinity of this domain for the N-terminal FERM (depicted in dark green). This leads to unmasking of binding sites for F-actin, for transmembrane proteins (such as CD44 and ICAM2; depicted in light blue) and for scaffolding proteins (for example, EBP50 and E3KARP; depicted in grey).

1.1.3 *Drosophila* Moesin, a key play in cellular and tissue morphogenesis

While part of the current knowledge on ERM function comes from vertebrates, the redundancy among the three paralogues has made genetic analyses complicated. Because *Drosophila* only has one ERM protein, research in this organism has proved useful in the understanding of how these proteins work. It has been established that the fly Moesin is essential for viability and is critical for epithelial integrity (Bourbon et al., 2002, Peter et al., 2002, Polesello et al., 2002). Furthermore, fly studies have reiterated that ERMs are activated upon phosphorylation of the C-terminal threonine residue (Thr559 in flies). Fly Moesin however appears to be phosphorylated by a single kinase, Slik (Hipfner and Cohen, 2003, Hipfner et al., 2004, Hughes and Fehon, 2006, Kunda et al., 2008, Carreno et al., 2008, Hughes et al., 2010). Interestingly, recent work suggests that

the homologous kinase, SLK, may also be the dominant one involved in ERM protein activation in vertebrates (Machicoane et al., 2014).

In flies, active Moesin has been implicated in multiple cellular and developmental processes. Below I present an overview of the most relevant of these.

1.1.3.1 Moesin is important for anterior-posterior polarity

Over a decade ago, two independent studies proposed that Moesin plays a key role in fly oogenesis (Jankovics et al., 2002, Polesello et al., 2002). By analysing mutant animals, the authors saw that loss of Moesin led to severe disorganisation of the actin cytoskeleton, including aberrant actin-membrane linkage and presence of ectopic clumps of actin in the cytoplasm. These defects affected localisation of the maternal determinant Oskar at the posterior cortex of the oocyte. As a consequence, mutant embryos lacked anterior-posterior polarity and exhibited dramatic shape defects (Jankovics et al., 2002, Polesello et al., 2002).

1.1.3.2 Moesin is crucial for epithelial morphogenesis and apical-basal polarity

It has long been proposed that Ezrin plays an important role in epithelial polarity and morphogenesis, for example, in the mammalian gut (Saotome et al., 2004, Casaletto et al., 2011). Studies in the fly provide further evidence that ERMs are indeed required for epithelial morphogenesis and for the integrity of the apical domain of epithelial cells. Remarkably, it was observed that genetic loss of Moesin, or its kinase Slik, leads to defects in the organisation of the developing larval wing disc, such that cells lose their apical-basal features and become extruded from the epithelium (Speck et al., 2003, Hipfner and Cohen, 2003, Hipfner et al., 2004, Hughes and Fehon, 2006). These studies also proposed that Moesin promotes epithelial integrity by counteracting the activity of the small GTPase Rho1. It was not clear however whether the genetic interactions between Rho1 and Moesin represent direct regulatory interactions between the two proteins, or are due to their both functioning through a common actin filament network. Moesin has also been implicated in photoreceptor morphogenesis, being required for correct actin organisation and membrane morphology at the cell apex (Karagiosis and Ready, 2004).

1.1.3.3 Moesin promotes cell rounding and cortical stiffness in cells in culture

More recently, we and others demonstrated that Moesin is required for cell shape changes and cortical rigidity during mitosis. We observed that Moesin-depleted cells failed to round up and assemble a stable actomyosin cortex upon mitotic entry. In consequence, spindle morphogenesis was defective, leading us to postulate that the cortex provides the structural foundation required to support spindle function (Carreno et al., 2008, Kunda et al., 2008, Kunda and Baum, 2009).

Together with other studies, our findings showed that the actin cortex is a key determinant in cellular morphogenesis. Like membrane-actin anchorage, other aspects of the actin cytoskeletal network, such as its molecular composition and mechanical properties, play a key role in mitosis. This is discussed in the next section of this chapter.

1.2 The cortex: a membrane-bound network of actin, myosin and actin-binding proteins

The cortex is a thin layer of actin filaments, myosin motors and actin-binding proteins that subtends the plasma membrane of animal cells. Because this network is tethered to the membrane, it plays an important role in the control of cell shape. One of the main functions of the cortex is to resist external mechanical forces (Bray and White, 1988). It also acts to oppose intracellular osmotic pressure (Stewart et al., 2011, Fischer-Friedrich et al., 2014), like the cell wall in plant cells and bacteria (Zimmermann et al., 1980, Koch, 1984, Verhertbruggen et al., 2013), helping shape animal cells. However, unlike cell walls, the cell cortex can be rapidly remodelled in response to internal and external cues, thus allowing cell shape changes (Kunda and Baum, 2009, Martin et al., 2009, Ren et al., 2009b, Goehring et al., 2011). This adaptive capacity of the cortex is due to the turnover of its molecular components and to mesh reorganisation through contractility. In this section I provide a brief characterisation of the actomyosin cortex. In particular, I discuss its molecular composition, network topology and mechanical properties.

1.2.1 Molecular composition of the cortex

Determining the protein composition of the cortex has mostly relied on techniques such as immunolabelling and expression of fluorescently tagged molecules. Furthermore, studies looking at blebbing have proved extremely useful in the identification of molecules involved in the formation and mechanics of the mammalian cell cortex (Charras et al., 2006). While blebs are devoid of cytoskeleton during expansion, they accumulate actin as they retract back towards the cell body. Perhaps unsurprisingly, most actin-binding proteins found in blebs are also found in other actin networks. Apart from ERMs, which I already highlighted in section 1.1, the list of cortical proteins includes other membrane linkers, such as filamin and myosin-I. Additionally, the cortex contains crosslinking and bundling proteins (including fimbrin, α-actinin and fascin), and

proteins involved in contractility (such as myosin-II motors, but also tropomyosin and tropomodulin) (Charras et al., 2006, Salbreux et al., 2012).

Assembly of filamentous actin at the cortex has been shown to depend on nucleators of the formin family (mDia1, mDia2 and Fhod1) and Arp2/3 complex (Tominaga et al., 2000, Eisenmann et al., 2007, Hannemann et al., 2008, Roh-Johnson et al., 2012). However, these findings were based on indirect evidence. A recent study in mammalian cells, which used a proteomic analysis of isolated blebs as well as immunocytochemistry, has proposed that the majority of cortical actin is generated by mDia1 and Arp2/3 (Bovellan et al., 2014), thus corroborating some of the earlier findings. Furthermore, ongoing work in our lab points to Diaphanous (the fly homologue of mDia1) being the main nucleator of actin filaments in the mitotic cortex of epithelial cells.

1.2.2 Topology of the cortical network

Scanning and transmission electron microscopy have been useful in dissecting the architecture of the actin cortex in various model systems (Hanakam et al., 1996, Charras et al., 2006, Charras et al., 2008, Bovellan et al., 2014). These studies suggest that the thickness of the cortical mesh is in the 50-100nm range. A recent study, which used a theoretical description of cortical geometry together with fluorescence microscopy to break the optical limit, has elegantly shown that the cortex of mitotic HeLa cells is ~190nm-thick.

Unravelling the exact three-dimensional arrangement of cortical actin filaments has proved challenging. Evidence suggests that the bulk of the actin network lies parallel to the membrane, while some filaments can also be oriented orthogonally (Charras et al., 2006, Morone et al., 2006). Importantly, the topology of the actin mesh depends on the activity of the aforementioned actin-binding proteins. For example, while filamin promotes crosslinking of actin filaments into loose and non-aligned networks, α-actinin promotes filament bundling (Fletcher and Mullins, 2010). Consequently, actin-binding proteins are key determinants of the mechanical properties of the cortex, namely cortical tension and elasticity.

1.2.3 The cortex is a viscoelastic and contractile structure

1.2.3.1 Viscoelasticity

The actin cortex exhibits viscoelastic behaviour upon deformation (Salbreux et al., 2012). This behaviour depends on cortical tension and protein turnover and it can be assessed by atomic force microscopy and optical stretching experiments (Haga et al., 2000, Guck et al., 2001). On short timescales, the cell cortex acts as an elastic solid in response to external perturbations. On timescales longer than the turnover of the cortical components, the cortex behaves like a viscous fluid, in that the energy of the deformation is dissipated as the network adjusts into new conformations. This is accompanied by changes in cell shape and behaviour (Levayer and Lecuit, 2012, Salbreux et al., 2012).

1.2.3.2 Contractility and cortical tension

Cortical tension is defined as the tension force exerted on a cortex cross-section by the surrounding cytoskeletal mesh, and because the cortex is attached to the membrane, it is the main determinant of cell surface tension (Lecuit and Lenne, 2007). Tension is mostly determined by myosin-II-directed contractility. myosin-II motors exist as hexamers: two essential light chains, two regulatory light chains and two heavy chains (Ikebe, 2008). These motors have ATPase activity, which allows binding and detaching to actin (Kull and Endow, 2013). Myosin can assemble into minifilaments composed of several hexamers, which generate contractility by sliding actin filaments in an antiparallel fashion (Huxley, 2000). Myosin activity is mostly controlled by phosphorylation. The regulatory chain of the myosin-II motor can be phosphorylated at conserved residues (Thr18 and Ser19) by a large plethora of kinases, such as Rho-associated kinase, citron kinase, MRCK and MLCK (Matsumura, 2005). The function of myosin-II is also modulated by phosphatases, in particular those of the PP1 family (Kirchner et al., 2007, Grusche et al., 2009).

1.3 The actomyosin cortex and cell shape changes at mitotic entry

Animal cells undergo drastic shape changes during mitosis: they round up at mitotic entry, elongate at anaphase and split into two at the end of cytokinesis. These shape changes at mitotic entry are accompanied by reorganisation of the actin cytoskeleton. In this section I present an overview of the mechanisms that drive mitotic rounding, especially those involving rearrangements of the actin cortex. I conclude by highlighting the importance of mitotic cell geometry in spindle function and epithelial morphogenesis.

1.3.1 Cell rounding and reorganisation of the actomyosin cortex at mitotic entry

It has long been observed that cells in culture leave their flat interphase morphology and adopt a spherical shape as they enter mitosis (Harris, 1973, Cramer and Mitchison, 1997). Early studies on mitotic rounding suggested that this was accompanied by a reduction in cell surface area (Sit et al., 1993, Sit et al., 1994). It was then suggested that this is most likely due to a decrease in the constitutive recycling of membrane at the G2/M transition (Boucrot and Kirchhausen, 2007, Boucrot and Kirchhausen, 2008). These studies proposed that at mitotic entry, the extent of exocytosis is lowered, while endocytosis is unchanged. However, earlier studies showed that endocytosis is actually inhibited in early mitosis (Sit et al., 1993, Raucher and Sheetz, 1999). These findings have been recently replicated (Kaur et al., 2014). Other studies have suggested that the apparent reduction in the surface area of mitotic cells does not represent the reality and is due to the formation of many small pits and spikes in the membrane (Porter et al., 1973, Sanger and Sanger, 1980, Sanger et al., 1984).

Along with changes in membrane topology, mitotic cell rounding is also accompanied by the reorganisation of the actin cytoskeleton, where interphase structures are disassembled and reassembled into new conformations (Thery and Bornens, 2006, Dao et al., 2009). Studies over the last decade have shed light on various molecular mechanisms controlling the rearrangement of actin networks at the onset of mitosis. One such study proposed that the small GTPase RhoA is

important for the accumulation of a thick actomyosin under the membrane, which leads to an increase in mechanical stiffening (Maddox and Burridge, 2003). These findings were later corroborated by a study in our lab, which identified the RhoA activator Ect2 as central regulator of mitotic rounding (Matthews et al., 2012). Importantly, this study unveiled a mechanistic link between the cell cycle machinery that initiates mitosis and the concurrent changes in cytoskeletal organisation. Other actin regulators implicated in mitotic cell rounding include WDR1 and LIM kinase, proteins known to promote the disassembly of filamentous actin (Fujibuchi et al., 2005, Kaji et al., 2008). Again this emphasizes the need for actin cytoskeletal remodelling during mitotic rounding.

As mentioned in section 1.1, ERM proteins are thought to be crucial players in the process of cell rounding and cortical stiffening at mitosis. We and others have shown that fly cells in culture depleted for Moesin (the only ERM protein expressed in Drosophila) fail to round up and acquire a stable actomyosin cortex at metaphase (Carreno et al., 2008, Kunda et al., 2008). The same was true upon depletion of Slik kinase. Conversely, expression of a constitutively active form of Moesin showed that this protein is indeed necessary and sufficient to trigger cortical stiffening (Kunda et al., 2008).

1.3.2 The importance of cell rounding and actin reorganisation in chromosome segregation and tissue morphogenesis

The main purpose of mitotic cell division is the faithful segregation of genetic material in two daughter cells. In order to achieve this, the spindle microtubules have to gather all chromosomes and bring them together to form a compact plate at the centre of the cell. Once all chromosomes have established proper attachments via kinetochore microtubules to the bipolar spindle, the SAC is satisfied and the genetic material is then separated. In a recent collaborative study, our lab proposed that mitotic rounding provides cells with the ideal cellular geometry for successful cell division (Lancaster et al., 2013). By flattening human cells in culture (either genetically or by confining cells in chambers of limited dimensions), we saw that chromosome capture and stability of the bipolar spindle were severely impaired, leading to aberrant DNA segregation. Moreover, it is likely that mitotic rounding facilitates spindle-cortex interactions, ensuring correct

spindle positioning (Cadart et al., 2014). This is important during both symmetric and asymmetric cell division (Green et al., 2012, Kotak and Gonczy, 2013).

While Lancaster and colleagues stressed the importance of cell rounding in mitosis, the actin cortex also plays a role in ensuring accurate spindle orientation. This is supported by studies in fly cells (Carreno et al., 2008, Kunda et al., 2008) and more recently in human cells (Machicoane et al., 2014), which showed that ERMs promote cortical integrity and proper spindle orientation. The spindle defects reported in these studies are likely due to impaired bridging between actin and astral microtubules, and due to defects in cell shape. On the other hand, it is also possible that additional defects arise from aberrant centrosome separation, since several studies have demonstrated that cortical contractility directly impinges on centrosome movements in prophase and subsequent bipolar spindle formation (Rosenblatt et al., 2004, Wang et al., 2008, Cao et al., 2010).

Recent *in vivo* studies have highlighted the importance of actin-dependent cell rounding for proper tissue homeostasis and morphogenesis, likely by controlling spindle orientation (Oliferenko et al., 2009, Panousopoulou and Green, 2014). Mitotic rounding is relevant in processes such as epithelial planar growth (Bosveld et al., 2012, Woolner and Papalopulu, 2012), tissue stratification and differentiation (Norden et al., 2009, Luxenburg et al., 2011, Meyer et al., 2011, Spear and Erickson, 2012, Nakajima et al., 2013) and tissue invagination (Kondo and Hayashi, 2013).

1.4 Polarisation of the actomyosin cortex at mitotic exit

At mitotic exit the actomyosin cortex becomes polarised. This polarisation is instructed by the anaphase spindle, which specifies the site of equatorial furrowing and directs the assembly of the contractile ring. In this section I start by presenting a description of the mechanism of central spindle assembly. I describe how this structure signals to the cortex to generate an equatorial zone of active RhoA, a key driver in the assembly of the contractile ring. Additionally, I take a brief look at the role of astral microtubules in aiding cortical polarisation, which likely cooperate with the central spindle in positioning the furrow. Finally, I highlight recent findings that unveil the importance of polar mechanics in the control of cell shape at cytokinesis.

1.4.1 The central spindle guides furrow positioning and ingression

It has long been proposed that the spindle controls cytokinetic furrowing. Early evidence supporting this model arose from simple experiments in large invertebrate egg cells with altered topology, where division occurred at sites at which there were overlapping antiparallel microtubules (reviewed in (Rappaport, 1996, Oegema and Mitchison, 1997)). The role of the central spindle in promoting equatorial contractility and furrow ingression is now well established and the molecular details underlying these processes have been thoroughly studied.

The central spindle, also known as midzone, is a bipolar microtubule array that forms between the segregating chromosomes (Green et al., 2012). This array is organised in a way that the plus ends of the microtubules emanating from one spindle pole are interdigitated with the plus ends from the microtubules of the opposite pole (Euteneuer and McIntosh, 1980). Formation of the central spindle requires a microtubule crosslinking protein (PRC1) and kinesin motors (namely, KIF4, MKLP2 and KIF14) (Gruneberg et al., 2006, Gaillard et al., 2008, Bieling et al., 2010) and is regulated by Aurora B and Plk1 (Carmena et al., 2009, Glotzer, 2009). Additionally, midzone assembly depends on the centralspindlin complex, which is composed of MKLP1 and RacGAP1 (Mishima et al., 2002, Zhao and Fang, 2005, D'Avino et al., 2006, Lekomtsev et al., 2012). The centralspindlin

promotes contractile ring assembly in two ways. It recruits the RhoGEF Ect2 to the central spindle (Nishimura and Yonemura, 2006) from where it becomes associated to the overlying plasma membrane (Su et al., 2011). In addition, the GAP domain of RacGAP1 has been proposed to promote Rac inactivation (Canman et al., 2008, Loria et al., 2012, Bastos et al., 2012); facilitating local Rho activation. The accumulation of active RhoA at the midzone then recruits proteins directly involved in the assembly and ingression of the contractile ring, such as formins, which nucleate and elongate filamentous actin (Bohnert et al., 2013), and the citron and Rho-associated kinases, which activate myosin-II (Kosako et al., 2000, Matsumura, 2005, Gruneberg et al., 2006). Constriction of the contractile ring also depends on the scaffolding protein anillin and membrane-associated septin filaments (Field et al., 2005, Piekny and Glotzer, 2008).

1.4.2 The astral microtubules aid cortical polarisation at mitotic exit

Early studies suggested that the spindle asters actively induce relaxation of the poles of cells in anaphase, thus contributing to the pattern of tension polarisation at mitotic exit (Wolpert, 1966, White and Borisy, 1983, Rappaport, 1996). While this may not be the primary signal, several studies in the last decade have proposed that furrow positioning is dependent on both astral and midzone microtubules (Bringmann and Hyman, 2005, Chen et al., 2008, Murthy and Wadsworth, 2008). In contrast to the stable microtubules of the midzone, the dynamic astral microtubules are thought to inactivate Rho function and myosin-II activation in non-equatorial regions. This was shown in studies where the behaviour of astral microtubules was pharmacologically or genetically perturbed (Werner et al., 2007, Foe and von Dassow, 2008, Odell and Foe, 2008, Rankin and Wordeman, 2010). Furthermore, it has been pointed out that astral microtubules have the capacity to induce cortical flow to physically transport actin and myosin from the poles to the equator (Foe et al., 2000, Chen et al., 2008, Zhou and Wang, 2008, Tseng et al., 2012).

1.4.3 The importance of polar contractility in cell shape during cytokinesis

Studies in *Dictyostelium* have shown that the polar cortex is involved in the global control of the shape of dividing cells. In this organism, which is thought to divide through multiple mechanisms (Uyeda and Nagasaki, 2004), accumulation of key actin crosslinkers, such as fimbrin and dynacortin, at cell poles during cytokinesis generates resistive forces that slow furrow ingression (Reichl et al., 2008, West-Foyle and Robinson, 2012). While this is an attractive model, many of the crosslinkers expressed in *Dictyostelium* do not have direct homologues in metazoans, in which the molecular composition of the polar cortex is not known. Nevertheless, a recent study in symmetrically-dividing animal cells has demonstrated that polar mechanics has a similar active role in controlling cell shape (Sedzinski et al., 2011). The authors showed that perturbation of the polar cortex causes shape oscillations, which resulted in furrow displacement and aneuploidy. Furthermore, they observed that polar blebbing can stabilise cell shape by alleviating excess cortical contractility.

The importance of myosin-driven polar contractility has also been validated in cases of asymmetric cell division. A study looking at mitotic neuroblasts demonstrated that myosin-II preferentially accumulates at one end of the cell, setting up an asymmetric pattern of contractility that can displace the furrow to generate an asymmetric division (Cabernard et al., 2010). Remarkably, this asymmetry was still observed in the complete absence of microtubules, in clear opposition to the dominant model of spindle-dependent cortical polarisation.

1.5 Phospho-regulation of the cell cycle

As discussed above (see section 1.3), animal cells undergo profound changes in shape as they pass from G2 into mitosis and divide. These shape changes must be precisely timed so that rounding occurs as the spindle is assembled, after which the cytokinetic ring must precisely partition the two masses of DNA. All these events are controlled by the cell cycle machinery. This machinery encompasses the mitotic kinases that drive mitotic entry and their counteracting phosphatases that drive mitotic exit. Through their direct or indirect regulation of local and global mitotic events, they can ensure that events happen at the right place and time. I discuss this in more detail in the following sections.

1.5.1 Serine/threonine kinases as triggers of mitosis

Entry into mitosis is mediated by the conserved serine/threonine kinase CDK1 and its associated cyclin B (O'Farrell, 2001). Studies in *Xenopus* and human cells have shown that activation of CDK1 is dependent on the abundance and subcellular localisation of cyclin B at the G2/M transition (Solomon et al., 1990, Fung and Poon, 2005, Santos et al., 2012). In addition, CDK1-cyclin B activity is modulated by specific proteins that phosphorylate/dephosphorylate the CDK subunit at key residues (Morgan, 1997). These proteins are at the core of feedback loops that generate sharp transitions in activity, which has been proposed to help provide directionality to the switch from interphase into mitosis (Coudreuse and Nurse, 2010). The best characterised of these regulators are the Wee1 kinase and the Cdc25 phosphatase. The former phosphorylates and inactivates CDK1 on a tyrosine residue, while the latter removes the inhibitory phosphate and promotes entry into mitosis (Harvey et al., 2005). Once active, CDK1 phosphorylates and activates a large plethora of targets that ensure correct mitotic progression (Morgan, 1997).

Another set of kinases implicated in cell cycle progression are the Polo-like kinases. This group includes four main kinases, named Plk1-4, of which Plk1 is the best understood. Interestingly, one of the main roles of this protein is to promote mitotic entry by impinging on CDK1 activity. It does so by inactivating

Myt1 and Wee1 and by activating Cdc25 (Barr et al., 2004). Plks are also known to control centriole and centrosome biogenesis (Bettencourt-Dias et al., 2005, Lee and Rhee, 2011). A third function of Plk1 is to regulate cohesion of the chromosomes (Clarke et al., 2005). Finally, at the end of mitosis, Plk1 has been shown to control assembly of the spindle midzone and trigger furrow ingression (D'Avino et al., 2007, Petronczki et al., 2007, Wolfe et al., 2009).

Proteins of the Aurora family constitute the third type of kinases with essential roles in mitosis. The most famous members of this family are Aurora A and B. Aurora A is the major driver of centrosome maturation and centrosome separation at mitotic entry (Hannak et al., 2001, Berdnik and Knoblich, 2002, Marumoto et al., 2003). Additionally, it has been shown that Aurora A can help chromosome alignment and microtubule stabilisation (Barros et al., 2005, Kinoshita et al., 2005, Hochegger et al., 2013). Aurora B is the core catalytic component of the chromosomal passenger complex, in which the kinase is associated with the INCENP, borealin and survivin (Terada, 2001, Carmena et al., 2012). This complex undergoes dynamic changes in its localisation during passage through mitosis, enabling it to regulate key events. These include chromosome biorientation, SAC activation, chromatid cohesion and, during mitotic exit, regulation of the spindle midzone and abscission (Dai et al., 2006, Douglas et al., 2010, Schmidt et al., 2010, Welburn et al., 2010, Dunsch et al., 2011, Nunes Bastos et al., 2013). Importantly, recent studies have proposed that Aurora A and B can also work together in regulating certain mitotic functions, such as chromosome congression in prometaphase and microtubule dynamics at anaphase (Kim et al., 2010, Hegarat et al., 2011).

1.5.2 Protein phosphatases counteract kinase activity during mitosis

Regulation of both entry and exit from mitosis involves the inactivation of mitotic kinases and the activation of counteracting protein phosphatases. Apart from the Cdc25 phosphatase (Busino et al., 2004), most phosphatases known to regulate mitotic progression are specifically targeted at serines and threonines (Bollen et al., 2009). Of these proteins, the most important are those in the PP1, PP2A and PP6 families (hereafter referred to as PPPs).

PPPs exist as holoenzyme complexes in which a conserved catalytic subunit associates with one or more regulatory subunits. The different combinations of subunits give these holoenzymes substrate specificity and regulation (Bollen et al., 2010, Barr et al., 2011). In general, phosphatases containing a PP1 catalytic subunit associate with a single regulatory subunit. This interaction depends on the presence of an RVXF motif in the PP1 interactors (Wakula et al., 2003). PP2A enzymes however, exhibit more sophisticated arrangements since they contain a catalytic subunit, a scaffolding subunit (A-subunit) and a variable B-subunit that ensures substrate specificity (Janssens et al., 2008). PP6 complexes are thought to have a similar architecture to PP2A (Barr et al., 2011).

As mentioned above, mitotic entry is driven by the activation of CDK1-Cyclin B, which depends on the levels of available cyclin and on the activities of Wee1 and Cdc25. However, PPPs are also known to tune the G2/M transition. In particular, it has been proposed that inhibition of the PP2A-B holoenzyme by the Greatwall/ENSA pathway in G2 propels CDK1 activation (Vigneron et al., 2009, Gharbi-Ayachi et al., 2010, Mochida et al., 2010). On the other hand, it has also been suggested that this PP2A complex can be inhibited by CDK1 independently of Greatwall (Okumura et al., 2014).

PPPs are also important during mitosis. For example, it has been demonstrated that the complex PP2A-B' counteracts the activity of Plk1 on the chromosomes, thereby ensuring centromeric cohesion throughout prometaphase (Kitajima et al., 2006). Another study has implicated PP6 in the regulation of spindle formation by counteracting Aurora A activity (Zeng et al., 2010). Importantly, spindle bipolarity and kinetochore-microtubule interactions rely on a balance between PP1 and Aurora B activities. This balance is achieved in various ways. On the one hand, PP1 can directly dephosphorylate and inactivate centromeric Aurora B (Posch et al., 2010). On the other hand, the phosphatase is able to counter the Aurora B-dependent phosphorylation of kinetochore components (Liu et al., 2010, Kim et al., 2010). Furthermore, recent studies have proposed that PP1, together with PP2A, controls the chromosomal targeting of Aurora B (Qian et al., 2011, Qian et al., 2013). It has been postulated that the balance between Aurora B and PP1 activities controls the SAC in fungi (Lesage et al., 2011), although it is unclear whether this is true in animals.

Once all chromosomes are correctly attached to the spindle and the SAC is satisfied, the APC/C complex targets cyclin B1 for proteasomal degradation. This leads to inactivation of CDK1 and initiation of chromosome separation (Pines, 2006). However, CDK1 inactivation alone is insufficient to drive mitotic exit, as the substrates of CDK1 and other kinases need to be dephosphorylated (Wurzenberger and Gerlich, 2011). This switch is performed by PPPs. Among many studies, recent reports have proposed, for example, that PP1 is important in chromosome segregation and subsequent decondensation by countervailing Aurora B activity (Wurzenberger et al., 2012, Afonso et al., 2014). Importantly, this timely progression through anaphase and cytokinesis is also aided by PP2A, as has been proposed last year (Cundell et al., 2013).

1.6 Experimental systems: the Drosophila notum and sensory organ precursor cells

1.6.1 The notum: a single-layered epithelium on the dorsal thorax of the fly

The notum constitutes a large portion of the *Drosophila* dorsal thorax (Fig. 1.2). It develops from two larval cell populations – the mesothoracic leg and wing imaginal discs –, which undergo eversion during pupal metamorphosis (Zeitlinger and Bohmann, 1999, Grieder et al., 2009). Given its topological simplicity, the developing pupal notum of *Drosophila* has been extensively used to understand multiple aspects of tissue morphogenesis and mechanics. Indeed, studies using the notum have shed light on mechanisms of epithelial cell division (Founounou et al., 2013, Guillot and Lecuit, 2013, Herszterg et al., 2013), asymmetric cell division (Morin and Bellaiche, 2011), cell delamination (Marinari et al., 2012), apoptosis (Koto et al., 2011) and planar polarisation (Olguin et al., 2011, Bosveld et al., 2012).

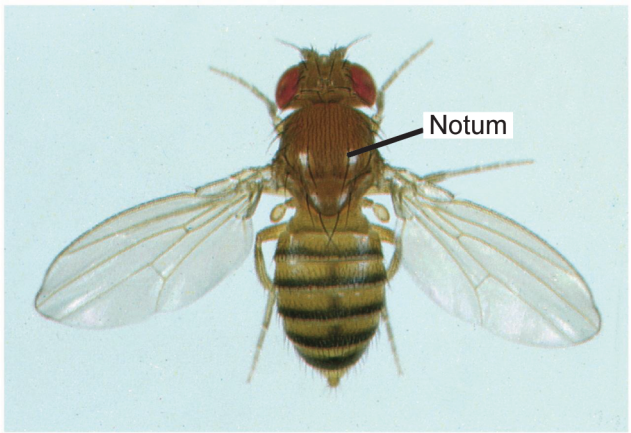

(Adapted from http://www.mun.ca/biology/scarr/)

Figure 1.2 – The adult *Drosophila* notum.
The notum is located on the dorsal side of the fly thorax. The adult dorsal thorax is covered by sensory bristles, macrochaetae and microchaetae, arranged in a characteristic pattern.

1.6.2 Sensory organ precursor cells as a paradigm of asymmetric cell division

The dorsal thorax is covered by two different types of external sensory organs: macrochaetae and microchaetae (de Celis et al., 1999). These sensory organs, also called bristles, are organised into stereotyped spatial arrays in which each bristle occupies a defined position (Simpson et al., 1999, Pistillo et al., 2002). The development of bristle precursor cells depends upon expression of the genes *achaete* and *scute*, which provide cells with neural potential during the larval and pupal stages (Cubadda et al., 1997, Wulbeck and Simpson, 2000, Pistillo et al., 2002). Expression of these genes is itself regulated by cis-regulatory elements and spatially restricted transcription factors such as Pannier (Garcia-Garcia et al., 1999, Calleja et al., 2000, Wulbeck and Simpson, 2000, Pistillo et al., 2002, Fromental-Ramain et al., 2008). Importantly, *achaete* and *scute* are at the core of a mechanism of lateral inhibition that allows correct fate specification and, in consequence, the patterning of the sensory precursors. This mechanism relies on Notch-Delta signalling (Heitzler et al., 1996, Castro et al., 2005). Once its fate is specified, the precursor cell (SOP/PI) gives rise to a lineage of five different cells, which will compose the sensory organ (Fig. 1.3). The first cell divides within the plane of the single-layered epithelium, along the anterior-posterior axis, to produce an anterior PIIb and a posterior PIIa cell. PIIb divides to form a glial cell and PIIIB, which in turn will give rise to two internal cells (neuron and sheath). PIIa divides to form two outer cells (hair and socket). The glial cell migrates away along the neuronal axon (Fig. 1.3). (Hartenstein and Posakony, 1989, Gho et al., 1999, Roegiers et al., 2001, Fichelson and Gho, 2003). The anterior-posterior polarisation of SOP cells is dictated by Frizzled receptor signalling (Bellaiche et al., 2004, Segalen et al., 2010). Frizzled and its cortical effector Dishevelled are localised to the posterior cortex of the SOP cell (Bellaiche et al., 2004). It has been suggested that Frizzled signalling controls the posterior localisation of the Par complex (Bazooka/Par-3, Par-6 and aPKC) and the anterior localisation of the Discs large/Partner of Inscuteable (Pins) complex, which in turn promotes the anterior localisation of the cell fate determinants Neuralized, Numb and the adaptor partner of Numb (Pon) (Bellaiche et al., 2001, Le Borgne and Schweisguth, 2003, Bellaiche et al., 2004, Emery et al., 2005, Wirtz-Peitz et al., 2008). In addition, it is thought that the actomyosin cortex is

required for asymmetric localisation of fate determinants at the plasma membrane (Knoblich et al., 1997, Lu et al., 1999, Barros et al., 2003, Erben et al., 2008). The co-segregation of Numb and Neuralized into the anterior cell is essential for Notch-mediated PIIa/PIIb fate decision (Rhyu et al., 1994, Le Borgne and Schweisguth, 2003, Emery et al., 2005).

While being an attractive model to study cell polarisation and asymmetric cell division, SOP cells have also been used to study cell morphology and actin dynamics (Georgiou and Baum, 2010). Given the fact that these cells have a specific identity and are not juxtaposed to one another, one can express fluorescently tagged protein or probes to follow shape transitions and protein dynamics during the cell cycle.

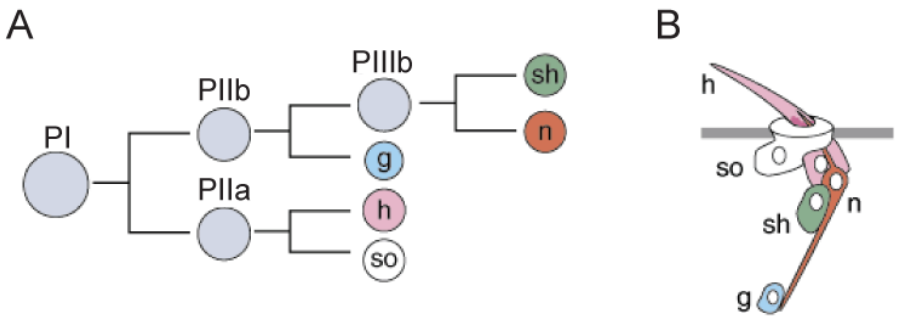

(Adapted from Roegiers et al., 2001)

Figure 1.3 – The SOP lineage.

A, B – The PI (SOP) cell divides to give rise to PIIb and PIIa (**A**). PIIb divides to form a glial cell and PIIIB. The latter divides to originate the neuron (n) and the sheath (sh) – the two internal cells of the sensory organ (see **B**). PIIa divides to give rise to the hair (h) and the socket (so) – the two external cells of the sensory organ (see **B**). The glial cell migrates away along the neuron.

1.7 Aims of my research

The introduction lays out much of what is known about Moesin function and regulation, as well as its role, alongside other actin regulators, in the changes in cell shape that accompany mitotic progression. In addition, it highlights the advantages of the notum as a model system to study cell shape dynamics and division.

Building on these themes, the aims of my research were to:

1. Study the function of Moesin during mitosis in the context of an epithelium.

2. Identify the mechanisms controlling the timely activation and inactivation of Moesin.

3. Determine how this is coupled to mitotic progression and the activity of mitotic kinases and their countervailing phosphatases.

In the following results chapters I discuss my major findings. These relate to the role and regulation of Moesin during mitotic entry, in metaphase and during mitotic exit.

Chapter 2

Materials and methods

2.1 *Drosophila* strains

Transgenic/mutant strains	Origin
w^{1118};;;	BL 3605
w^{*}; UAS-mCherry-α-Tubulin;;	BL 25774
w^{1118};; UAS-Lifeact-GFP;	F. Schnorrer
w^{1118};; *neur*-GAL4;	Y. Bellaiche
w^{1118};; *pnr*-GAL4;	BL 3039
w^{1118}; *neur*-GMA	B. Baum
w^{1118}, UAS-Slik;;;	D. Hipfner
w^{*}; tubP-GAL80^{ts}; TM2/TM6B;	BL 7108
w^{*};; *sqh*-Sqh-mCherry;	E. Wieschaus
w^{1118};; *phyl*-PON-GFP;	B. Baum
w^{1118}; *neur*-RFP;;	Y. Bellaiche
w^{1118}; *ubi*-RFP-Cnn;;	J. Raff
;; Asl^{mecD}/TM6B;	J. Raff
w^{*}; sna^{Sco}/CyO; tubP-GAL80^{ts};	BL 7018
w^{1118}; UAS-Sds22-GFP; TM2/TM6B	B. Thompson
w^{1118}; EM462-GAL4;;	G. Morata
w^{*};; gSpc25-mRFP;	C. Lehner
w^{1118}; UAS-PON-GBP/CyO;;	M. Gonzalez-Gaitan
w^{1118};; UAS-Moesin-GFP;	F. Payre
w^{1118};; UAS-MoesinT559-GFP;	F. Payre

Transgenic strains expressing inducible hairpin RNAi constructs				
TID or Line #	Origin	Annotation ID **Target gene**	19-mers*	Off-targets – 19-mer hits (Annotation)
TID42051	VDRC	CG5851 **Sds22**	377	0
TID43783	VDRC	CG4527 **Slik**	323	1 (CG1954)
TID35025	VDRC	CG5650 **PP1-87B**	293	15 (CG6593); 5 (CG9156); 3 (CG8822); 1 (CG1668); 1 (CG2096)
TID38989	VDRC	CG32707 **APC4**	333	1 (CG10210); 1 (CG10375); 1 (CG10631); 1 (CG11111); 1 (CG30020); 1 (CG6205); 1 (CG7583); 1 (CG9906)
TID103914	VDRC	CG1768 **Diaphanous**	341	0
TID104675	VDRC	CG9774 **Rok**	488	0
HM05265	DRSC	CG10701 **Moesin**	NA	NA
HMS01417	DRSC	CG13345 **Tumbleweed/RacGAP1**	NA	NA
HMS01752	DRSC	CG11451 **Spc105r/KNL1**	NA	NA
10701R-3	NIG-FLY	CG10701 **Moesin**	482 (siRNA count)	0

*This is the maximum number of 19-nucleotide fragments that can be generated by Dicer from the inducible hairpin indicated, as predicted by Dietzl and colleagues (Dietzl et al., 2007). They defined 'target gene' as any gene hit by at least 80% of the 19-mers generated by the inducible construct. Any gene hit by fewer 19-mers, but at least one, was defined as an 'off-target' gene (Dietzl et al., 2007).

2.2 *Drosophila* husbandry and genetic techniques

To express protein-coding constructs or RNA hairpins in fly tissues I made use of the GAL4/upstream activating sequence (UAS) system. This system is based on the ability of the yeast GAL4 transcription factor to control gene expression by binding to UAS cis-regulatory sites (Brand and Perrimon, 1993, Busson and Pret, 2007). The two components are carried in separate fly strains that can be crossed in multiple combinations. Because GAL4 can be driven under specific promoters, the system allows UAS-dependent expression in a temporal and tissue-specific manner. In the case of RNAi-mediated gene silencing, UAS-flanked inverted repeats are transcribed into RNA hairpins, which are processed by Dicer into siRNAs. These small fragments can then bind to their complementary mRNA and silence gene expression (Dietzl et al., 2007, Mummery-Widmer et al., 2009). In my experiments, I did not make use of a Dicer transgene to enhance RNAi efficiency, although this has been demonstrated and recommended (Dietzl et al., 2007).

In my work, protein constructs or RNA hairpins were expressed under the following promoters: *pannier* (central region of the notum) (Calleja et al., 2002), *neuralized* (SOP cells only) (Bellaiche et al., 2001), *phyllopod* (proneural clusters) (Pi et al., 2004), *oddstriped*^{EM462} (lateral domains along the thorax) (Hartmann and Jackle, 1995) and ubiquitous promoters (namely, *tubulin*, *sqh* and *ubi*).

In all experiments, flies were grown at 18°C or 25°C during embryonic and larval stages and moved to 25°C or 29°C at the beginning of puparium formation for 14-15h. In cases where early development was severely impaired or compromised, I used a GAL80 temperature-sensitive transgene, GAL80^{ts}, (Matsumoto et al., 1978, McGuire et al., 2003) to dampen protein expression or RNAi-mediated gene silencing. In *Drosophila*, this tool allows regulation of the GAL4/UAS system in a temperature-dependent manner. At 18°C GAL80^{ts} represses GAL4 activity, while at temperatures of 25°C or higher the GAL80 mutant is inactive thus allowing GAL4-dependent gene expression (Suster et al., 2004, Elliott and Brand, 2008). Experimental details about the temperature at which specific genotypes were generated are indicated in the figure legends in Chapters 3-5.

2.3 Pupal dissection and live imaging

At the start of each experiment, I collected pupae at 0h APF. Pupae were then kept at 25°C (or 29°C) for ~14-15h, at which time SOP cells start dividing. Then I attached each pupa, ventral side down, to a slide with double-sided tape (Zitserman and Roegiers, 2011). The operculum of the pupal case was then removed with forceps. Next, I cut a small section of the case over the thorax, thereby exposing the developing notum. A coverslip with a thin layer of halocarbon oil was placed over the notum, supported by a stash of coverslips (acting as spacers) (Georgiou and Baum, 2010). Live imaging began immediately after dissection. Time-lapse movies of notal development were acquired using a Leica SPE scanning confocal microscope with a 40X lens (NA 1.3).

2.4 Notum dissection and immunocytochemistry

Pupae were setup as described above and dissected at ~14-15h APF. To dissect the notum, each pupa was pinned (dorsal side down) onto the bottom of a dish and immersed in PBS. Using forceps and scissors I then cut and discarded the pupal head and thorax, exposing the notum. Pupal nota were promptly fixed in 10% Trichloroacetic acid or 4% formaldehyde for 20 minutes at room temperature, before being permeabilised in PBS containing 0.1% Triton X-100. Subsequently, I incubated these nota in a blocking solution composed of 5% BSA and 3% FBS (in PBS). Once immunostained and mounted, tissues were imaged using a Leica SP5 confocal microscope and 60X oil objective (NA 1.4). I used the following antibodies and dyes for immunostainings: Rabbit anti-p-ERM (CS, 3141S, 1/100), Rabbit anti-p-MRLC2 (S19) (CS, 3671S, 1/30), Mouse anti-α-Tubulin (Abcam, DM1A, 1/100), Guinea pig anti-Centrosomin (1/1000, a gift from F. Pichaud), Rabbit anti-Moesin (1/10000, a gift from D. Kiehart), Mouse anti-GFP (Abcam, 1/500), Mouse anti-MPM-2 (Millipore, #05-368, 1/200), Guinea pig anti-Slik (1/250, a gift from D. Hipfner) and DAPI (Molecular Probes, 1μg/ml). I used Alexa conjugated antibodies for the counterstainings. All time-lapse and fixed staining images in the thesis are single confocal cross-sections.

2.5 Graph representation and statistical analysis

Various types of graphs are shown in chapters 3-5: box-and-whisker plots with 10-90 percentiles (Figures 3.3B, 3.4B, 3.7B, 3.10B, 4.2B, 4.9B, 4.12A, 4.12B, 4.13B, 5.4C, 5.5B, 5.8C, 5.13D, 5.14B, 5.14C, 5.18D, 5.19C and 5.19D); bar graphs of the mean with standard deviation (Figures 3.5B, 3.9B, 4.8B, 4.8D, 5.2B, 5.4B, 5.4D, 5.5C, 5.6B, 5.8B, 5.9E, 5.13B, 5.15C and 5.17C); rosette plots (Figures 4.11C and 5.7B); dotplots with median (Figures 5.4A, 5.20B and 5.20C); scatter plots with linear regression (Figure 5.10H); XY line plots (Figures 4.3B, 4.3D, 4.3F, 4.10B, 4.10C, 5.9C, 5.9D, 5.13C, 5.14A and 5.18C). The two-tailed unpaired t-test with Welch's correlation was used to calculate statistical significance in all analyses of this thesis except in those shown in Figures 4.9B, 5.20B and 5.20C, where I used the one-way analysis of variance with Tukey's multiple comparison test. $p<0.05$: significant, $p<0.01$: very significant, $p<0.001$: extremely significant.

2.6 Image analysis and quantifications

FIJI software (http://fiji.sc/Fiji) was used to quantify protein levels at the cortex by retrieving the mean grey value of fluorescence signal in a small region of membrane. This can be seen in Figures 3.3, 3.5, 4.8B and 4.8D, where the cortical levels of protein were normalised against the nuclear region (in the same fluorescence channel).

To calculate the relative levels of actin at the pole in early and mid anaphase (seen in Figures 5.4B, 5.8B, 5.9E and 5.13B) I performed the following: first, a kymograph of the radial cross-section was assembled for each actin-labelled cell (as seen in Fig.5.9A-B, yellow box denotes the cross-section). Then, the mean actin intensity was systematically measured over time by placing a 9-pixel square region onto the polar cortex at every time-point along the kymographic profile. Values were then normalized against the actin levels in metaphase. To generate the bar graphs of the actin levels, the values obtained for each cell represent the average of five values measured during a 50sec period either before or after the onset of cell elongation.

To assess the heterogeneity of the actin cortex (seen in Figures 4.2 and 4.9) I measured the mean grey values of GMA signal for all four cortical quadrants and retrieved the standard deviation (s.d.) between them. The closer s.d. is to zero, the more uniform the cortex is.

FIJI software (http://fiji.sc/Fiji) was also used to generate the kymographs of the cell perimeter over time seen in Figures 4.5, 5.2, 5.10 and 5.15. To build these, I drew a line scan over the perimeter of the cell during mitosis (one line per time, 10sec resolution). The lines were then straightened and combined in the form of a space/time plot (as seen in Figure 5.10B, D). In the case of Figures 5.10E-G and 5.11C-D, these space/time plots were subsequently saved in a text image format and then binned into 9x9 grids of mean grey values (not shown). Subsequently, these 9x9 grids of actin intensity values were then 'overlaid' to obtain an average plot of actin levels/time for all cells analysed (seen in Fig. 5.10F). Alongside this, I measured the DNA-cortex distances d1-9 (as seen in Fig. 5.10C) in each cell during early anaphase, obtaining a 9x9 grid of distance/time (as seen in Fig. 5.10E). Similarly to the actin plots, the distance/time grids of all 10 cells analysed were 'overlaid' to obtain an average plot distance/time (seen in Fig. 5.10G). Matlab (MathWorks) was used to present the plots aforementioned in the form of colormaps.

The analysis of cell roundness, circularity and area (shown in Figures 4.3, 4.5, 5.19 and 5.20) was also performed using FIJI.

Chapter 3

Results: The spatio-temporal dynamics of Moesin during mitotic progression

3.1 Introduction

Animal cell division is accompanied by dramatic shape transitions. Over many decades, studies using cultured cells have shown how these retract their protrusions and attain a rounded shape at the onset of mitosis (Harris, 1973, Cramer and Mitchison, 1997, Kunda and Baum, 2009, Dao et al., 2009). Similar morphological changes have been described for cells embedded in tissue contexts (Norden et al., 2009, Meyer et al., 2011, Kondo and Hayashi, 2013). At mitotic exit cells undergo yet another shape transition as they elongate in preparation for cytokinesis. In doing so, they accommodate spindle elongation and the segregation of the genetic material, which will be equally parted between the daughter cells.

Remodelling of the actomyosin cytoskeleton has been implicated in the various cell shape transitions during mitosis, as detailed in chapter 1. A few years ago studies from two labs showed that Moesin, which provides linkage between actin filaments and the plasma membrane, plays a key role in reorganising the actin cytoskeleton in mitotic fly cells in culture (Carreno et al., 2008, Kunda et al., 2008). In particular, these reports revealed that Moesin is required for cell rounding and formation of a rigid actin cortex, thereby ensuring correct spindle morphogenesis. Importantly, this has since been confirmed in metaphase cells in tissue contexts (Cheng et al., 2011, Luxenburg et al., 2011, Nakajima et al., 2013). While well characterised in early mitosis, the functions of Moesin and concurring remodelling of the cortex in cells exiting mitosis are not currently understood.

In this chapter I first present a concise description of the morphological changes that fly SOP cells undergo when passing through mitosis. I then succinctly characterise how the cytoskeleton of actin filaments is reorganised as mitotic cells change their shape (a thorough examination of this reorganisation will be presented in Chapters 4 and 5). Next I provide a detailed assessment of the spatio-temporal pattern of Moesin in cells at the different stages of mitosis. Finally, I elucidate how the activity of this actin-membrane crosslinker is regulated during mitosis, by analysing the roles of two of its major phospho-regulators – the Ste20-like kinase Slik and the serine/threonine phosphatase PP1.

3.2 Characterisation of the morphological changes and the reorganisation of actin cytoskeleton during mitosis

3.2.1 Morphological changes and reorganisation of the actin cytoskeleton upon mitotic entry

To begin my studies, I first decided to characterise the behaviour of SOP cells as they enter mitosis. These cells sit within the developing notum of the *Drosophila* fly. They are arranged in a spaced pattern, in that they are not juxtaposed to one another but are separated by epithelial cells (Cubadda et al., 1997, Simpson et al., 1999, Wulbeck and Simpson, 2000). Given their identity, tools have been engineered to allow expression of protein markers specifically in these cells (Le Borgne and Schweisguth, 2003), as can be done for any cell type/lineage in the fly. For these reasons, SOP cells constitute an excellent model system to examine shape transitions and protein function/localisation with high accuracy.

I began my experiments by visualising flies where SOP cells express a GFP-tagged form of the F-actin-binding peptide Lifeact (Riedl et al., 2008) and Cherry-tagged Tubulin. Using scanning confocal microscopy, I imaged these cells as they entered mitosis. As illustrated in Figure 3.1, which depicts an SOP cell representative of those analysed, interphase cells exhibit actin-rich protrusions at various apical-basal levels. This is more prominent in the middle of the tissue (at Z=0μm) and basal levels (Georgiou and Baum, 2010, Cohen et al., 2010). As cells reach prophase, marked by the separation of the centrosomes (see white arrowheads in Fig. 3.1A), most of the protrusions are lost. At this point, cells have also attained a largely rounded morphology. At the prophase-prometaphase transition, when the nuclear envelope breaks down and the spindle begins to form, a drastic increase in F-actin levels at the cortex is observed (see Fig. 3.1B and yellow arrowheads in Fig. 3.1A). Importantly, this cortical rearrangement is concomitant with the rounding process, which is consistent with previous findings (Maddox and Burridge, 2003, Matthews et al., 2012, Lancaster et al., 2013, Nakajima et al., 2013). Also, note the presence of blebbing in the basal domains of the cell (see blue arrowheads). This blebbing may reflect an increase in

myosin-dependent contractility (Maddox and Burridge, 2003, Kunda et al., 2008, Carreno et al., 2008, Kondo and Hayashi, 2013). Once cells reach metaphase they are highly rounded, indicated by the circular shape and the smooth edge of the representative cell (evident in all apical-basal sections). Importantly, the cortex of the cell is now homogeneously enriched with F-actin. Interestingly, I also noticed that the apical microvilli present in the early stages of rounding have largely disappeared by the time cells reach metaphase (see z=3μm cross-sections) (Porter et al., 1973, Sanger et al., 1984). To determine if this is the case, one will have to image these cells in electron microscopy.

3.2.2 Morphological changes and reorganisation of the actin cytoskeleton during mitotic exit

Having observed the changes in cell shape and the accompanying rearrangement of the cortical actin cytoskeleton in early mitosis, I now wanted to gain insight into the equivalent processes in cells exiting mitosis. Using a similar setup to that explained in the previous section, I filmed SOP cells expressing Cherry-tagged Tubulin (in this case, also expressed in epithelial cells) and the GMA actin-binding probe (expressed in SOP cells only, to facilitate visualisation). Figure 3.2 shows intermediate confocal sections of a representative cell at metaphase, anaphase and telophase. As can be appreciated, the cortical levels of F-actin drop considerably at the poles as cells elongate at anaphase (see arrowheads; also clear in the 'Actin profiles'). Simultaneously, a clear enrichment of F-actin is observed in the equatorial regions of the cell edge, where the constriction of the cytokinetic ring and membrane furrowing will occur (Reichl et al., 2008, Zhou and Wang, 2008, Pollard, 2010). At telophase, when new nuclei begin to form (as indicated by the exclusion of Tubulin signal – see blue arrowheads), furrowing has almost reached completion and the midzone anti-parallel microtubules begin to bundle to form the midbody (Guse et al., 2005). Interestingly, F-actin re-accumulates at the polar cortices at this stage. Moreover, the new daughter cells acquire a homogenous actin cortex and a highly rounded morphology, like cells in metaphase.

An in-depth exploration of the shape and cortical dynamics in anaphase and cytokinetic cells will be presented later in this thesis.

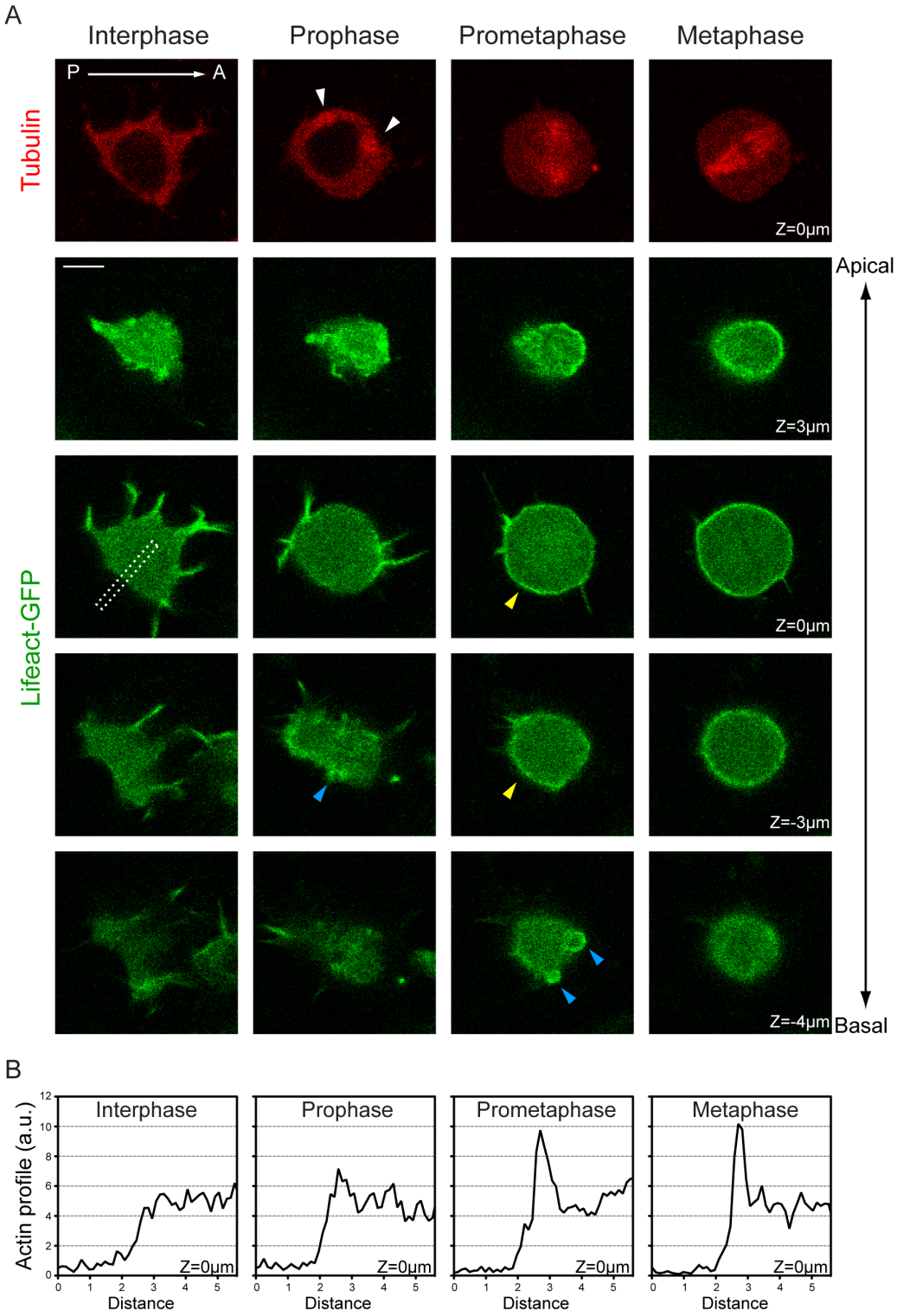
A
Interphase
Prophase
Prometaphase
Metaphase
P
A
Tubulin
Z=0µm
Apical
Z=3µm
Lifeact-GFP
Z=0µm
Z=-3µm
Z=-4µm
Basal
B
Actin profile (a.u.)
Interphase
Prophase
Prometaphase
Metaphase
Z=0µm
Distance

Figure 3.1

Figure 3.1 – Actin reorganisation and shape changes in SOP cells entering mitosis.

A – Panel of confocal cross-sections of a representative SOP cell imaged at interphase, prophase, prometaphase and metaphase. A-P, Anterior-Posterior axis. White arrowheads point to the centrosomes. Yellow arrowheads point to actin accumulation at the cortex in early mitosis. Blue arrowheads point to basal blebbing. Lifeact-GFP labels actin filaments. mCherry-Tubulin transgene was expressed to label spindle microtubules. Scale bar = 5µm. Genotype:

w^{-}; UAS-mCherry-αTubulin/+; UAS-Lifeact-GFP/*neur*-GAL4;

Note: flies were grown at 25°C through early development and pupariation.

B – Fluorescence intensity profiles of the radial cross-section shown in **A** (dotted box), highlighting the cortical accumulation of actin in prometaphase and metaphase.

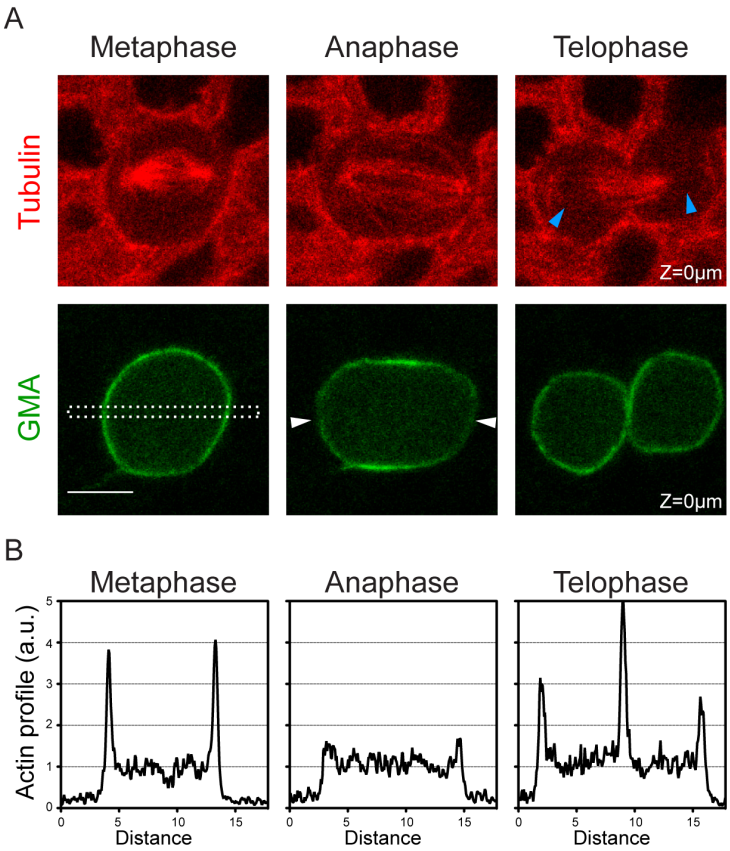

Figure 3.2 – Actin reorganisation and shape changes in SOP cells exiting at mitotic exit.

A – Panel of confocal cross-sections of a representative SOP cell imaged at metaphase, anaphase and telophase. White arrowheads point to actin clearance from the poles. Blue arrowheads indicate Tubulin exclusion from the reforming nuclei at telophase. mCherry-Tubulin transgene was expressed to label spindle microtubules. GMA labels filamentous actin. Scale bar = 5µm. Genotype:

w^{-}; *neur*-GMA, UAS-mCherry-αTubulin/+; *pnr*-GAL4/+;

Note: flies were grown at 25°C through early development and pupariation.

B – Fluorescence intensity profiles of the radial cross-section shown in A (dotted box), highlighting the drop of polar actin at anaphase and cortical re-enrichment at telophase.

3.3 Moesin is activated at the cell cortex upon mitotic entry

As mentioned in chapter 1, it is currently accepted that the function of ERMs in anchoring actin filaments to the plasma membrane is dependent on their activation. This occurs in two steps: interaction with PIP2 (Blin et al., 2008, Roch et al., 2010, Ben-Aissa et al., 2012) and phosphorylation at the conserved threonine residue in the actin-binding domain by the Ste20-like kinase Slik (Simons et al., 1998, Fehon et al., 2010, Machicoane et al., 2014).

Studies with cultured fly cells have demonstrated that the cortical levels of the activated form of Moesin increase dramatically at the onset of mitosis, which leads to cell rounding and cortical stiffening (Carreno et al., 2008, Kunda et al., 2008).

Having characterised the changes in morphology and the reorganisation of the actin cortex in SOP cells at the onset of mitosis, I therefore wanted to determine the dynamic pattern of localisation and activation of Moesin in this context. To do so, I started by fixing and staining notum explants against Moesin, Tubulin and DNA. Figure 3.3 depicts a panel of stained epithelial cells at various stages of mitotic entry, which exhibit an identical pattern of Moesin localisation as that seen in SOP cells. In interphase, the signal of Moesin around the cell edge is very low and diffuse. The cortical levels of the protein increase gradually as cells enter mitosis and reach metaphase. At this stage, the cortical signal of Moesin is almost twice as high as that observed in interphase. It is striking that Moesin appears to decorate the cortex of mitotic cells at basolateral levels (intermediate section, Z=0μm), since most studies have focused on the apical localisation and function of this protein. Interestingly, Moesin-rich protrusions are also observed in the basal domain of cells entering mitosis (Kosodo et al., 2008, Nakajima et al., 2013).

Next I wanted to gauge the profile of localisation of activated, phosphorylated Moesin during mitotic entry. To do so, I stained tissue explants with an antibody against the phosphorylated form of Moesin (epitope containing Thr559) and an MPM-2 antibody to identify mitotic cells (Renzi et al., 1997, Wu et al., 2010). As shown in Figure 3.4, the levels of cortical p-Moesin appear to be very low in interphase cells. At prophase/prometaphase, I observed a sharp

increase in the amount of active Moesin around the cell edge, in agreement with previous reports (Kunda et al., 2008, Carreno et al., 2008). Cortical levels of p-Moesin continue rising as cells progress into metaphase. By the time cells assumed a highly rounded geometry, the cortical levels of p-Moesin had increased ~5-fold above those seen in metaphase.

Given the patterns of localisation of total Moesin and its phosphorylated form, it is possible that the cortical accumulation of Moesin is not exclusively dependent on its phosphorylation at Thr559. As has been mentioned before, activation and binding to plasma membrane by Moesin also depends on PIP2 and other adaptor proteins (Fievet et al., 2004, Roch et al., 2010, Hughes et al., 2010, Fehon et al., 2010, Blin et al., 2008, Ben-Aissa et al., 2012).

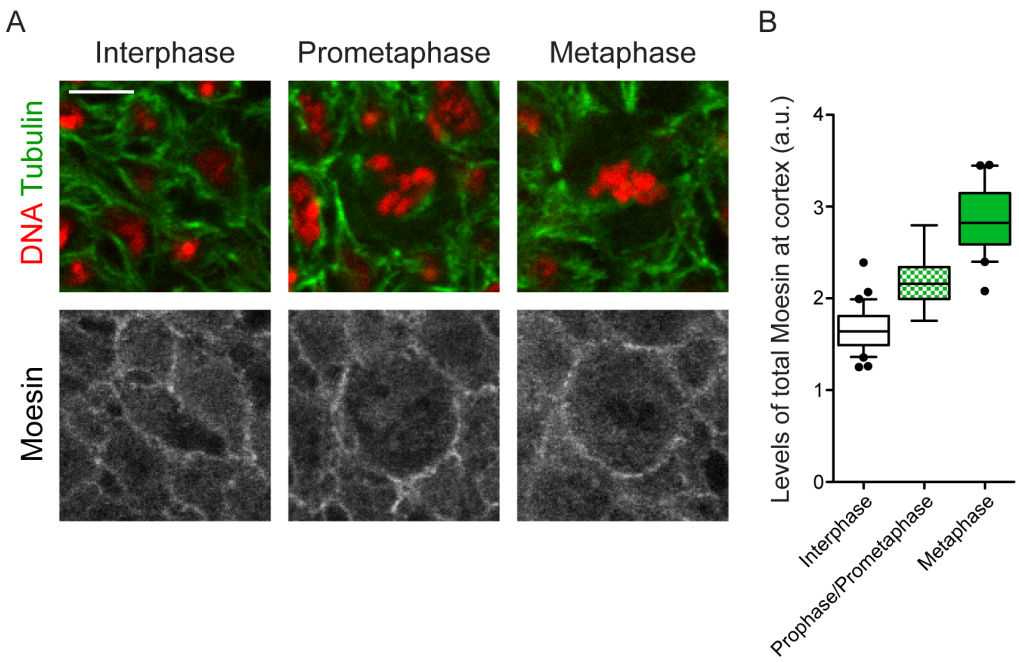

Figure 3.3 – Moesin accumulates at the cortex upon entry into mitosis.

A – Representative epithelial cells at different points of mitotic entry. Tissues were fixed and stained for DNA, Tubulin and total Moesin. Scale bar = 5µm. Genotype: w^{1118};;;

Note: flies were grown at 25°C through early development and pupariation.

B – Quantification of the levels of Moesin at the cortex of interphase, prophase/prometaphase and metaphase. Values are the normalised levels cortex/nuclear region. Mean±SD (a.u.) – Interphase: 1.66±0.25, 30 cells; Prophase/prometaphase: 2.19±0.31, 8 cells; and Metaphase: 2.84±0.38, 20 cells; ≥ 3 animals analysed.

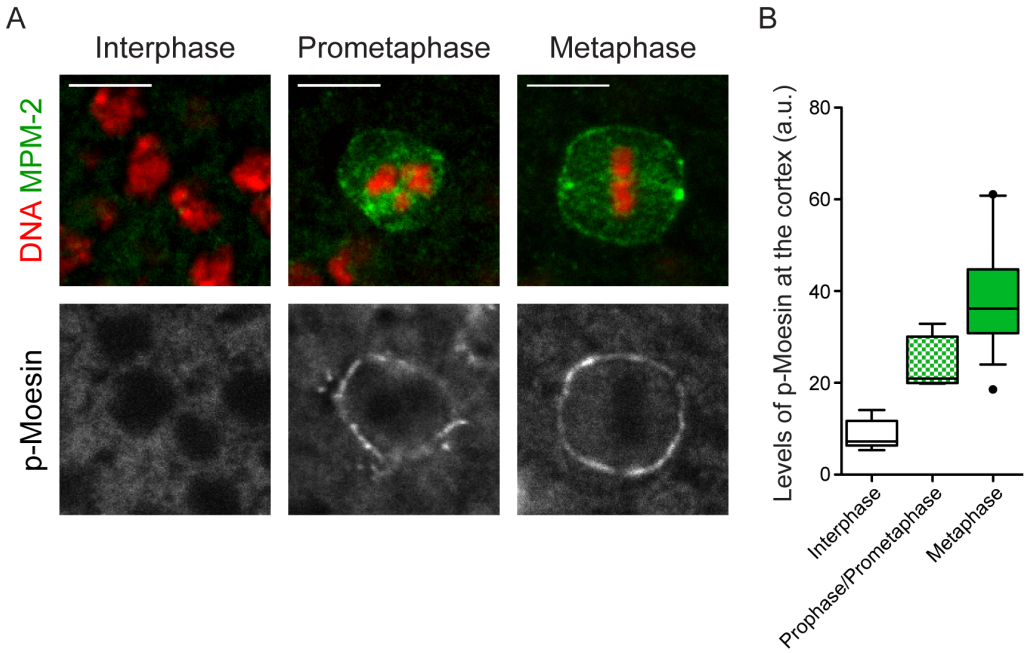

Figure 3.4 – The cortical signal of p-Moesin is highly increased at mitosis.

A – Representative epithelial cells at different points of mitotic entry. Tissues were fixed and stained for DNA, MPM-2 and p-Moesin. Scale bar = 5µm. Genotype:

w^{-};; *pnr*-GAL4/+;

Note: flies were grown at 25°C through early development and pupariation.

B – Quantification of the levels of p-Moesin at the cortex of interphase, prophase/prometaphase and metaphase. Mean±SD (a.u.) – Interphase: 8.59±3.14, 8 cells; Prophase/prometaphase: 23.65±6.19, 4 cells; Metaphase: 38.77±11.79, 14 cells; ≥ 3 nota analysed.

3.4 Slik kinase is required for localised activation of Moesin at the cortex in early mitosis

The Ste20-like kinase Slik has been shown to activate Moesin in multiple contexts. Several lines of evidence have demonstrated that loss of Slik leads to impaired epithelial integrity (Hipfner and Cohen, 2003, Hipfner et al., 2004, Hughes et al., 2010). Importantly, depletion of Slik in fly and human cells in culture causes strong defects in cell rounding, cortical rigidity and spindle morphogenesis/orientation (Kunda et al., 2008, Carreno et al., 2008, Machicoane et al., 2014).

To investigate whether Slik is required for the activation of Moesin in mitosis *in vivo*, I depleted Slik in the fly notum by RNA interference. In agreement with *in vitro* studies, this caused a dramatic and significant drop in the levels of p-Moesin at the metaphase cortex (Figure 3.5). I also performed the reverse experiment to test the defects of expressing exogenous Slik. Since fly pupae with increased levels of Slik showed drastic morphological defects making them difficult to dissect, I used a temperature-sensitive Gal80 transgene to control Slik expression (Matsumoto et al., 1978, McGuire et al., 2003) (as detailed in Chapter 2). In control cells, a strong pool of kinase was found concentrated at the cortex (Fig. 3.6). This cortical accumulation was enhanced upon expression of exogenous Slik (Fig. 3.6). Strikingly, in the latter background, the cortical levels of p-Moesin are remarkably higher than those seen in control cells, especially in the mitotic stages (see bottom panel of Fig. 3.7A and Fig. 3.7B). Even though significant, the increase in the levels of active Moesin in interphase cells expressing Slik is almost negligible. These data point to a complex view of Slik-dependent activation of Moesin in mitosis, in that the activity and/or subcellular localisation of the kinase might be cell cycle-regulated. Further experiments will be required to validate this.

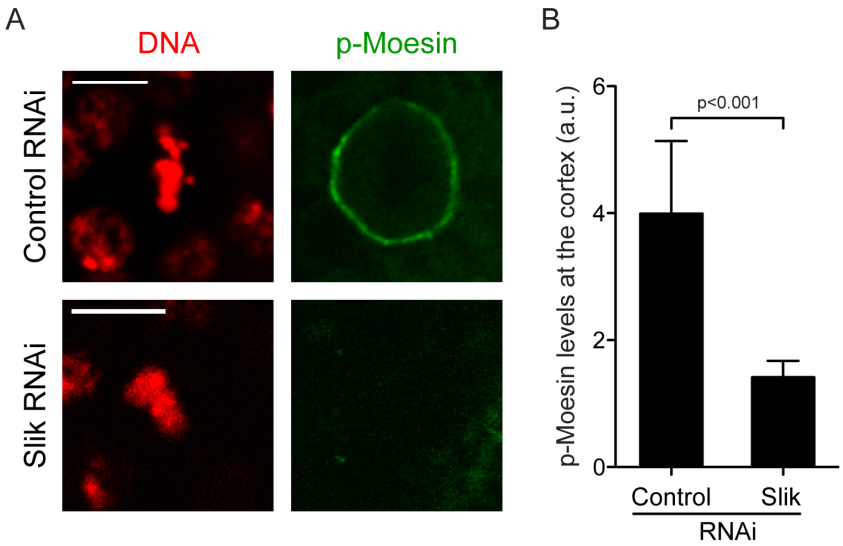

Figure 3.5 – Depletion of Slik leads to reduced levels of p-Moesin at the metaphase cortex.

A – Two representative cells in control and Slik RNAi tissues. Tissues were fixed and stained for DNA and p-Moesin. Scale bar = 5µm. Genotypes:

w^{-};; *pnr*-GAL4/+;

w^{-}; UAS-Slik-IR/+; *pnr*-GAL4/+;

Note: flies were grown at 25°C during early development and at 29°C during pupariation.

B – Quantification of the levels of p-Moesin at the cortex of control and Slik RNAi cells. Values are the normalised levels cortex/nuclear region. Mean±SD (a.u.) – Control RNAi: 3.99±1.14, 14 cells; Slik RNAi: 1.14±0.26, 13 cells; ≥ 3 nota were analysed.

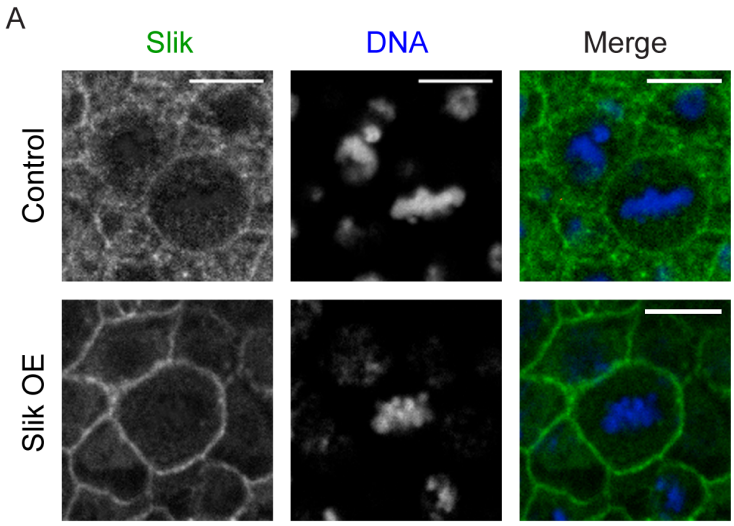

Figure 3.6 – Slik is concentrated around the cell edge of mitotic cells.

A – Representative cells in control and Slik-overexpression tissues. Tissues were fixed and stained for DNA and Slik. Scale bar = 5µm. Genotypes:

w^-; tubP-GAL80^{ts}/+; *pnr*-GAL4/+;

w^-, UAS-Slik/Y; tubP-GAL80^{ts}/+; *pnr*-GAL4/+;

Note: flies were grown at 18°C during early development and at 29°C during pupariation.

3.5 PP1-87B phosphatase and its regulatory subunit Sds22 are negative regulators of Moesin in mitosis

While many mechanisms of ERMs activation have been established, less is known about the molecular machineries that inactivate them. In the pursuit of negative regulators of Moesin, a few years ago our lab performed an RNA interference screen targeting 83 predicted phosphatases in *Drosophila* Kc167 cells (Kunda et al., 2012). This screen identified the serine/threonine phosphatase PP1-87B, whose depletion caused a profound increase in the amounts of cellular p-Moesin. Interestingly, many studies have implicated the fly PP1-87B and its yeast and human homologues in regulating the mitotic checkpoint, chromosome segregation and cytoskeletal dynamics (Chen et al., 2007, Kirchner et al., 2007, Pinsky et al., 2009, Vanoosthuyse and Hardwick, 2009). Following on from these findings, I decided to investigate how this phosphatase is regulating the dynamic changes in Moesin phosphorylation and localisation during mitosis.

Using a similar experimental setup to that described above, I expressed a Gal4-responsive hairpin dsRNA targeting PP1-87B in transgenic flies. The levels of active Moesin were vastly increased in cells with lowered levels of PP1-87B phosphatase relative to control cells. This increase in cortical p-Moesin was evident in the early stages of mitosis but was most prominent at metaphase (Fig. 3.7).

Given the multitude of regulatory proteins that bind PP1 phosphatases (Bennett et al., 2006, Bollen et al., 2010, Barr et al., 2011), it was important to identify the targeting subunit acting with PP1-87B in the regulation of Moesin at mitosis. I focused on the phosphatase regulatory subunit Sds22, because this protein has been implicated in the regulation of events at the metaphase-to-anaphase transition in various model systems (Ohkura and Yanagida, 1991, MacKelvie et al., 1995, Posch et al., 2010, Wurzenberger et al., 2012) and has been shown to control the activity of Moesin and myosin-II in *Drosophila* epithelia (Grusche et al., 2009, Jiang et al., 2011). It is important to highlight that even though Sds22 is known to bind all four PP1 catalytic isoforms in flies (Bennett et al., 2006, Grusche et al., 2009), PP1-87B was the isoform that led to the strongest phenotype in the screen aforementioned. On the other hand,

depletion of regulatory subunits like Mbs and MYPT-75D, previously ascribed putative roles in cytoskeletal organisation (Fukata et al., 1998, Eto et al., 2005), did not lead to a significant increment in p-Moesin levels (Kunda et al., 2012).

Mitotic cells with reduced levels of Sds22 exhibited elevated amounts of phosphorylated Moesin decorating the cortex, as observed in epithelia depleted for PP1-87B (Fig. 3.7). Taken together, these results indicate that PP1-87B and Sds22 act together in the regulation of Moesin activity.

Because both PP1 phosphatase and its subunit Sds22 have both been implicated in the control of mitotic progression, I sought to determine whether the accumulation of p-Moesin observed at metaphase could be due to a delay in the onset of anaphase (Chen et al., 2007, Kunda et al., 2012). To test this, I depleted flies from APC4, a subunit of the anaphase-promoting complex, which led to a severe mitotic delay (Fang et al., 1998, Peters, 2002). Strikingly, the levels of active Moesin at the cortex of mitotic cells were not altered in APC4-depleted cells in relation to control cells. This strongly suggested that the effects of PP1-87B and Sds22 in Moesin regulation are independent of their effects in mitotic progression.

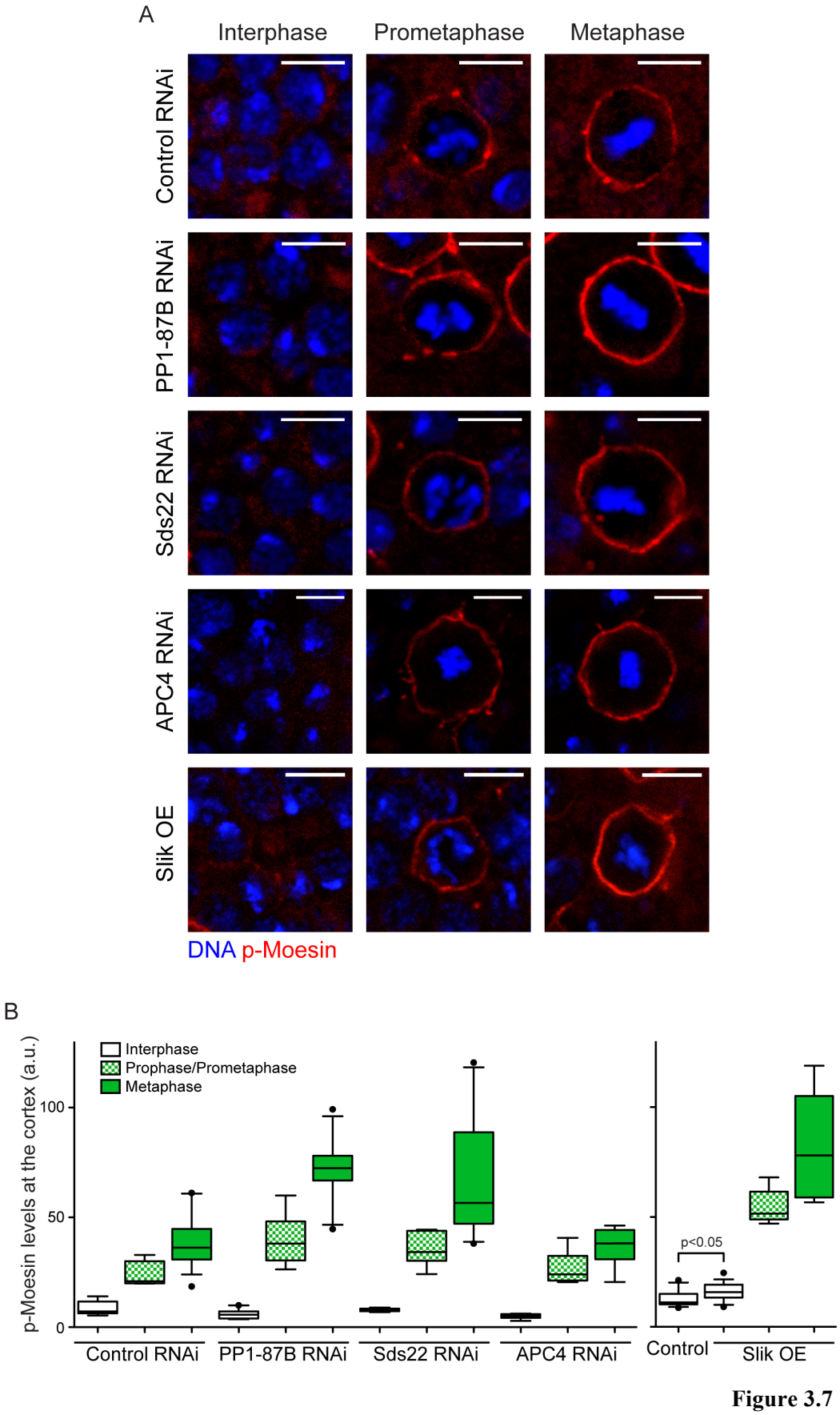
A
Interphase
Prometaphase
Metaphase
Control RNAi
PP1-87B RNAi
Sds22 RNAi
APC4 RNAi
Slik OE
DNA p-Moesin
B
p-Moesin levels at the cortex (a.u.)
Interphase
Prophase/Prometaphase
Metaphase
100
50
0
p<0.05
Control RNAi
PP1-87B RNAi
Sds22 RNAi
APC4 RNAi
Control
Slik OE

Figure 3.7

Figure 3.7 – Depletion of PP1-87B and Sds22 phosphatase subunits, or expression of exogenous Slik, all lead to increased levels of p-Moesin at the mitotic cortex.

A – Representative cells in control, PP1-87B RNAi, Sds22 RNAi, APC4 RNAi and Slik overexpression backgrounds at different points of mitosis. Cells are stained for DNA and p-Moesin (and counterstained for Tubulin to identify the mitotic stages – not shown). Scale bar = 5µm. Genotypes:

w^-; tubP-GAL80^{ts}/+; *pnr*-GAL4/+;

w^-; tubP-GAL80^{ts}/UAS-PP1-87B-IR; *pnr*-GAL4/+;

w^-; tubP-GAL80^{ts}/UAS-Sds22-IR; *pnr*-GAL4/+;

w^-; tubP-GAL80^{ts}/UAS-APC4-IR; *pnr*-GAL4/+;

w^-, UAS-Slik/Y; tubP-GAL80^{ts}/+; *pnr*-GAL4/+;

Note: flies were grown at 18°C during early development and at 29°C during pupariation.

B – Quantification of the levels of p-Moesin at the cortex of cells in all backgrounds shown in **A**. Mean±SD (a.u.) – Control RNAi: 8.59±3.14 (interphase, 8 cells), 23.65±6.19 (prop/prom, 4 cells), 38.77±11.79 (metaphase, 14 cells); PP1-87B RNAi: 5.92±2.10 (interphase, 9 cells), 39.66±11.14 (prop/prom, 8 cells), 72.18±14.32 (metaphase, 11 cells); Sds22 RNAi: 7.82±0.74 (interphase, 6 cells), 35.41±7.75 (prop/prom, 7 cells), 66.49±26.70 (metaphase, 10 cells); ACP4 RNAi: 4.92±1.16 (interphase, 7 cells), 26.30±8.18 (prop/prom, 5 cells), 36.32±8.40 (metaphase, 9 cells). Plot on the right – Control: 12.62±3.81 (interphase, 14 cells) Slik OE: 16.03±4.02 (interphase, 17 cells), 54.51±7.82 (prop/prom, 7 cells), 80.40±24.07 (metaphase, 9 cells); ≥3 animals for each genetic background.

3.6 Moesin shows a dynamic pattern of inactivation and reactivation in mitotic exit

So far, I have presented evidence that highlights how the actin cytoskeleton is rearranged at the onset of mitosis by way of actin accumulation at the cortex as cells reach metaphase. I have also shown that the cortical levels of active Moesin increase upon mitotic entry, in a process that is regulated by Slik and PP1-87B/Sds22. Taken together, these data suggest that Moesin is required for the concentration of filamentous actin at the cell edge, likely ensuring proper cell rounding and mechanical stability. These aspects will be thoroughly analysed in chapter 4.

In section 3.2.2, I showed that the actin cytoskeleton is subject to drastic rearrangements during mitotic exit. At anaphase, as cells elongate and chromosome segregation ensues, the pattern of filamentous actin becomes polarised. Actin is lost from the cell poles and begins accumulating at the nascent cytokinetic furrow.

To investigate how the pattern of actin Moesin changes during this process, I performed identical immunofluorescence experiments to those described above. As depicted in Figure 3.8, p-Moesin is lost from the cell poles at anaphase, which concurs with the polar loss of actin described earlier. Then, at telophase, the cortex of the newly formed cells becomes re-enriched with high amounts of Actin and p-Moesin. Thus, the patterns of localisation of actin and Moesin change concomitantly, implicating Moesin in the remodeling of cortical actin and control of mitotic shape changes.

As mentioned earlier, the localisation of ERM proteins to the membrane is dependent on multiple factors. While phosphorylation is crucial for the activation of ERMs, binding to PIP2 and various scaffolding proteins is also required for their activation and membrane localisation. I then expressed GFP-tagged Moesin in nota and performed an analysis where I could appreciate the pattern of p-Moesin and total Moesin in anaphase cells.

Using antibodies against a GFP epitope and against p-ERM, I was able to detect that, in anaphase, the levels of inactive Moesin at the poles were higher than those of phosphorylated protein (Fig. 3.9). This was reflected in the different

patterns of cortical distribution of the inactive and active forms of Moesin (see inset in Fig. 3.9). These data suggest the presence of a spatio-temporal cue that triggers the transient dephosphorylation of Moesin at the poles but does not affect its membrane-binding capacity. I did notice however, that the signal of inactive Moesin itself appeared to be a little bit reduced at the tip of the cell poles (compare white arrowhead to pink arrowheads in Fig. 3.9). This observation may be in line with data presented by Roubinet and colleagues, who argued that loss of PIP2 from the cell poles and accumulation of this lipid at the equator could affect the cortical distribution of total Moesin in cells as they prepare to elongate at cytokinesis (Roubinet et al., 2011). However, in comparison to that report, my double-immunolabelling analyses (to probe active and inactive Moesin) are clearer in pointing to the existence of a second pathway that instructs the dephosphorylation of Moesin and that is not directly responsible for the unbinding/detachment of Moesin from the plasma membrane (at least transiently).

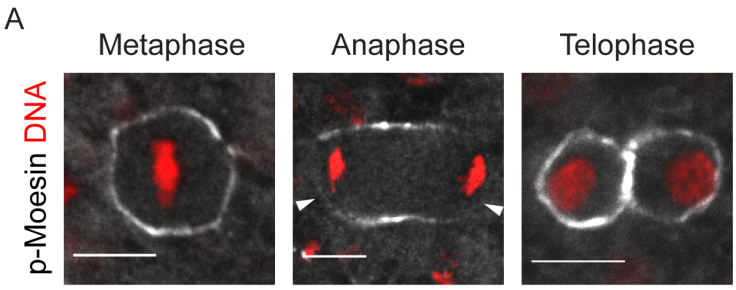

Figure 3.8 – Cortical p-Moesin is dynamically redistributed during mitotic exit.

A – Representative epithelial cells at different points of mitotic exit. Tissues were fixed and stained for DNA and p-Moesin. White arrowheads point to actin clearance from the poles. Scale bar = 5µm. Genotype:

w^{1118};;;

Note: flies were grown at 25°C through early development and pupariation.

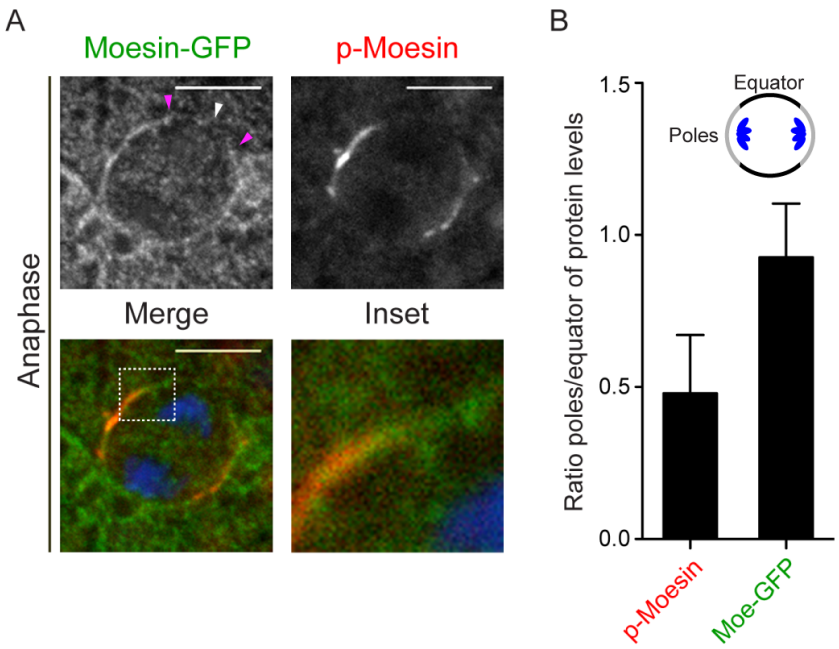

Figure 3.9 – Moesin is inactivated at the cell poles in anaphase.

A – Representative anaphase cell in a Moesin-GFP-expressing tissue. Tissues were fixed and stained for GFP (total Moesin), p-Moesin and DNA. Inset of the dotted region is shown. Arrowheads point to the polar cortex. White arrowhead points to the pole tip (i.e., the cortical point that is furthest from the cell centre; see text for more details). Scale bar = 5µm. Genotype:

w^{-};; *pnr*-GAL4/UAS-Moesin-GFP;

Note: flies were grown at 25°C through early development and pupariation.

B – Ratio poles/equator of Moesin-GFP (total Moesin) or p-Moesin levels in anaphase cells. Mean±SD – p-Moesin: 0.48±0.19; Moesin-GFP: 0.92±0.18; 5 cells, 2 different animals were analysed.

3.7 PP1-87B phosphatase and its regulatory subunit Sds22 control the activity of Moesin in anaphase

Having seen that the levels of p-Moesin at the cell poles drop as cells begin to exit mitosis, I sought to determine whether PP1/Sds22 contributes to Moesin inactivation.

Figure 3.10 shows representative anaphase cells in various genetic backgrounds stained for p-Moesin. As can be easily appreciated, cells lacking either PP1-87B or Sds22 are incapable of clearing p-Moesin from their poles. As a result they fail to polarise the ERM protein (as seen in control cells). This is unlikely due to a checkpoint defect since loss of p-Moesin from the poles was unaffected in APC4-depleted cells. This is interesting since both APC/C and PP1 are known to be directly or indirectly involved in SAC silencing, at which point CDK1 inactivation and sister chromatid separation ensue (Peters, 2002, Vanoosthuyse and Hardwick, 2009, Lesage et al., 2011, Musacchio, 2011).

Conversely, cells expressing high levels of Slik did not fail to clear p-Moesin from their poles (Figure 3.10). Moreover, in this genetic background, Slik appears to localise uniformly around the cell edge in anaphase (also observed in cells that only express endogenous levels of the kinase – see Fig. 3.11). This strongly suggests that Slik is not relocalised at anaphase. Therefore, to eliminate p-Moesin at the poles, Slik must be either transiently inactivated or its activity rendered irrelevant by PP1-87B at this point of mitosis. This will be in explored further in chapters 5 and 6.

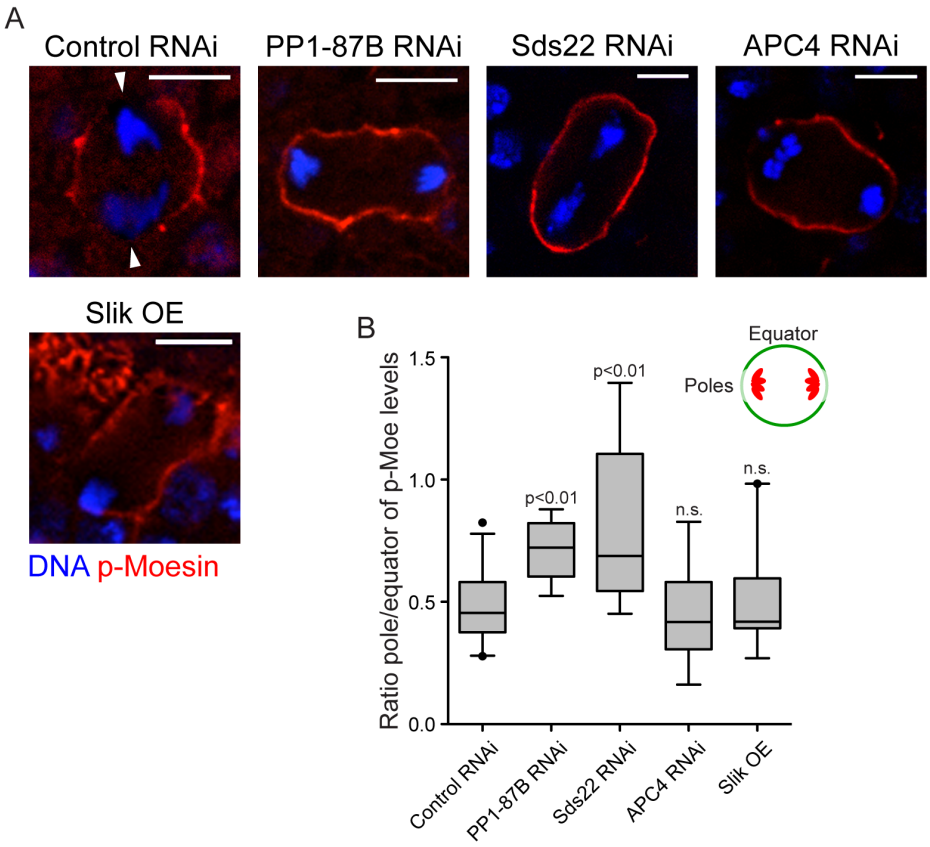

Figure 3.10 – Depletion of PP1-87B or Sds22 leads to impaired loss of p-Moesin from the cell poles in anaphase.

A – Representative anaphase cells in control, PP1-87B RNAi, Sds22 RNAi, APC4 RNAi and Slik overexpression backgrounds. Tissues were fixed and stained for DNA and p-Moesin. White arrowheads point to p-Moesin clearance from the poles. Scale bar = 5µm. Genotypes:

w^{-}; tubP-GAL80^{ts}/+; *pnr*-GAL4/+;

w^{-}; tubP-GAL80^{ts}/UAS-PP1-87B-IR; *pnr*-GAL4/+;

w^{-}; tubP-GAL80^{ts}/UAS-Sds22-IR; *pnr*-GAL4/+;

w^{-}; tubP-GAL80^{ts}/UAS-APC4-IR; *pnr*-GAL4/+;

w^{-}, UAS-Slik/Y; tubP-GAL80^{ts}/+; *pnr*-GAL4/+;

Note: flies were grown at 18°C during early development and at 29°C during pupariation.

B – Ratio poles/equator of p-Moesin levels in anaphase cells in all backgrounds shown in **A**. Mean±SD – Control RNAi: 0.48±0.16, 12 cells; PP1-87B RNAi: 0.71±0.12, 9 cells; Sds22 RNAi: 0.81±0.33, 9 cells; ACP4 RNAi: 0.45±0.22, 7 cells; Slik OE: 0.49±0.21, 9 cells; ≥ 3 animals for each genetic background.

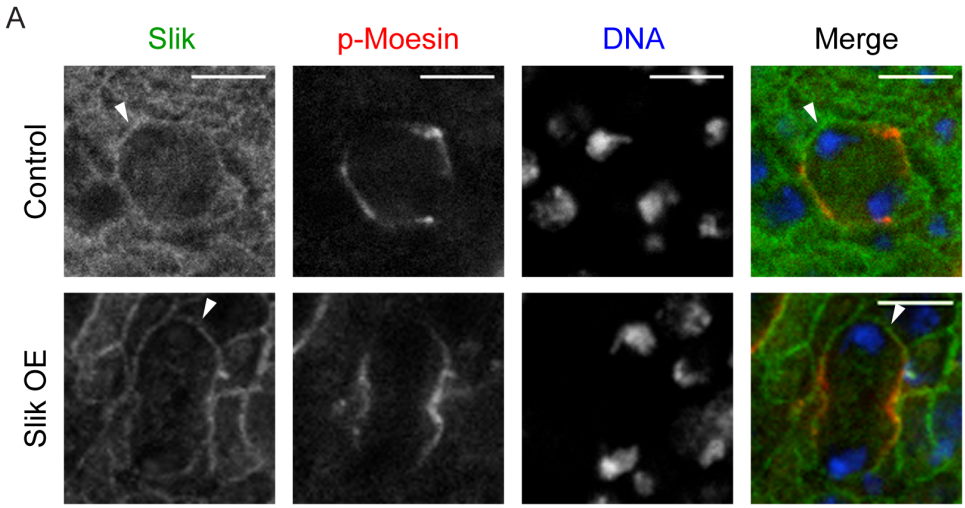

Figure 3.11 – Slik is evenly distributed around the cell edge in anaphase cells.

A – Two representative cells in control and Slik-overexpression tissues. Tissues were fixed and stained for DNA, Slik and p-Moesin. White arrowheads point to Slik localisation at the cell poles. Scale bar = 5µm. Genotypes:

w^-; tubP-GAL80^{ts}/+; *pnr*-GAL4/+;

w^-, UAS-Slik/Y; tubP-GAL80^{ts}/+; *pnr*-GAL4/+;

Note: flies were grown at 18°C during early development and at 29°C during pupariation.

3.8 Conclusions

In this chapter I described the morphological changes and reorganisation of the actin cortex in cells progressing through mitosis. Using time-lapse confocal microscopy, I showed that fly SOP cells retract their interphase protrusions and attain a round shape at metaphase, which is accompanied by the formation of a homogenous, actin-rich cortex. Moreover, I showed that the activity of the ERM protein Moesin is upregulated in early mitosis, likely to ensure the reorganisation of the actin cortex in round metaphase cells. I demonstrated that the levels of Moesin at the cortex are controlled by the kinase Slik and by the PP1-87B/Sds22 phosphatase holoenzyme. While depletion of Slik led to lowered levels of p-Moesin around the cell edge in metaphase, overexpression of this kinase and depletion of PP1 protein levels both caused an increase of cortical Moesin signal. At mitotic exit, cells elongate and divide at the middle, giving rise to two new cells. I observed that both actin and Moesin become polarised along the cortex of anaphase cells, such that these proteins clear from the poles and become concentrated along the cell equator. I demonstrated that this transient event is dependent on the activity of PP1-87B and its subunit Sds22 and is independent of Slik function.

In the next two chapters I will address whether Moesin is functionally relevant in the stabilisation of the actin cortex in metaphase, and whether this might be important for spindle function and for accumulation of fate determinants at the membrane. I will also provide insights into the mechanism of Moesin-dependent polar relaxation at anaphase. In particular, I will show the detailed molecular mechanism by which the PP1 phosphatase triggers inactivation of Moesin to allow initiation of cell elongation and help cytokinesis progression.

Chapter 4

Results: Active Moesin is required for stabilisation of the actin cortex and cell shape in metaphase

4.1 Introduction

Mitotic rounding is thought to be universal among animal cells. As detailed in chapters 1 and 3, multiple studies using cultured cells have began to shed light on the mechanisms of mitotic cell rounding. This involves retraction of the cell margin and protrusions (Cramer and Mitchison, 1997, Maddox and Burridge, 2003), changes in cell surface topology (Porter et al., 1973, Sanger et al., 1984, Boucrot and Kirchhausen, 2007), and cytoskeletal rearrangements (Thery and Bornens, 2006, Kunda and Baum, 2009, Matthews et al., 2012). More recent publications have also demonstrated that mitotic rounding is determined by the interplay between tension of the actomyosin cortex and internal hydrostatic pressure (Stewart et al., 2011, Fischer-Friedrich et al., 2014). As mentioned in section 3.1, it is thought that mitotic rounding is important for correct cell geometry in both cultured cells (Kunda et al., 2008, Carreno et al., 2008, Lancaster et al., 2013) and tissue contexts (Norden et al., 2009, Meyer et al., 2011, Kondo and Hayashi, 2013).

In chapter 3 I presented a brief characterisation of the shape changes and rearrangements of the actin cytoskeleton at the onset of mitosis. These are accompanied by an increase in the levels of cortical p-Moesin.

While studies in cultured cells have stressed the requirement of Moesin in cell rounding, cortical rigidity and spindle assembly (Kunda et al., 2008, Carreno et al., 2008), the role of this protein in mitotic epithelial cells is largely unknown. Therefore, the goal here was to carry out a functional analysis of Moesin in the context of mitosis by analysing tissues depleted for Moesin/Slik.

4.2 Moesin and its activating kinase Slik are dispensable for mitotic rounding in SOP cells

To investigate whether Moesin and its regulator Slik are required for cell shape changes at mitotic entry (described in section 3.2.1), I started by depleting these proteins in fly nota expressing a marker to visualise filamentous actin. Cells depleted for Moesin or Slik rounded up as they passed from interphase into prophase, as can be seen in Figure 4.1, despite displaying some protrusion remnants. These results suggest that Moesin activity is likely dispensable for early rounding events *in vivo* at the G2/M transition. However, based on these data, it is unclear whether Moesin/Slik-depletion may cause morphological defects in the basal regions of the mitotic cells. Furthermore, given the fact that RNAi-dependent protein depletion may be incomplete, in the future, it will be important to assess the impact of genetic mutations in the Moesin and Slik chromosomal loci in mitotic cell rounding. Additionally, it will be essential to determine the involvement of other cytoskeletal components, such as myosin-I and myosin-II, in the morphological changes of cells entering mitosis.

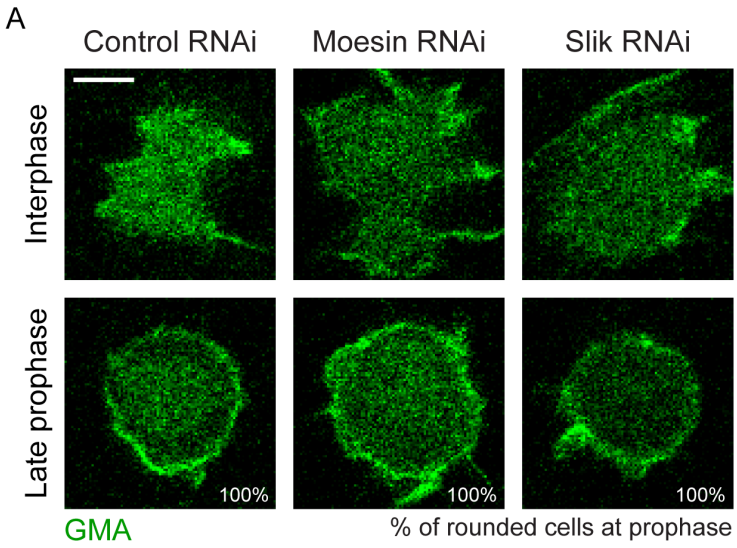

Figure 4.1 – Depletion of Moesin or Slik does not affect mitotic rounding in SOP cells.

A – Three representative SOP cells in control RNAi, Moesin RNAi and Slik RNAi tissues imaged at interphase and late prophase. Percentage of rounded cells at prophase is indicated. GMA labels filamentous actin. Scale bar = 5µm. Genotypes:

w^-; *neur*-GMA/+; *pnr*-GAL4/+;

w^-, UAS-Moesin-IR/Y; *neur*-GMA/+; *pnr*-GAL4/+;

w^-; *neur*-GMA/UAS-Slik-IR; *pnr*-GAL4/+;

Note: flies were grown at 25°C during early development and at 29°C during pupariation.

4.3 Moesin is required for the stabilisation of the actin cortex and cell roundness in prometaphase and metaphase

Although my work showed that cells depleted for Moesin or Slik were able, strikingly so, to retract their protrusions and round up as they entered mitosis, they exhibited a disorganised actin cortex in metaphase (Fig. 4.2). To quantify these defects, I defined a 'heterogeneity' parameter as a measure of the uniformity of actin distribution at the cell boundary (see chapter 2 for more details). This has a value of zero in cells exhibiting an even accumulation of cortical actin. As can be seen in the boxplot chart (Fig. 4.2B), control cells show a drop in cortical heterogeneity as they transit from early prometaphase into metaphase. In contrast, cells devoid of Moesin or Slik are unable to achieve an even distribution of actin around the perimeter as they advance toward the onset of anaphase. These data imply that Moesin is required for the even accumulation of filamentous actin at the membrane in metaphase cells.

I also noticed that control cells assumed a round shape soon after NEB and maintained this morphology during prometaphase and metaphase (Fig. 4.3A,B), whereas cells lacking Moesin or Slik failed to attain a stable, rounded shape as they progressed through mitosis (Fig. 4.3C-F). This result partly corroborates previous findings from our lab (Matthews et al., 2012), which revealed that the RhoGEF Ect2 is exported from the nucleus into the cytoplasm just before NEB, thereby activating RhoA to promote the formation of a round, stiff metaphase cortex. In contrast, cells with lowered amounts of Moesin or Slik exhibited a pattern of shape instability throughout prometaphase, as can be appreciated in the plots of cell roundness over time (Fig 4.3).

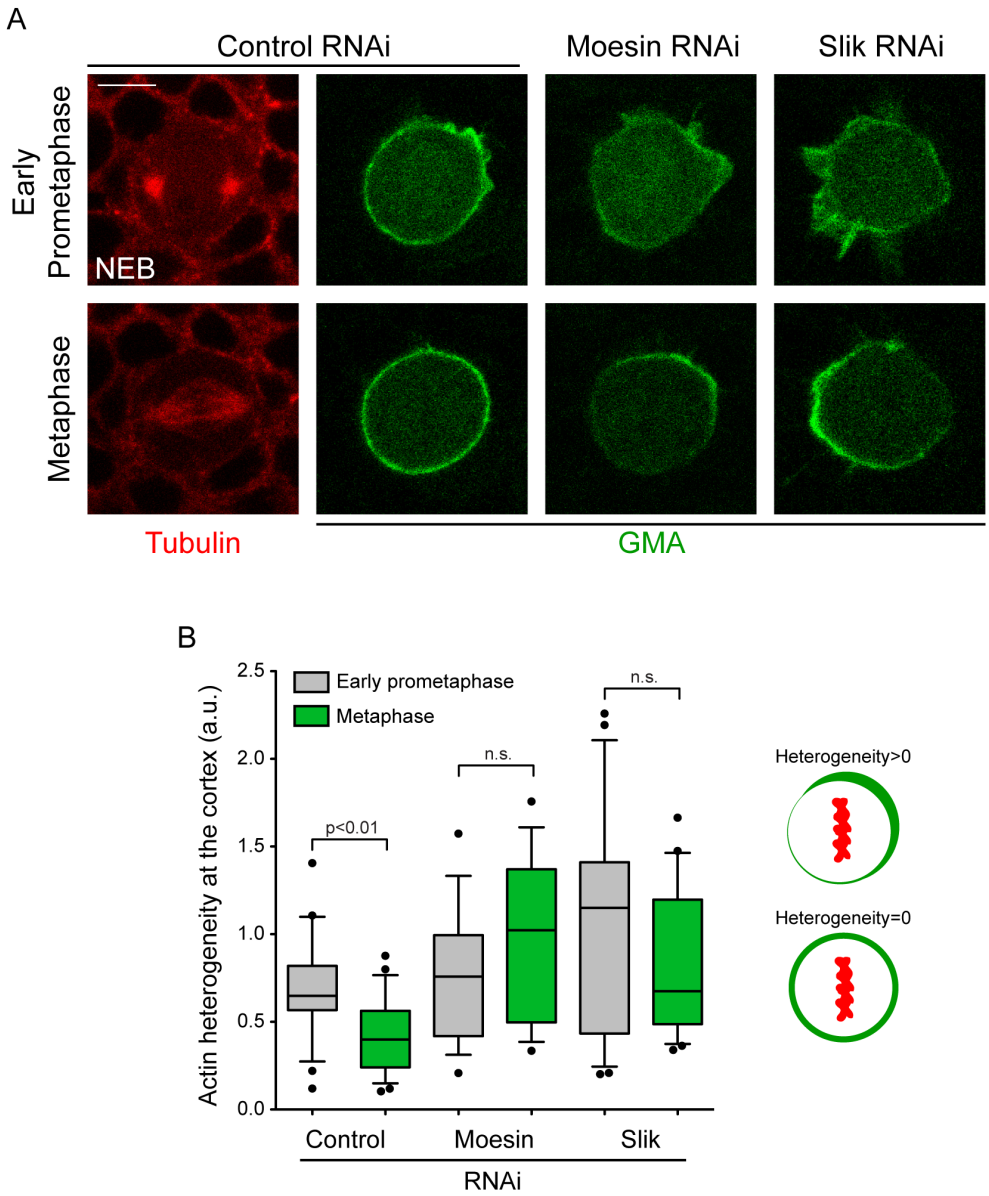
A
Control RNAi
Moesin RNAi
Slik RNAi
Early Prometaphase
Metaphase
NEB
Tubulin
GMA
B
Early prometaphase
Metaphase
Actin heterogeneity at the cortex (a.u.)
2.5
2.0
1.5
1.0
0.5
0.0
p<0.01
n.s.
n.s.
Control
Moesin
Slik
RNAi
Heterogeneity>0
Heterogeneity=0

Figure 4.2

Figure 4.2 – Depletion of Moesin or Slik causes disorganisation of the actin cortex in SOP cells.

A – SOP cells in control RNAi, Moesin RNAi and Slik RNAi tissues imaged at early prometaphase and late metaphase. mCherry-Tubulin transgene was expressed to label spindle microtubules. GMA labels filamentous actin. Scale bar = 5µm. Genotypes:

w^-; *neur*-GMA, UAS-mCherry-αTubulin/+; *pnr*-GAL4/+;

w^-, UAS-Moesin-IR/Y; *neur*-GMA, UAS-mCherry-αTubulin/+; *pnr*-GAL4/+;

w^-; *neur*-GMA, UAS-mCherry-αTubulin/UAS-Slik-IR; *pnr*-GAL4/+;

Note: flies were grown at 25°C during early development and at 29°C during pupariation.

B – Quantification of heterogeneity of the actin cortex at early prometaphase and metaphase in SOP cells in the genetic backgrounds indicated in **A**. Mean±SD (a.u.) – Control RNAi (23 cells): 0.68±0.30 (early prometaphase), 0.42±0.21 (metaphase); Moesin RNAi (15 cells): 0.75±0.35 (early prometaphase), 0.99±0.46 (metaphase); Slik RNAi (21 cells): 1.08±0.61 (early prometaphase), 0.86±0.41 (metaphase). ≥ 3 animals analysed in each genetic background.

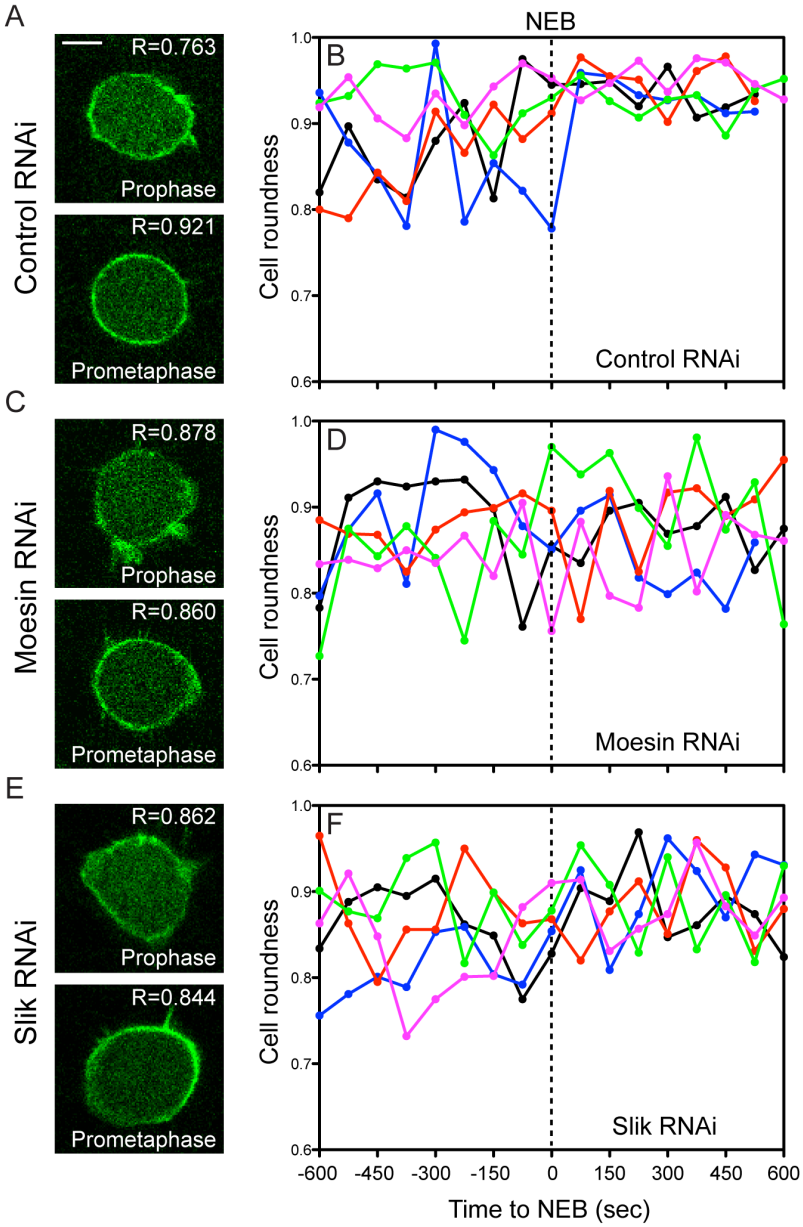

Figure 4.3 – Moesin- or Slik-depletion leads to shape instabilities during mitosis.

A, C, E – SOP cells in control RNAi, Moesin RNAi and Slik RNAi tissues imaged at prophase and prometaphase. Roundness, R, is indicated. GMA labels filamentous actin. Scale bar = 5µm. Genotypes:

w^-; *neur*-GMA/+; *pnr*-GAL4/+;

w^-, UAS-Moesin-IR/Y; *neur*-GMA/+; *pnr*-GAL4/+;

w^-; *neur*-GMA/UAS-Slik-IR; *pnr*-GAL4/+;

Note: flies were grown at 25°C during early development and at 29°C during pupariation.

B, D, F – Plots of cell roundness monitored before and after NEB. Plots show five representative SOP cells in each of the genetic backgrounds seen in **A**, **C** and **E** imaged at a 75-second resolution. 2 animals per condition were analysed.

4.4 Depletion of Moesin or Slik levels leads to oscillations of cortical actin during metaphase

To learn more about the cortical defects caused by Moesin/Slik depletion, I performed time-lapse confocal imaging of mitotic SOP cells at high temporal resolution. In doing so, I would gain insight into the mechanism driving the stabilisation of the metaphase actin cortex. Figure 4.4 shows a panel of four representative cells in control, Moesin RNAi and Slik RNAi backgrounds progressing through the last few minutes of metaphase (0sec marks the metaphase-to-anaphase transition, monitored by Tubulin labelling). While control cells displayed a fairly even accumulation of cortical actin throughout metaphase, cells depleted for Moesin or Slik exhibited a dynamic pattern of actin patches that seem to oscillate between different cortical positions. To investigate the nature of these oscillations further, I created kymographs to illustrate cortex dynamics over time (see chapter 2 for details). Figure 4.5 shows the kymographs for each of the cells depicted in Figure 4.4. As expected, Cell 1 exhibited a stable actin cortex, where actin was evenly distributed at the boundary. This is representative of over 90% of the cells analysed (Fig. 4.5C). The large majority of Moesin- or Slik-depleted cells show a pulsatile pattern of actin oscillations (Moesin RNAi: 73%; Slik RNAi: 82%). These cells displayed pulses of accumulation/dismantling of cortical actin (clearly visualised in the kymograph of Cell 3), where actin patches appeared to 'bounce' between cortical sites that are diametrically opposed to each other. In rarer instances, I observed a rotating pattern of cortical actin (as that seen in Cell 4). In this case, a small crescent of actin revolved around the cell in a continuous and steady manner. These oscillatory phenomena have not been reported in previous studies on the role of Moesin in cell shape changes.

A lot remains to be understood regarding the cortical behaviour observed in cells with impaired Moesin function. On the one hand, the oscillations of actin documented above could simply be explained by an overall defect in Moesin-dependent actin-membrane anchorage. On the other hand, it is possible that such wave-like behaviour relies on the same mechanisms that drive events of protrusion-retraction in the lamellipodium of migratory cells. I speculate about these ideas in more detail in Chapter 6.

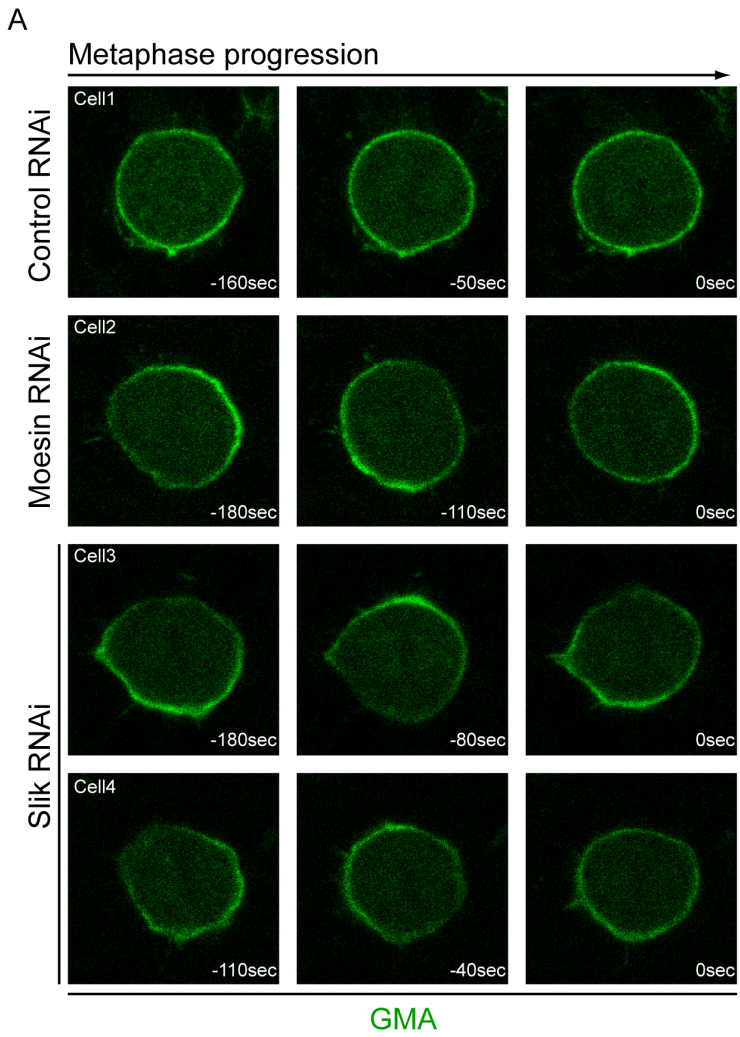

Figure 4.4 – Moesin- and Slik-depleted cells exhibit cortical instabilities during metaphase.

A – SOP cells in control RNAi, Moesin RNAi and Slik RNAi tissues imaged during metaphase. Time before anaphase onset is indicated. GMA labels filamentous actin. Scale bar = 5µm. Genotypes:

w^-; *neur*-GMA/+; *pnr*-GAL4/+;

w^-, UAS-Moesin-IR/Y; *neur*-GMA/+; *pnr*-GAL4/+;

w^-; *neur*-GMA/UAS-Slik-IR; *pnr*-GAL4/+;

Note: flies were grown at 25°C during early development and at 29°C during pupariation.

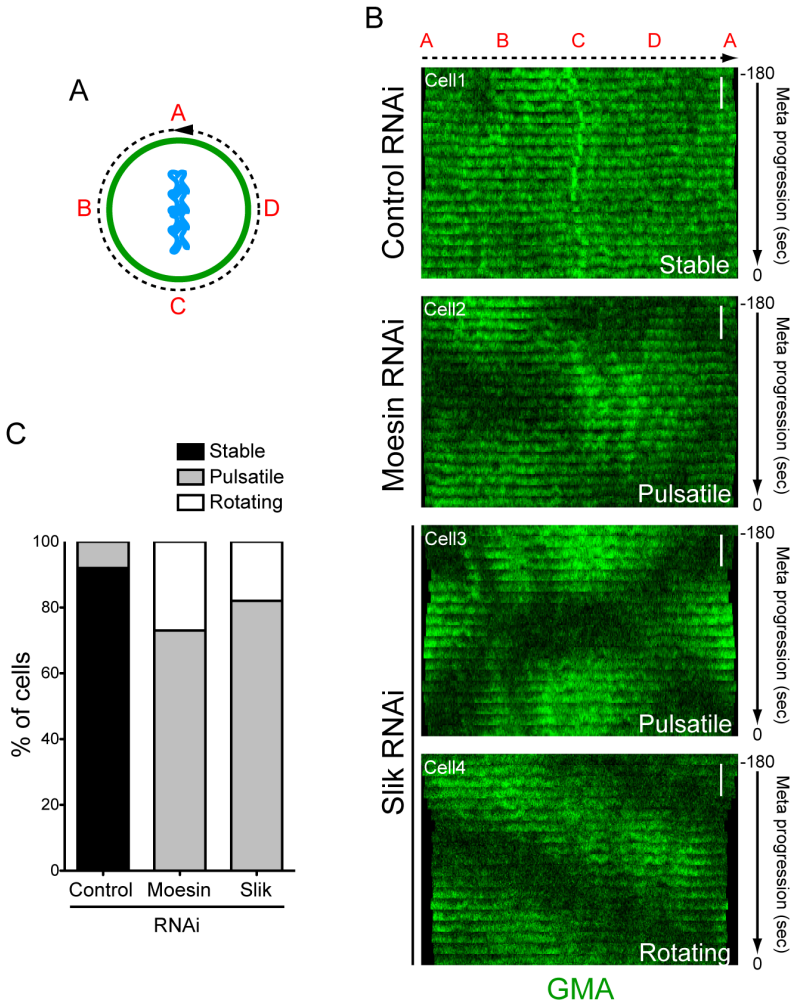
A
A
B
D
C
B
A
B
C
D
A
Cell1
-180
Meta progression (sec)
0
Control RNAi
Stable
Cell2
Moesin RNAi
Pulsatile
Cell3
Slik RNAi
Pulsatile
Cell4
Rotating
GMA
C
Stable
Pulsatile
Rotating
% of cells
100
80
60
40
20
0
Control
Moesin
Slik
RNAi

Figure 4.5

Figure 4.5 – Depletion of Moesin or Slik causes oscillations of the actin cortex during metaphase progression.

A – Scheme depicting a cross-section of a cell with the actin cortex in green and the chromosomes in blue.

B – Kymographs of 4 representative SOP cells (same as seen in Fig. 4.4) of the cortical perimeter imaged during late metaphase. Points A-D (in red), as seen in **A**. Phenotype of cortical stability is indicated. GMA labels filamentous actin. Time before anaphase onset is indicated. Scale bar = 30sec. Genotypes:

w^-; *neur*-GMA/+; *pnr*-GAL4/+;

w^-, UAS-Moesin-IR/Y; *neur*-GMA/+; *pnr*-GAL4/+;

w^-; *neur*-GMA/UAS-Slik-IR; *pnr*-GAL4/+;

Note: flies were grown at 25°C during early development and at 29°C during pupariation.

C – Quantification of cells showing stable, pulsatile or rotating behaviour of the actin cortex in all genetic backgrounds shown in **B**. Total of cells scored: control RNAi, 40 cells; Moesin RNAi, 15 cells; Slik RNAi, 22 cells. ≥ 5 animals analysed in each genetic background.

4.5 Depletion of Diaphanous abolishes the cortical instabilities in cells with impaired Moesin activity

It is thought that actin waves and accompanying membrane movements observed in motile cells depend on activation and inhibition feedbacks in actin dynamics (Asano et al., 2009, Carlsson, 2010, Ryan et al., 2012b, Allard and Mogilner, 2013). Experimental and theoretical findings suggest that initiation and propagation of these actin waves are regulated by the activity of nucleation-promoting factors, like the Arp2/3 complex (Asano et al., 2009, Bretschneider et al., 2009, Carlsson, 2010, Ryan et al., 2012a). Interestingly, a recent study in mammalian cells has demonstrated that Arp2/3 and the formin mDia are the two major nucleators of F-actin at the cortex (Bovellan et al., 2014). However, ongoing work in our lab (Rosa et al., in revision) indicates that Arp2/3-dependent actin polymerisation is not required for the formation of an actin cortex in epithelial and SOP cells, such that depletion of the Arp3 subunit in such cells did not compromise the homogeneous enrichment of F-actin around the cell boundary at metaphase. Instead, Rosa and colleagues have demonstrated that Diaphanous is the major orchestrator of actin polymerisation at the mitotic cortex.

Given Rosa's findings, I investigated whether a decrease in Diaphanous levels in cells depleted for Moesin or Slik would be sufficient to attenuate or abolish the actin oscillations seen in Figures 4.4 and 4.5. Remarkably, I observed that the large majority of cells depleted for both Diaphanous and Moesin were completely devoid of a rich actin cortex, and therefore, did not shown any detectable pattern of actin fluctuations (Fig. 4.6).

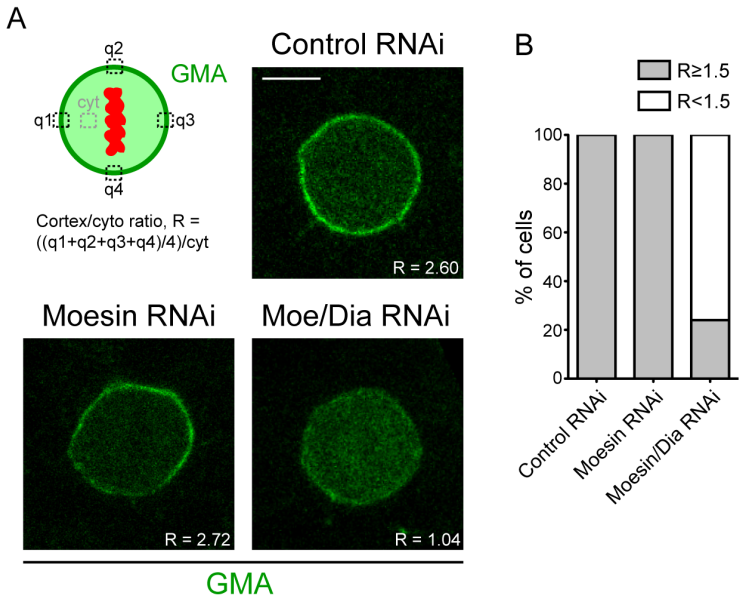

Figure 4.6 – Reduced levels of Diaphanous abolish the cortical instabilities in Moesin-depleted cells.

A – Stills of SOP cells in control RNAi, Moesin RNAi and Moesin/Diaphanous RNAi tissues taken at metaphase. GMA labels filamentous actin. Ratio cortex/cytoplasm of GMA signal, R, is indicated. Scale bar = 5µm. Genotypes:

w$^-$; *neur*-GMA/+; *pnr*-GAL4/+;

w$^-$, UAS-Moesin-IR/Y; *neur*-GMA/+; *pnr*-GAL4/+;

w$^-$; *neur*-GMA/UAS-Diaphanous-IR; *pnr*-GAL4/+;

Note: flies were grown at 25°C during early development and at 29°C during pupariation except in the case of Diaphanous RNAi (early development – 18°C; pupariation – 25°C).

B – Quantification of cells with R ≥ 1.5 or R< 1.5 in all genetic backgrounds seen in **A**. Total of cells scored: control RNAi, 16 cells; Moesin RNAi, 18 cells; Moesin/Diaphanous RNAi, 17 cells. ≥ 3 animals analysed in each genetic background.

4.6 The stability of the metaphase cortex depends on the coordinated activities of Moesin and Myosin-II

To investigate the dynamics of both actin and myosin-II in mitotic SOP cells, I imaged nota co-expressing GMA and Cherry-tagged myosin-II (known as *spaghetti squash* in flies) at high resolution. Both cytoskeletal components exhibited a uniform distribution around the edge of round metaphase cells (Fig 4.7A). At a coarse-grained level, this homogenous accumulation of actin and myosin-II at the cortex appeared to be stable over time (see kymographs in Fig. 4.7A2). Upon depletion of Slik, however, I observed a heterogeneous accumulation of myosin-II at the cortex (see arrowheads in Fig 4.7B1). When looking at the kymographs, it was clear that the patterns of actin and myosin-II pulses were not synchronised. As depicted by the inset (Fig. 4.7B2), the accumulation of myosin-II at the cell edge was only detectable 36 ± 7sec after the accumulation of actin. These findings appear to be consistent with the model for bleb retraction and cortical reassembly previously proposed (Charras et al., 2006), in which newly polymerised actin recruits myosin-II, which in turn constricts the actin meshwork. Furthermore, the burst of actin and myosin accumulation occurred at sites where the membrane appeared deformed, likely due to internal hydrostatic pressure (Charras et al., 2006, Stewart et al., 2011, Clark et al., 2013).

Theoretical studies have stated that myosin-II-generated contractility can help wave propagation (Wolgemuth, 2005, Shlomovitz and Gov, 2007). To perturb the activity of myosin-II in my system, I used RNAi to deplete Rok levels. This led to a significant drop in the p-myosin-II signal at the metaphase cortex (Fig. 4.8A, B), without affecting the levels of p-Moesin (Fig. 4.8C, D). This contradicts work in mammalian cells, which demonstrated that Rok kinase can phosphorylate the ERM at the conserved C-terminal threonine residue (Matsui et al., 1998, Jeon et al., 2002). Then, I co-depleted Moesin and Rok in fly tissues. Strikingly, upon knockdown of both proteins, I could no longer observe significant disorganisation of the actin cortex in mitotic cells (Fig. 4.9), nor did I see the spatio-temporal pattern of oscillations featured in Moesin-depleted cells. Taken together, these novel data imply that in the absence of functional Moesin, myosin-II-generated contractility drives cortical instability.

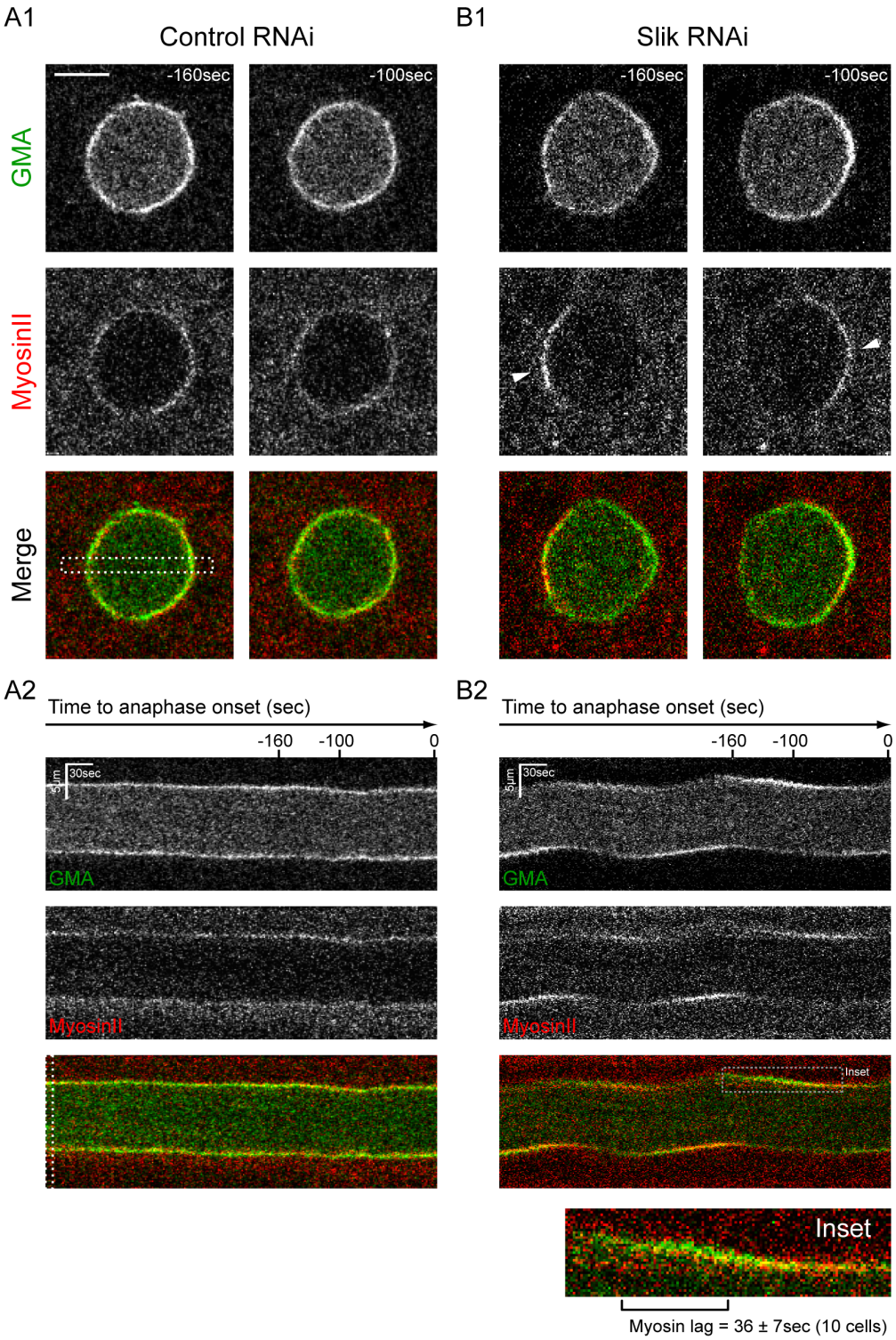
A1
Control RNAi
B1
Slik RNAi
-160sec
-100sec
GMA
MyosinII
Merge
A2
B2
Time to anaphase onset (sec)
-160
-100
0
5μm
30sec
GMA
MyosinII
Inset
Myosin lag = 36 ± 7sec (10 cells)

Figure 4.7

Figure 4.7 – Myosin-II drives cortical instability in the absence of active Moesin.

A1, B1 – Stills of SOP cells in control RNAi (A1) and Slik RNAi (B1) at two different time-points of metaphase. GMA labels filamentous actin. Sqh-mCherry labels myosin-II. White arrowheads point to heterogeneous accumulation of myosin-II. Scale bar = 5µm.

A2, B2 – Kymographs of the diametrical cross-section of the cells shown in **A1** and **B1** imaged throughout metaphase (see dashed box in **A1**). Imaging performed at 5sec resolution. Inset of the dashed box seen in **B2** is shown at the bottom of the figure. Genotypes:

w^-; *neur*-GMA/+; *pnr*-GAL4, *sqh*-Sqh-mCherry/+;

w^-; *neur*-GMA/UAS-Slik-IR; *pnr*-GAL4, *sqh*-Sqh-mCherry/+;

Note: flies were grown at 25°C during early development and at 29°C during pupariation.

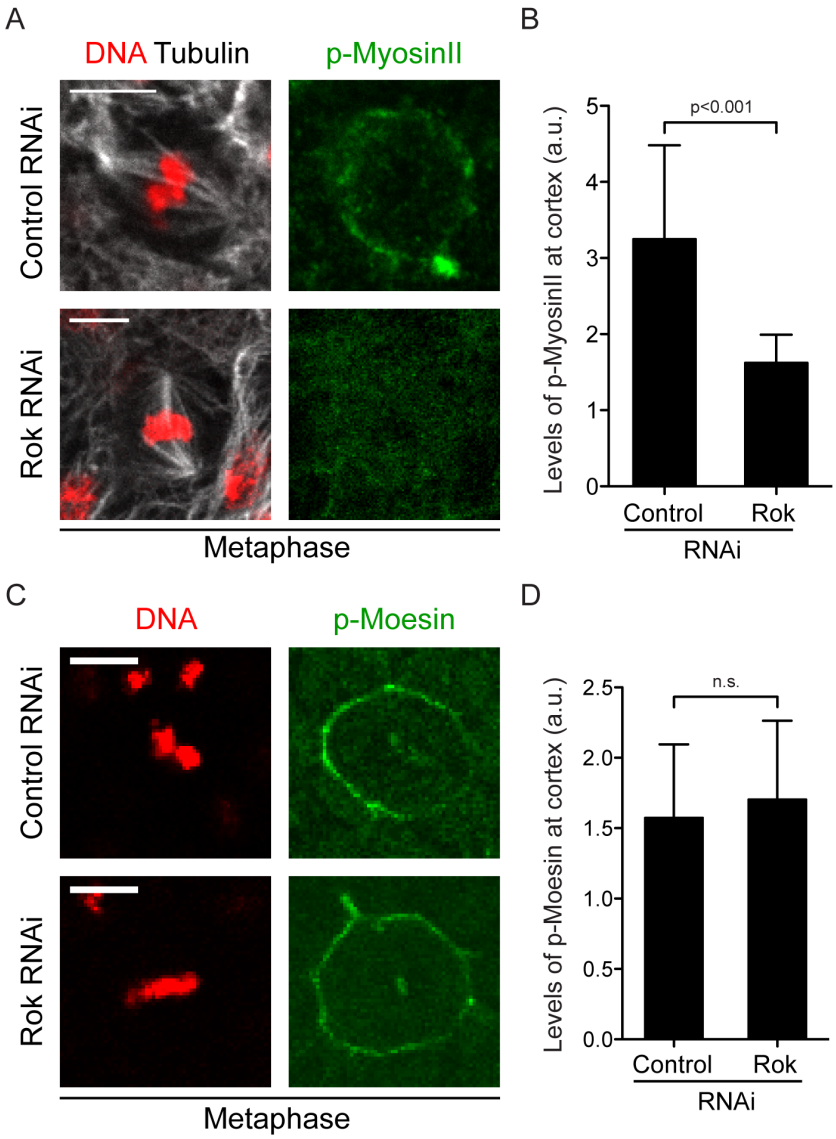

Figure 4.8 – Depletion of Rok leads to reduced p-Myosin-II levels and unaltered p-Moesin levels at the metaphase cortex.

A – Two representative cells in control and Rok RNAi tissues. Tissues were fixed and stained for DNA, Tubulin and p-myosin-II. Scale bar = 5µm.

B – Quantification of the levels of p-myosin-II at the cortex of control and Rok RNAi cells. Values are the normalised levels cortex/nuclear region.

C – Two representative cells in control and Rok RNAi tissues. Tissues were fixed and stained for DNA and p-Moesin. Scale bar = 5µm.

D – Quantification of the levels of p-Moesin at the cortex of control and Rok RNAi cells. Values are the normalised levels cortex/nuclear region. Genotypes:

w^{-};; *pnr*-GAL4/+;

w^{-}; UAS-Rok-IR/+; *pnr*-GAL4/+;

Note: flies were grown at 18°C during early development and at 25°C during pupariation.

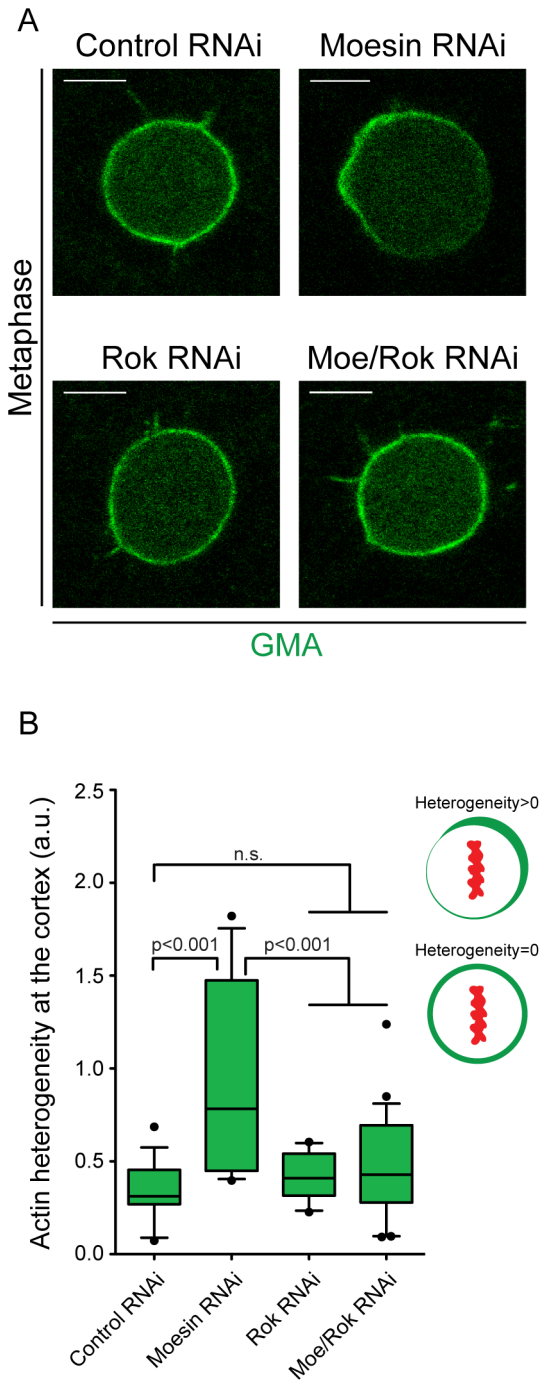
A
Control RNAi
Moesin RNAi
Rok RNAi
Moe/Rok RNAi
Metaphase
GMA
B
Actin heterogeneity at the cortex (a.u.)
2.5
2.0
1.5
1.0
0.5
0.0
n.s.
p<0.001
p<0.001
Heterogeneity>0
Heterogeneity=0
Control RNAi
Moesin RNAi
Rok RNAi
Moe/Rok RNAi

Figure 4.9

Figure 4.9 – Reduced levels of Rok alleviate the cortical instability observed in Moesin-depleted SOP cells.

A – Representative SOP cells in control RNAi, Moesin RNAi, Rok RNAi and Moesin/Rok RNAi imaged at metaphase. GMA labels filamentous actin. Scale bar = 5µm. Genotypes:

w^-; *neur*-GMA/+; *pnr*-GAL4/+;

w^-; *neur*-GMA/+; *pnr*-GAL4, UAS-Moesin-hairpin/+;

w^-; *neur*-GMA/UAS-Rok-IR; *pnr*-GAL4/+;

w^-; *neur*-GMA/UAS-Rok-IR; *pnr*-GAL4, UAS-Moesin-hairpin/+;

Note: flies were grown at 18°C during early development and at 25°C during pupariation.

B – Quantification of heterogeneity of the actin cortex at metaphase in SOP cells in the genetic backgrounds indicated in **A**.

4.7 Mitotic spindle function is unaltered in the presence of cortical instabilities in SOP cells

The crosstalk between spindle microtubules and the cell cortex has been extensively studied. This communication is known to control spindle function in processes like meiosis (Bezanilla and Wadsworth, 2009), furrow positioning (Glotzer, 2005, Kotak and Gonczy, 2013), and asymmetric and oriented cell division (Knoblich, 2010, Morin and Bellaiche, 2011). Multiple publications have emphasised the interplay between actin networks and the spindle apparatus (Schuh and Ellenberg, 2008, Woolner et al., 2008, Fink et al., 2011, Castanon et al., 2013, Spiro et al., 2014). Because impairment of ERM activity in cultured cells has been shown to cause spindle defects (Carreno et al., 2008, Kunda et al., 2008, Machicoane et al., 2014), I was then propelled to check whether the same is true in tissue cells.

By imaging mitotic SOP cells labelled for actin and Tubulin (as depicted in Fig. 4.2), I could observe small spindle oscillations in the plane of the epithelium (Fig. 4.10). These were not affected by depletion of Moesin or Slik, even though cells in these backgrounds exhibit profound cortical instabilities (documented in sections 4.3-4.6). These data appear to be in contrast with the results obtained from experiments with cultured cells (Carreno et al., 2008, Kunda et al., 2008). On the other hand, unlike cultured cells, Moesin-depleted SOP cells have a rounded geometry, a key requirement for correct spindle assembly (Kunda et al., 2008, Lancaster et al., 2013).

It was also possible that Moesin- and Slik-depleted cells, while showing no spindle instabilities in late metaphase, could present errors in spindle orientation early in mitosis. Therefore, I measured the spindle angle to the A-P axis in cells at prophase, prometaphase and metaphase in control and Moesin/Slik depletion backgrounds. I noticed that in all three conditions the majority of cells are able to correct the orientation of the spindle to ensure its alignment with the A-P axis (Fig. 4.11). It is important to highlight that SOP division is controlled by the PCP pathway, in which Frizzled signalling orchestrates the localisation of polarity molecules and spindle tethering (Gho and Schweisguth, 1998, Segalen et

al., 2010, Olguin et al., 2011). These data suggest that there is limited crosstalk between the actin cortex and the spindle in SOP cells.

Since defects in spindle function can activate the mitotic checkpoint to delay the onset of anaphase, I checked whether the timing of mitosis is affected in SOP cells with impaired Moesin activity. I detected no difference in the duration of NEB-Ana onset between control and Slik-depleted cells (Fig. 4.12). In an additional study, I also measured the timing of mitosis in epithelial cells sitting in Moesin- or Slik-depleted nota. Note that these cells, while being instructed by PCP signalling like SOP cells (Gray et al., 2011, Olguin et al., 2011), do not necessarily divide along the A-P axis and their behaviour is more easily influenced by tissue topology and mechanics (Bosveld et al., 2012). Again these cells showed no defects in mitotic progression (Fig. 4.12). Although preliminary, these findings do not support there being intimate crosstalk between the cortex and spindle.

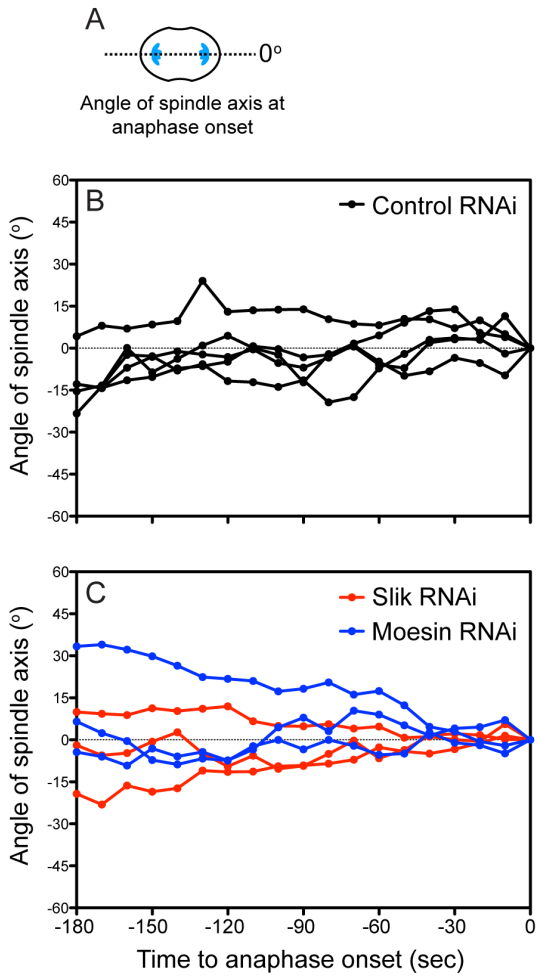

Figure 4.10 – Depletion of Moesin or Slik levels does not affect spindle stability in metaphase SOP cells.

A – Scheme of a dividing SOP cell. Angle of the spindle axis is 0° at the onset of anaphase.

B, C – Plots of spindle axis angle monitored during late metaphase in SOP cells. Control RNAi (**B**): 5 cells, 3 animals; Moesin RNAi (**C**): 3 cells, 2 animals; Slik RNAi (**C**): 3 cells, 2 animals. Time to anaphase onset is indicated. Imaging performed at 10sec resolution. Genotypes:

w$^-$; *neur*-GMA, UAS-mCherry-αTubulin/+; *pnr*-GAL4/+;

w$^-$, UAS-Moesin-IR/Y; *neur*-GMA, UAS-mCherry-αTubulin/+; *pnr*-GAL4/+;

w$^-$; *neur*-GMA, UAS-mCherry-αTubulin/UAS-Slik-IR; *pnr*-GAL4/+;

Note: flies were grown at 25°C during early development and at 29°C during pupariation.

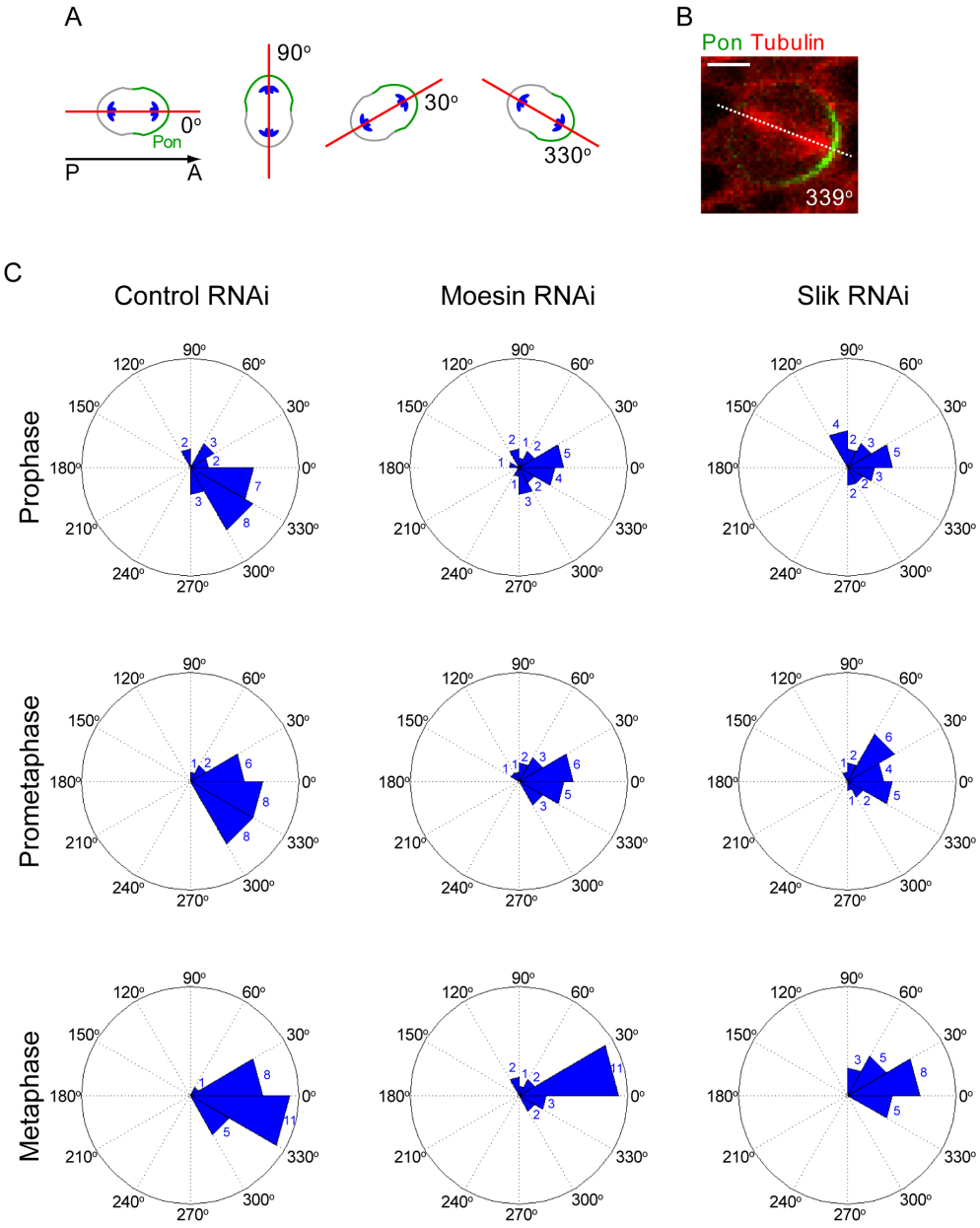
A
90°
0°
Pon
P
A
30°
330°
B
Pon Tubulin
339°
C
Control RNAi
Moesin RNAi
Slik RNAi
Prophase
Prometaphase
Metaphase

Figure 4.11

Figure 4.11 – Depletion of Moesin or Slik levels does not affect the spindle A-P orientation in mitotic SOP cells.

A – Scheme of SOP cells dividing at different angles. A-P axis = 0°. Pon (in green) localises to the anterior cortex in these cells.

B – Metaphase SOP cell expressing Pon and Tubulin markers. Scale bar = 5µm.

C – Rosette plots of spindle axis angle measured in SOP cells at prophase, prometaphase and metaphase in control RNAi, Moesin RNAi and Slik RNAi backgrounds. Control RNAi, 25 cells; Moesin RNAi, 21 cells; Slik RNAi, 21 cells. 3 animals analysed in each genetic background. Genotypes:

w^-; UAS-mCherry-αTubulin/+; *pnr*-GAL4, *phyl*-PON-GFP/+;

w^-, UAS-Moesin-IR/Y; UAS-mCherry-αTubulin/+; *pnr*-GAL4, *phyl*-PON-GFP/+;

w^-; UAS-mCherry-αTubulin/UAS-Slik-IR; *pnr*-GAL4, *phyl*-PON-GFP/+;

Note: flies were grown at 25°C during early development and at 29°C during pupariation.

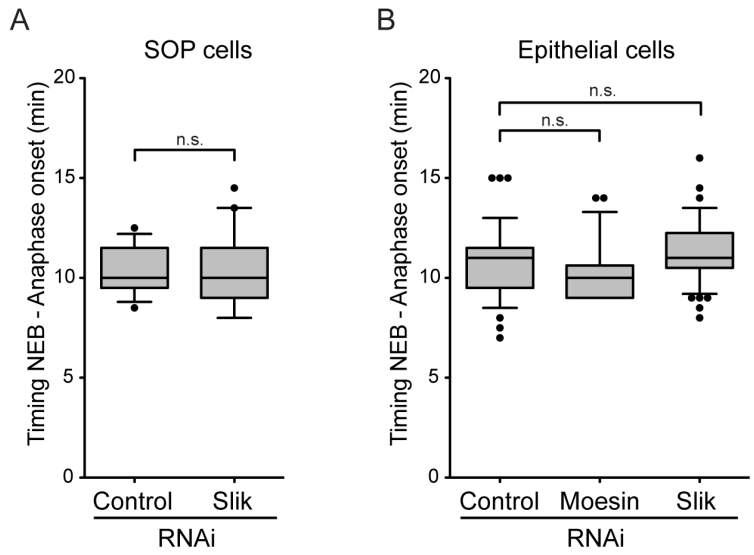

Figure 4.12 – Timing of mitosis is not affected upon Moesin or Slik depletion.

A, B – Timing between NEB and the onset of anaphase in SOP cells (**A**) and in epithelial cells (**B**) in control RNAi, Moesin RNAi and Slik RNAi backgrounds. Mean±SD (sec) – Control RNAi: 10.33±1.18 (**A**, 15 cells) and 10.80±1.76 (**B**, 56 cells); Slik RNAi: 10.42±1.71 (**A**, 19 cells) and 11.25±1.55 (**B**, 53 cells); Moesin RNAi: 10.31±1.45 (**B**, 26 cells). ≥ 3 animals analysed in each genetic background. Genotypes:

w^-; UAS-mCherry-αTubulin/+; *pnr*-GAL4, *phyl*-PON-GFP/+;

w^-, UAS-Moesin-IR/Y; UAS-mCherry-αTubulin/+; *pnr*-GAL4, *phyl*-PON-GFP/+;

w^-; UAS-mCherry-αTubulin/UAS-Slik-IR; *pnr*-GAL4, *phyl*-PON-GFP/+;

Note: flies were grown at 25°C during early development and at 29°C during pupariation.

4.8 Moesin-dependent stabilisation of the cortex is important for efficient localisation of Pon at the plasma membrane

As mentioned in Chapter 1, SOP cells divide asymmetrically, such that fate determinants are unequally segregated into the daughter cells (Knoblich, 2010, Morin and Bellaiche, 2011). To accomplish this, cells have to ensure that these determinants are asymmetrically distributed around the metaphase cortex. It has been shown that the actomyosin cortex is important in the cortical accumulation of fate determinants (Knoblich et al., 1997, Lu et al., 1999). In light of this, I investigated whether Moesin-dependent stabilisation of the cortex is required for the correct localisation of fate determinants in SOP cells.

In conducting my investigations, I imaged tissues expressing GFP-fused Pon in control and Moesin- or Slik-RNAi conditions. Remarkably, depletion of Moesin or Slik led to a significant decrease in the cortical levels of Pon (Fig. 4.13). However, its position at the anterior pole was unaffected. This appears to be in contrast to previous work (Knoblich et al., 1997, Lu et al., 1999, Barros et al., 2003, Erben et al., 2008), in which genetic or pharmacological perturbations of the actin cortex in fly neuroblasts impaired the accumulation of fate determinants into cortical crescents. Nevertheless, my data suggest that instabilities of the actomyosin cortex can perturb the accumulation of Pon at the membrane. Interestingly, depletion of Moesin led to a larger drop in Pon levels at the cortex than depletion of Slik. While further work is needed to verify this, my findings indicate that Moesin function is likely regulated by various upstream inputs. Furthermore, it is unclear how cortical instabilities triggered by loss of Moesin/Slik affect the cortical association of Pon at the cortex. It is tempting to speculate that oscillations of the actin cortex might hinder a mechanism of lateral transport of Pon molecules along the membrane, as has been proposed (Lu et al., 1999, Erben et al., 2008). On the other hand, it is possible that a stable actin cortex may help retain Pon at the cell boundary, thereby averting its dissociation into the cytoplasm (Mayer et al., 2005).

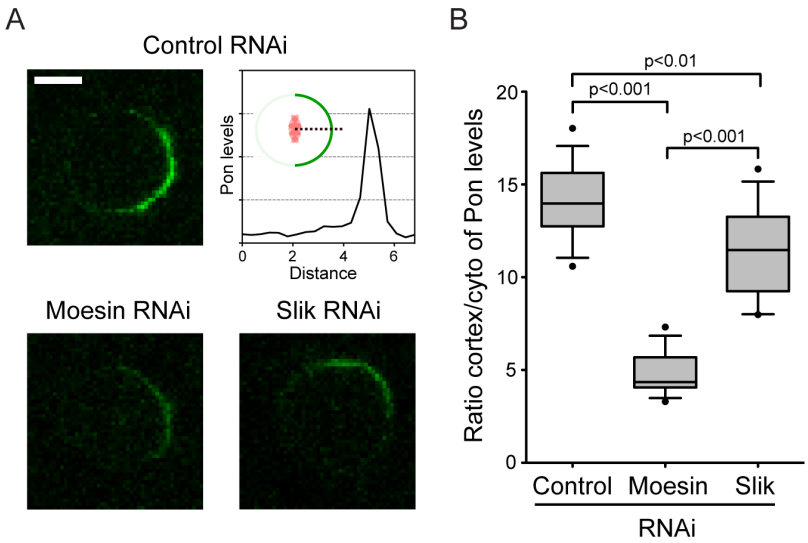

Figure 4.13 – Moesin and Slik are required for efficient accumulation of Pon at the cortex.

A – Representative SOP cells in control RNAi, Moesin RNAi and Slik RNAi backgrounds expressing GFP-tagged Pon. Scale bar = 5µm. Genotypes:

w^-; UAS-mCherry-αTubulin/+; *pnr*-GAL4, *phyl*-PON-GFP/+;

w^-, UAS-Moesin-IR/Y; UAS-mCherry-αTubulin/+; *pnr*-GAL4, *phyl*-PON-GFP/+;

w^-; UAS-mCherry-αTubulin/UAS-Slik-IR; *pnr*-GAL4, *phyl*-PON-GFP/+;

Note: flies were grown at 25°C during early development and at 29°C during pupariation.

B – Ratio cortex/cytoplasm of Pon levels in SOP cells in the genetic backgrounds shown in **A**. Ratio is the normalisation of GFP intensity at cortex against cytoplasm (see scheme in **A**). Mean±SD – Control RNAi: 14.19±2.00, 15 cells; Moesin 4.84±1.15, 15 cells; Slik RNAi: 11.30±2.51, 15 cells. 3 animals analysed in each genetic background.

4.9 Conclusions

One of my research goals was to elucidate the role of Moesin in cell shape transitions and actin reorganisation at mitotic entry. In this chapter I showed that Moesin and its activating kinase are dispensable for mitotic cell rounding. These results are in apparent opposition to previous findings from our team and other labs, who proposed that the fly ERM is required for the rounding of cultured cells entering mitosis (Carreno et al., 2008, Kunda et al., 2008). Furthermore, they showed that Moesin ensures that cells form a rigid, stable cortex underneath the membrane at metaphase. Importantly, I observed that depletion of Moesin or Slik leads to instabilities of the actin cortex in metaphase SOP cells. Interestingly, these instabilities displayed oscillatory features, such that the majority of cells with impaired Moesin activity exhibited a pattern of fluctuating patches of actin that moved from one side of the cell to another over time. I demonstrated that these oscillations depended on myosin-II-generated contractility and on the activity of the actin nucleator Diaphanous. Surprisingly, instabilities of the actomyosin cortex did not affect spindle stability or orientation in SOPs, which indicates that orientation of division is likely orchestrated by external and internal polarity cues that surpass a potential involvement of actin in the process. However, I demonstrated that failure to attain a stable cortex in metaphase led to defective cortical accumulation of Pon, a key fate determinate in SOP cell division.

One of the next challenges will be to dissect the molecular details underlying the cortical oscillations that I observed in cells with impaired Moesin activity. To understand their nature, it would be important to use techniques such as single-molecule speckle microscopy or fluorescence recovery after photobleaching (FRAP). These techniques will help gain insight into parameters of protein diffusion and turnover, and understand the dynamics of actin wave behaviour.

Chapter 5

Results: Kinetochore-localised PP1/Sds22 triggers cortical relaxation to initiate anaphase cell elongation

5.1 Introduction

In the previous chapter I demonstrated that Moesin is required for the stabilisation of the actin cortex and cell shape in mitosis. In this chapter I explore in depth how cells disengage from this molecular and mechanical isotropy to begin elongating in anaphase, before splitting into two.

Decades of work have shed light on the mechanisms that drive cortical polarisation in cells exiting mitosis. To initiate cytokinesis, the equator becomes more contractile than the poles (Bray and White, 1988, DeBiasio et al., 1996, Rappaport, 1996). It is well established that the mitotic spindle directs this pattern of cell polarisation. To do so, the central spindle and a small subset of astral microtubules are thought to induce accumulation and activation of myosin-II at the equatorial cortex, leading to a local increase in contractility (Rappaport, 1996, Green et al., 2012, White and Glotzer, 2012). In addition, work in echinoderms and nematodes suggests that the astral microtubules promote polar relaxation, thereby helping to maintain the site of furrow specification (Werner et al., 2007, Murthy and Wadsworth, 2008, Odell and Foe, 2008, Tse et al., 2011). Given this knowledge, I sought to understand how spatio-temporal changes in Moesin (shown in chapter 3) contribute to the polarisation of the actomyosin cortex as cells transit from metaphase to anaphase. As such, in this chapter I first explore how the inactivation of Moesin and dismantling of the polar cortex are coupled to furrow specification and ingression. This identified a novel mechanism encompassing the spatio-temporal de-phosphorylation of Moesin in polar relaxation at mid-anaphase.

5.2 Actin and Myosin-II exhibit distinct patterns of cortical polarisation in anaphase

In section 3.2.2 I presented a brief description of the changes in actin organisation and cell morphology in SOP cells exiting mitosis. To understand how the cortex becomes polarised to initiate cytokinesis, I studied the spatio-temporal dynamics of both actin and myosin-II at mitotic exit. Figure 5.1 shows a representative SOP cell labelled for actin in green (GMA) and myosin-II in red (Sqh-mCherry). In metaphase, both cortical components appeared to localise uniformly around the cell boundary. At anaphase, as cells elongated along the spindle axis, the cortex became highly polarised. The levels of both actin and myosin-II dropped significantly at the cell poles and increase at the equator, where the cleavage furrow ingresses. These data are in agreement with the current knowledge of furrow constriction at cytokinesis, since both actin and myosin-II are required in this process (Chen et al., 2008, Yumura et al., 2008, Vale et al., 2009, Pollard, 2010). At telophase however, actin re-accumulates evenly throughout the cortex of the nascent daughter cells (evident in the confocal stills and the kymographs – Fig. 5.1). Strikingly, at this stage, myosin-II appeared to be completely absent at the cells poles and strongly localised at the furrow. This distinct pattern of localisation of actin and myosin-II indicates that the dynamics of these proteins must be, at least in part, uncoupled at the end of mitosis. While my observations require further validation, they appear to contrast with those of Sedzinski and colleagues (Sedzinski et al., 2011), who showed evidence for myosin-II-dependent contractility at the cell poles in cytokinesis.

To look in more detail into the spatio-temporal differences in the repolarisation of actin and myosin-II during anaphase, I performed an analysis similar to that described in section 4.4. Figure 5.2 depicts an SOP cell leaving mitosis expressing actin and myosin probes. As can be appreciated in the 'Merge' panel, the pattern of cortical actin does not precisely match that of myosin-II during anaphase (see white arrowheads). This is even clearer when looking at the kymographs of the cell perimeter over time. At ~60 seconds after the onset on anaphase, myosin-II cleared from the pole and rapidly concentrates at the equator, while the cortical redistribution of actin appeared to be more gradual. I quantified

this by measuring the length of myosin-II and actin 'tails' along the perimeter of multiple cells at mid-anaphase (Fig. 5.2B). These data suggest that the redistribution of actin along the anaphase cortex cannot depend on myosin-powered contractility alone. While there is evidence for interdependence in myosin-II and actin accumulation at the equator (Murthy and Wadsworth, 2005, Zhou and Wang, 2008, Reichl et al., 2008), my data is in agreement with many reports that have shown that myosin-II can be recruited to the equator independently of its actin-binding capacity (Dean et al., 2005, Piekny and Glotzer, 2008, Uehara et al., 2010, Takaine et al., 2014). In addition, it has been shown that actin can concentrate at the cleavage site via microtubules independently of myosin-II activity (Chen et al., 2008, Tseng et al., 2012).

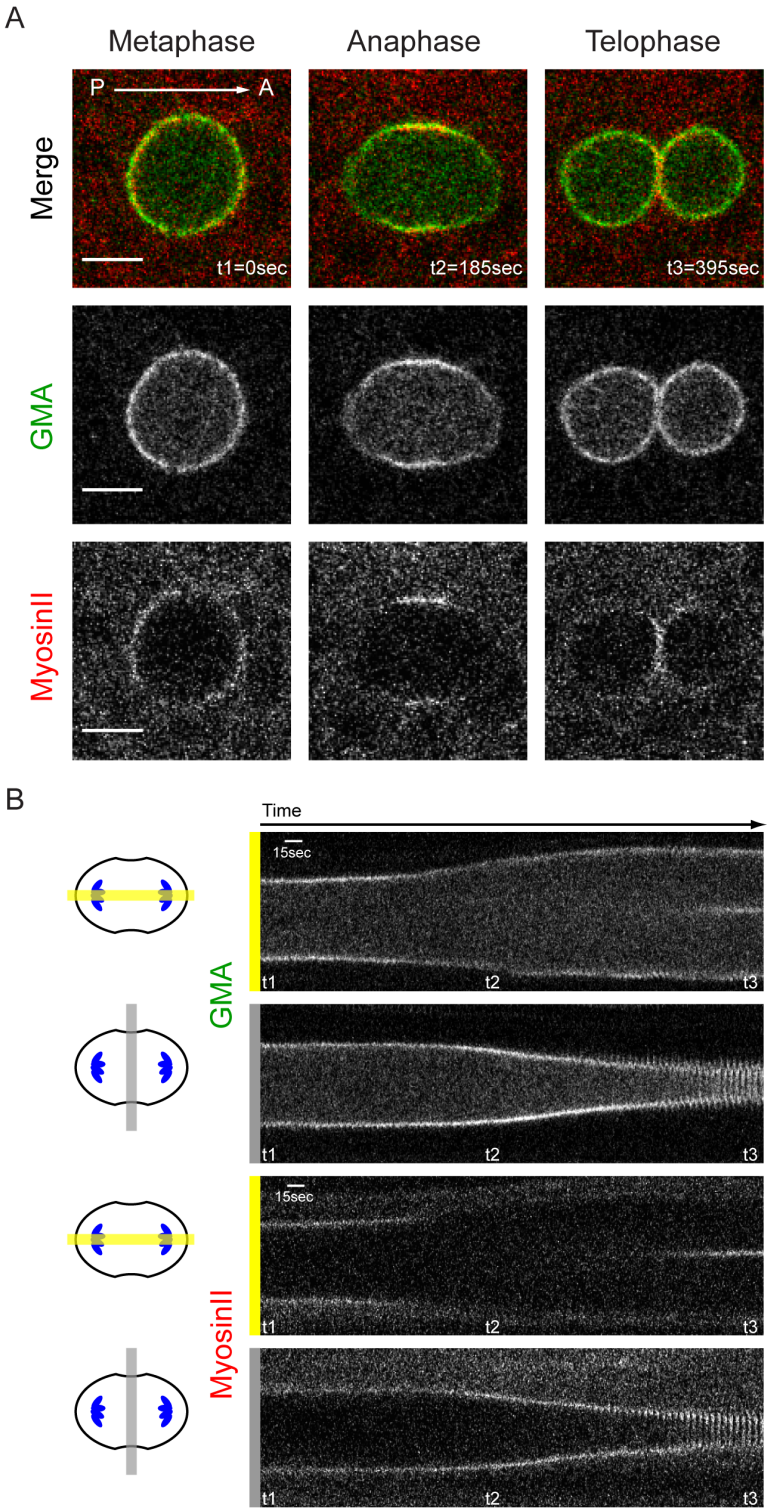
A
Metaphase
Anaphase
Telophase
Merge
P
A
t1=0sec
t2=185sec
t3=395sec
GMA
MyosinII
B
Time
15sec
GMA
t1
t2
t3
15sec
MyosinII

Figure 5.1

Figure 5.1 – Actin and Myosin-II cortical dynamics during mitotic exit.

A – Stills of an SOP cell expressing markers for filamentous actin (GMA) and myosin-II (Sqh-Cherry) imaged during mitotic exit. A-P is indicated. Scale bar = 5μm.

B – Kymographs of the polar (yellow) and equatorial (grey) cross-sections of the cell shown in **A** over time. Anaphase onset = 0sec. Genotype:

w^{-}; *neur*-GMA/+; *pnr*-GAL4, *sqh*-Sqh-mCherry/+;

Note: flies were grown at 25°C through early development and pupariation.

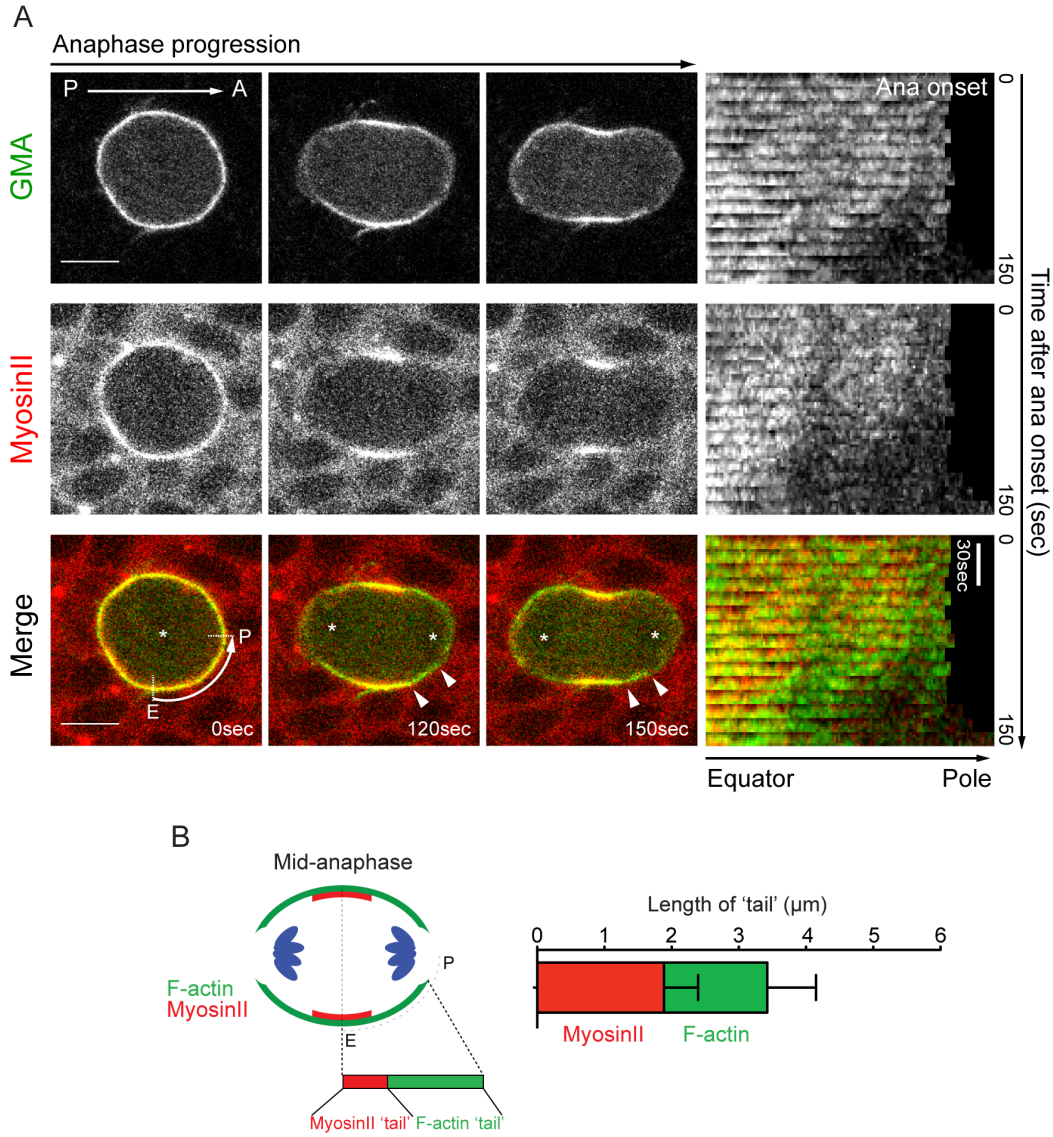

Figure 5.2 – Actin and MyosinII show different redistribution patterns at the cortex during anaphase.

A – Time-lapse imaging of an SOP cell fluorescently labelled for myosin-II and actin filaments. Arrowheads point to the actin 'tail' lagging behind myosin. A-P axis is indicated. Asterisks mark the chromosomes. Anaphase onset = 0sec. Scale bar = 5µm (right). Kymographs of cortical perimeter (see E-P domain on the left). Genotype: w^{-}; *neur*-GMA/+; *pnr*-GAL4, *sqh*-Sqh-mCherry/+;

Note: flies were grown at 25°C through early development and pupariation.

B – Quantification of the 'tail' length of cortical myosin-II and actin at mid-anaphase. Mean±SD (µm) – myosin-II tail: 1.88±0.51; F-actin tail: 1.54±0.72. 12 cells, ≥ 3 animals analysed.

5.3 Polar relaxation is independent of furrow ingression

5.3.1 Actin clearance from the poles is independent of equatorial furrowing

In section 5.2 I showed that the actomyosin cortex becomes highly polarised as cells initiate furrow ingression. One of the key drivers of cleavage furrowing is the centralspindlin complex. This is composed of MKLP1 and RhoGAP1 and localises to antiparallel microtubules of the central spindle (Mishima et al., 2002, D'Avino et al., 2006, White and Glotzer, 2012). It promotes furrow specification and ingression (Zavortink et al., 2005, Zhao and Fang, 2005), inhibition of Rac1 activity (Canman et al., 2008, Bastos et al., 2012) and accumulation and activation of RhoA at the equatorial cortex (Nishimura and Yonemura, 2006, Loria et al., 2012). To determine whether polar relaxation and furrow ingression are mechanistically uncoupled, it was important to perturb the function of centralspindlin in anaphase SOP cells.

I began my analyses by depleting RacGAP1 in flies. Strikingly, the notum of these flies showed severe morphogenetic defects in early pupariation, likely due to faulty cell division. To overcome this, I used a temperature-sensitive Gal80 transgene to control RacGAP1 dsRNA levels (Matsumoto et al., 1978, McGuire et al., 2003) (see Chapter 2 for more details). As expected based on previous results (Loria et al., 2012), the majority of the SOP cells analysed in this genetic background showed a dramatic delay in furrow initiation and completion (Fig. 5.3 and 5.4A). A smaller proportion of cells failed cytokinesis completely. Remarkably, while the levels of equatorial actin in RacGAP1-depleted cells were lower than in control cells (as indicated by the ratio pole/equator shown in Figure 5.4C), those cells showed efficient clearance of actin from the poles at mid-anaphase (see arrowheads in Fig. 5.3 and 5.4B). In line with this, in human cells in culture, where RNAi can be used to induce a complete loss of function of RacGAP1, Sergey Lekomtsev observed polar relaxation without furrow ingression. Taken together, these findings suggest that polar relaxation can occur independently of furrow ingression. This has not been previously documented.

5.3.2 Anaphase cell elongation is driven by polar relaxation and furrow ingression

Next I investigated the extent to which furrow formation and polar relaxation contribute to cell elongation during anaphase. I observed that cells elongated by ~40% from their metaphase width before they began furrowing at the equator (Fig. 5.3 and 5.4D). During furrow invagination, cells elongated an extra ~20% along their division axis. RacGAP1-depleted cells, which showed defects in furrow ingression, were able to elongate to the same extent as control cells in the early stages of cytokinesis, but did elongate during furrow ingression (Fig. 5.3 and 5.4D). These data support there being a furrow-independent component in the process of cell elongation. This was confirmed by measuring elongation in RacGAP1-depleted cells that cytokinesis completely. These cells elongated by ~30% as they passed from metaphase into anaphase (Fig. 5.4D).

While it is known how constriction of the contractile ring alters the surface topology of the cell equator (Green et al., 2012, Salbreux et al., 2012), its contribution to axial elongation has rarely been considered. However, my data suggest that anaphase cell elongation is largely driven by polar relaxation, independently of furrow constriction. These data are largely in agreement with a model proposed previously (Hickson et al., 2006), which pinpoints distinct regulatory mechanisms contributing to cell elongation during mitotic exit. Hickson and colleagues suggested that polar relaxation and broad accumulation of actomyosin at the furrow account for most of cell elongation. This is followed by focal constriction of the equator, which also contributes to axial elongation.

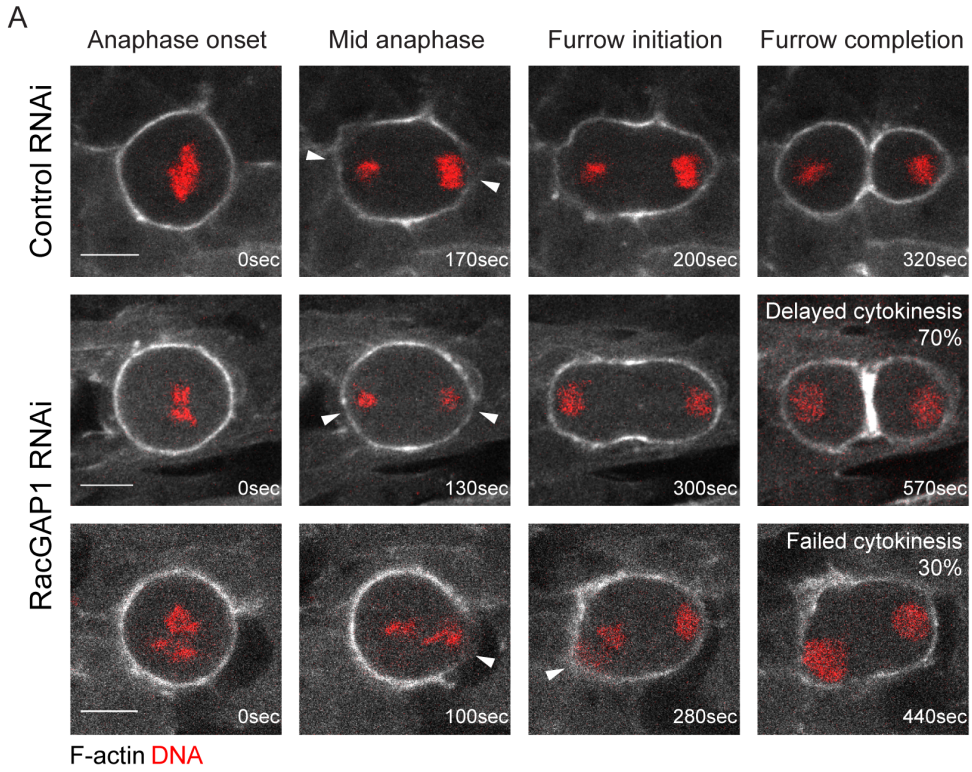

Figure 5.3 – Depletion of RacGAP1 in SOP cells does not affect polar relaxation.

A – Time-lapse imaging of SOP cells in control and RacGAP1-depleted backgrounds. White arrowheads indicate actin clearance at the poles. Lifeact-GFP labels filamentous actin. *neur*-RFP labels the chromosomes. Anaphase onset = 0sec. Scale bar = 5µm. Genotypes (also for Figure 5.4):

w^{-}; *neur*-RFP/+; *pnr*-GAL4, UAS-Lifeact-GFP/+;

w^{-}; *neur*-RFP/tubP-GAL80^{ts}; *pnr*-GAL4, UAS-Lifeact-GFP/UAS-Tumbleweed-hairpin;

Note: flies were grown at 18°C during early development and at 29°C during pupariation except in the case of Tumbleweed/RacGAP1 RNAi (pupariation – 25°C).

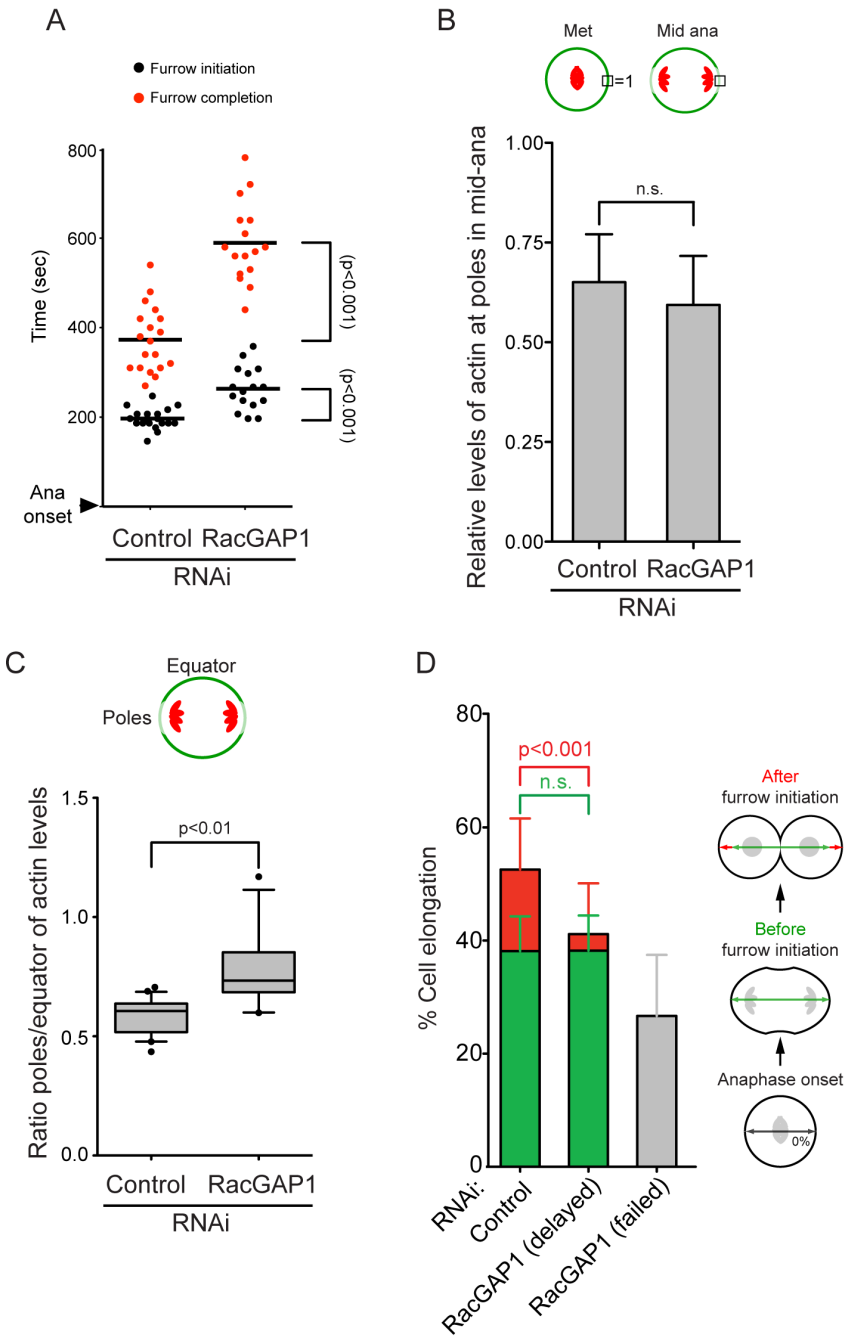

Figure 5.4 – Depletion of RacGAP1 in SOP cells does not affect actin clearance from the poles or cell elongation at anaphase.

A – Plotting of time period between anaphase onset and furrow initiation or furrow completion. Control RNAi: 19 cells; RacGAP1 RNAi: 16 cells. Black lines, median.

B – Relative levels of polar actin in SOP cells. Control RNAi: 12 cells; RacGAP1 RNAi: 12 cells.

C – Ratio poles/equator of cortical actin in anaphase cells. Mean±SD – Control RNAi: 0.58±0.07, 20 cells; RacGAP1 RNAi: 0.78±0.17, 13 cells.

D – Cell length measured in SOP cells before and after furrow initiation. Control RNAi: 19 cells; RacGAP1 RNAi: 16 cells. ≥ 4 animals analysed in each genetic background.

5.4 The centrosomes and astral microtubules are dispensable for polar relaxation

5.4.1 The centrosomes are in close proximity to the cell cortex during anaphase

Work in various model organisms has suggested that the astral microtubules prevent furrowing in non-equatorial regions, by inhibiting Rho accumulation and myosin-II activation (Werner et al., 2007, Murthy and Wadsworth, 2008, Odell and Foe, 2008, Tse et al., 2011). Moreover, some studies have suggested that centrosomes have a direct role in the polarisation of the cell cortex (O'Connell et al., 2000, Cowan and Hyman, 2004, Munro et al., 2004, von Dassow et al., 2009). These considerations propelled me to investigate whether the centrosomes and astral microtubules are required for polarisation of Moesin and Actin at anaphase in fly epithelia.

First, I decided to explore the spatio-temporal dynamics of the spindle poles in relation to the cell cortex during anaphase. This helped me understand whether clearance of polar actin correlates with the distance of the centrosome to the cortex. I imaged SOP cells in flies expressing RFP-tagged Cnn, which labels the centrosomes (Li and Kaufman, 1996), together with chromatin and F-actin markers, and followed cells as they transited from metaphase to anaphase, filmed every 10 seconds. As can been seen in Figure 5.5, each centrosome sits very close to the cortex at the onset of anaphase, showing that the spindle spans across the entire cell. As cells begin elongating, the posterior centrosome maintains a small distance to the cortex (0.54 ± 0.23μm, at mid anaphase), whereas the anterior pole appears to be completely apposed to the cortex (Fig. 5.5A, B). These results are identical to previous findings (Roegiers et al., 2001). Interestingly, actin is cleared from both anterior and posterior poles (see arrowheads in Fig. 5.5A). Therefore, despite the slight bias of the spindle toward the anterior pole, there does not appear to be a close correlation between distance of centrosome-cortex and polar relaxation at mid-anaphase.

5.4.2 The centrosomes and astral microtubules are not required for the cortical polarisation of Moesin and actin in anaphase

To assess the functional relevance of the centrosomes and astral microtubules in polar relaxation and actin clearance at anaphase, I used flies homozygous for a severe loss-of-function allele of the gene Asterless, called Asl^{mecD} (Blachon et al., 2008). As shown in various reports, these mutants show impaired centriole duplication, and therefore lack functional centrosomes (Bonaccorsi et al., 1998, Varmark et al., 2007, Blachon et al., 2008). I confirmed this by fixing dissected pupal nota and staining them for Cnn to assess the presence of centrosomal organelles. As shown in Figure 5.6, Asl^{mecD} cells lack discrete centrosomes, indicated by the absence of Cnn signal in the spindle poles. Importantly, Asl^{mecD} cells are still able to form functional spindles through alternative mechanisms and accomplish cell division (Basto et al., 2006, Meunier and Vernos, 2012). However, the morphology of the spindle in Asl^{mecD} cells is aberrant, such that the kinetochore-fibres irradiated from the DNA toward the cortex in a parallel array (see white arrowheads in Fig. 5.6), as previously reported (Goshima et al., 2005, Moutinho-Pereira et al., 2009). Furthermore, I observed that the orientation of division in Asl^{mecD} SOP cells was randomised (Fig. 5.7) (Gho and Schweisguth, 1998, Fichelson and Gho, 2003).

Next I imaged SOP cells expressing actin and Cnn markers in both control and Asl^{mecD} mutant tissues. At mid-anaphase, the drop in actin levels at the anterior pole was identical in control and Asterless mutant cells (Fig. 5.8A, B). The same was true for the other pole (relative levels of actin in control: 0.65 ± 0.12, 12 cells; Asl^{mecD}: 0.63 ± 0.10, 16 cells; $p<0.001$).

Given that in my model actin clearance from the poles is caused by the local inactivation of Moesin, I fixed nota obtained from both control and Asl^{mecD} homozygous flies and stained them for p-Moesin. Loss of polar p-Moesin appeared identical in control and Asl^{mecD} cells (Fig. 5.8C). Additionally, work from our lab showed that human cells in culture with disrupted astral microtubules display no defects in cortical clearance of p-ERM (performed by Sergey Lekomtsev). Together, these findings show that the centrosomes and astral microtubules do not act as an important trigger for Moesin inactivation and actin clearance from the poles in anaphase.

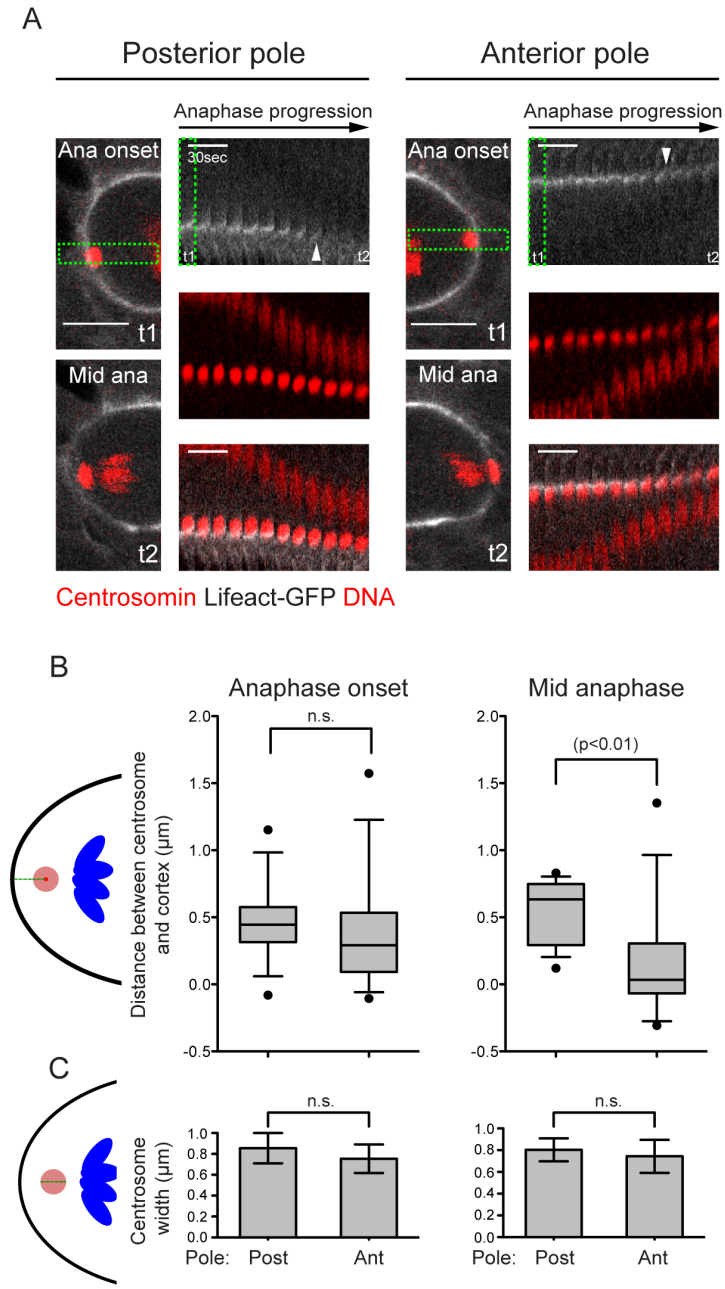

Figure 5.5 – The centrosomes are in close apposition to the cortex of SOP cells during mitotic exit.

A – Representative SOP cell imaged during mitotic exit. Arrowheads point to actin clearance. Lifeact-GFP labels filamentous actin. *neur*-RFP labels the chromosomes. RFP-Cnn labels the centrosomes. Scale bar (on the stills) = 5µm. Genotype:

w^{-}; *neur*-RFP/*ubi*-RFP-Cnn; *pnr*-GAL4, UAS-Lifeact-GFP/+;

Note: flies were grown at 25°C during early development and at 29°C during pupariation.

B, C – Quantification of the distance between centrosome and cortex (**B**) and centrosome width (**C**) at both cell poles at the anaphase onset and in mid-anaphase. 14 cells, ≥ 3 animals analysed.

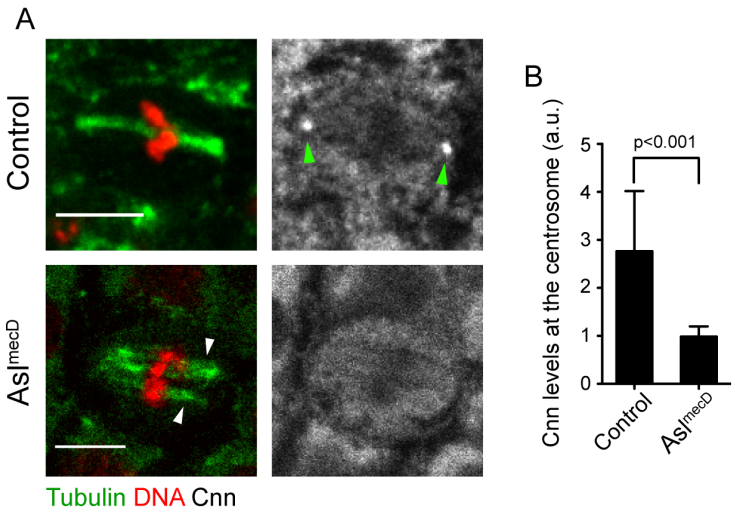

Figure 5.6 – Asterless mutant cells lack functional centrosomes.

A – Epithelial cells immunostained for centrosomin, Tubulin and DNA. Green arrowheads indicate the presence of centrosomes in control cells. White arrowheads point to the parallel arrangement of spindle microtubules. Scale bar = 5µm. Genotypes:

w^-; *neur*-GMA/*ubi*-RFP-Cnn;;

w^-; *neur*-GMA/*ubi*-RFP-Cnn; Asl^{mecD}/Asl^{mecD};

Note: flies were grown at 25°C through early development and pupariation.

B – Quantification of the relative levels of centrosomin on the centrosome. Control: 25 cells (50 centrosomes); Asl^{mecD}: 26 cells (52 'centrosomes'); ≥ 3 animals analysed in each genetic background.

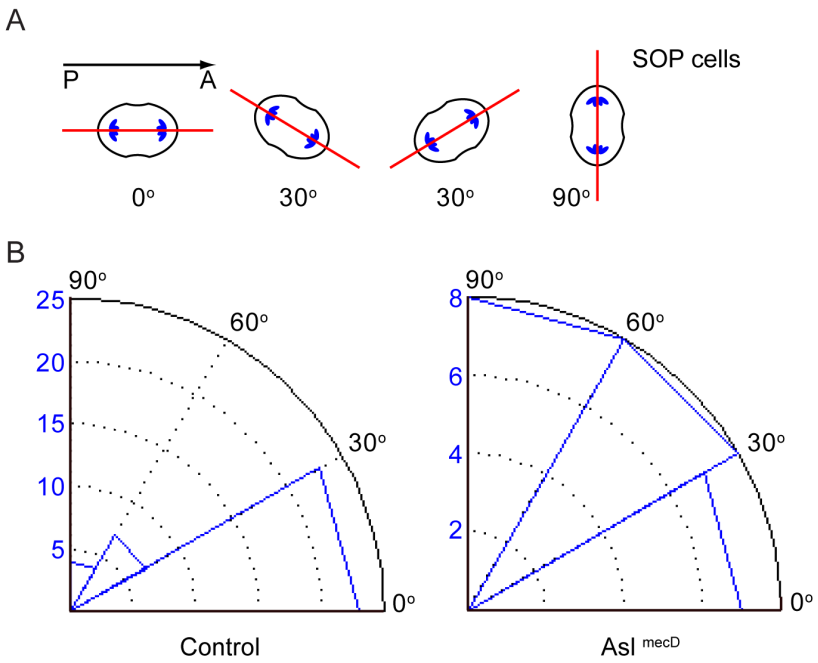

Figure 5.7 – The orientation of division in Asterless mutant SOP cells is randomised.

A – Scheme of SOP cells dividing in different orientations. A-P axis = 0°.

B – Rosette plots of spindle axis angle measured at the onset of anaphase. Control: 34 cells; Asl^{mecD}: 23 cells; ≥ 3 animals analysed in each genetic background. Genotypes (same for Figure 5.8):

w^{-}; *neur*-GMA/*ubi*-RFP-Cnn;;

w^{-}; *neur*-GMA/*ubi*-RFP-Cnn; Asl^{mecD}/Asl^{mecD};

Note: flies were grown at 25°C through early development and pupariation.

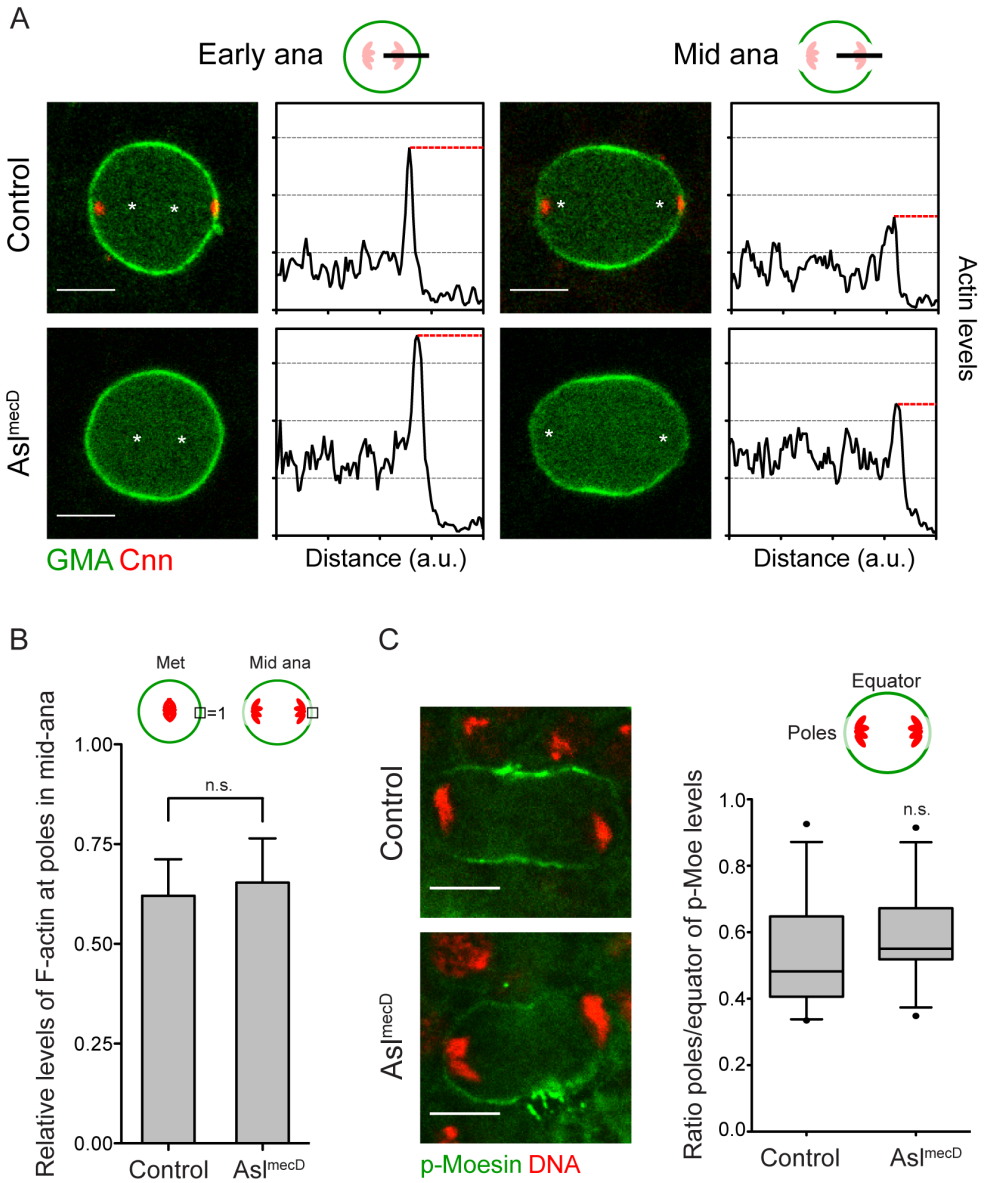

Figure 5.8 – Actin clearance from the poles is independent of centrosomes and astral microtubules.

A – Time-lapse stills of SOP cells taken at early and mid-anaphase in control and Asl^{mecD} mutant backgrounds and plot profiles denoting the actin levels across the cell. GMA labels filamentous actin. RFP-Cnn labels the centrosomes. Asterisks mark the chromosomes. Scale bar = 5µm.

B – Relative levels of polar actin in SOP cells. Control: 12 cells; Asl^{mecD}: 16 cells.

C – Epithelial cells immunostained for p-Moesin and DNA (left). Ratio poles/equator of p-Moesin in anaphase cells (right). Mean±SD – Control: 0.53±0.18, 12 cells; Asl^{mecD}: 0.59±0.14, 11 cells. Scale bar = 5µm. ≥ 3 animals analysed in each genetic background (in **B** and **C**).

5.5 Polar relaxation is sensitive to the proximity of the chromatin mass to the cell cortex

So far I established that polar relaxation occurs independently of furrow ingression and helps the polarisation of the cortex in early cytokinesis. Having excluded the centrosomes and astral microtubules as potential triggers of polar relaxation, I sought to determine whether mitotic chromosomes could elicit this symmetry breaking event. By imaging SOP cells labelled for F-actin and DNA during anaphase progression, I noticed that clearance of polar actin appeared to occur when the segregating chromosomes came into close proximity to the cell boundary (see arrowheads in Fig. 5.9A). To confirm this observation, I assembled kymographs (Fig. 5.9B) to precisely monitor the dynamics of cell elongation (D1), separation of the chromosomes (D2), and the approach of the chromosomes to the cell cortex (D3) (Fig. 5.9C, D). The kymograph of the representative cell shown in Figure 5.9 shows that polar expansion begins when the chromatin mass reaches a small distance to the cell cortex (1.05 ± 0.28μm at the anterior pole). At this point, the amount of polar actin drops significantly (Fig. 5.9D, E). Identical results were obtained for the posterior pole (relative actin levels at pole before elongation: 0.94 ± 0.28; after elongation: 0.68 ± 0.22; $p<0.05$, 12 cells). These data point to a strong spatio-temporal correlation between polarisation of actin, initiation of pole expansion and chromosome movements.

While I observed that polar expansion is concomitant with a drop in local actin levels (Fig. 5.9D, E), I decided to monitor the cortical integrity along the anterior side of the cell before the elongation onset (i.e. early anaphase). This would clarify whether the cortex becomes gradually weakened before the pole begins expanding (Charras et al., 2006, Charras and Paluch, 2008). Figure 5.10A and B depict an SOP cell as it progresses through early anaphase, where t=0sec marks the beginning of pole elongation. After assembling a kymograph of the straightened cell perimeter over time it became evident that the levels of cortical actin drop gradually during early anaphase, particularly at the pole (i.e. regions c4-6, Fig. 5.10C, D). Strikingly, there was a linear relationship between the distance of the chromosome mass and the amount of cortical actin. To obtain this correlation I measured the levels of actin in nine regions of the anterior cortex (c1-

c9) and the distance from those regions to the DNA (d1-d9) (Fig. 5.10C-H). Interestingly, the clearance of actin on the posterior pole (Fig. 5.11A, C) was less pronounced than on the anterior pole during the same time period (Fig. 5.11A-D). This is possibly due to the anterior bias in spindle positioning in SOP cells (Fig. 5.5 and (Roegiers et al., 2001)), such that the anterior portion of DNA appears to be in closer apposition to the cortex than the posterior one (see arrowheads in Fig. 5.11A, B).

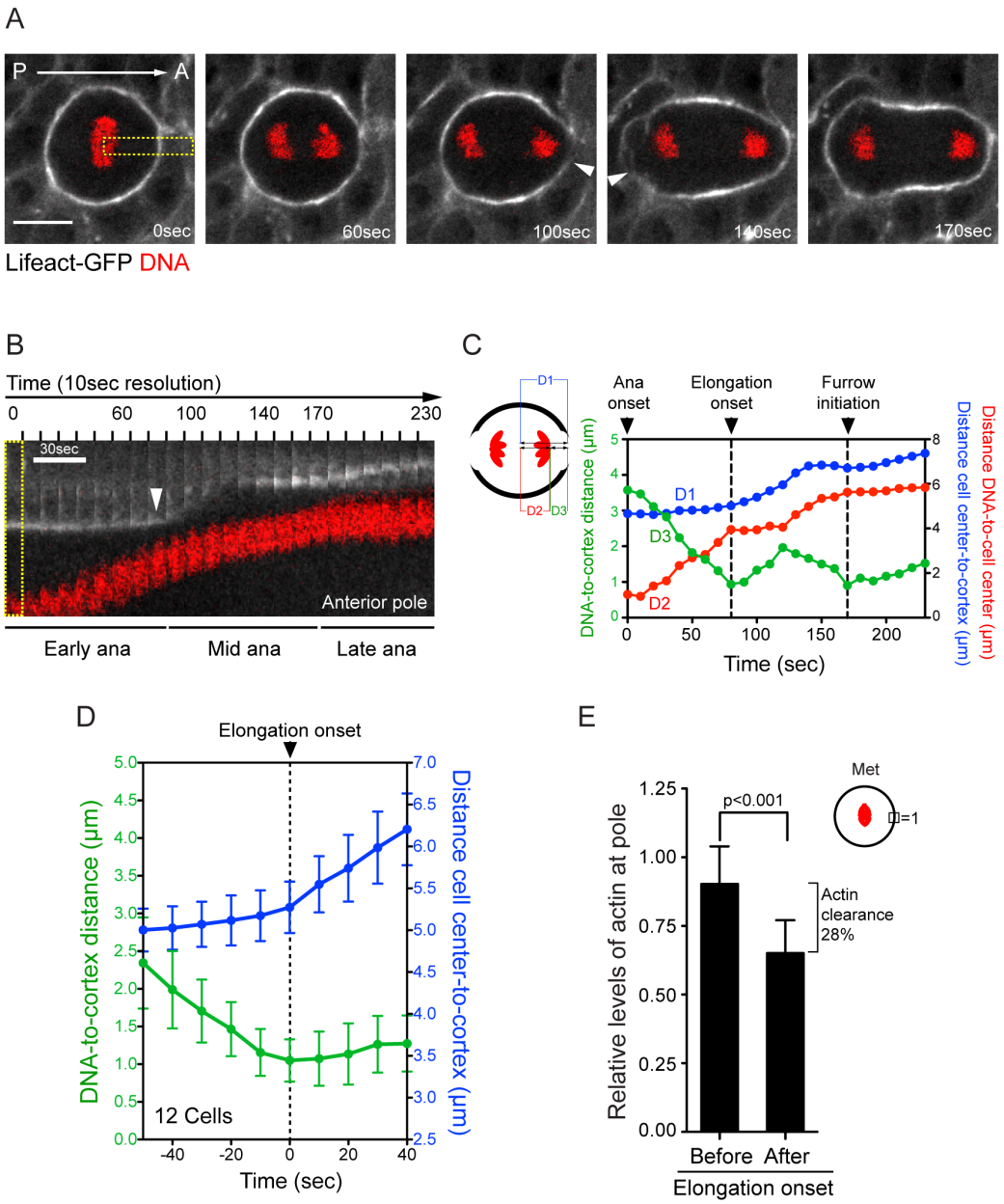

Figure 5.9 – Polar relaxation is triggered by chromatin proximity at mid-anaphase.

A – SOP cell undergoing anaphase. Lifeact-GFP labels filamentous actin. *neur*-RFP labels the chromosomes. Anaphase onset = 0sec. Scale bar = 5µm. Arrowheads indicate polar relaxation. Genotype: w^{-}; *neur*-RFP/+; *pnr*-GAL4, UAS-Lifeact-GFP/+;

Note: flies were grown at 25°C during early development and at 29°C during pupariation.

B – Kymograph of anaphase progression (see dotted box in **A**). Arrowhead indicates elongation onset.

C – Distances D1, D2 and D3 plotted during anaphase (refers to **A** and **B**).

D – D1 and D3 plotted before and after elongation onset (0sec offset).

E – Relative levels of actin at the anterior pole before and after elongation onset. n=12 cells, ≥ 3 animals analysed.

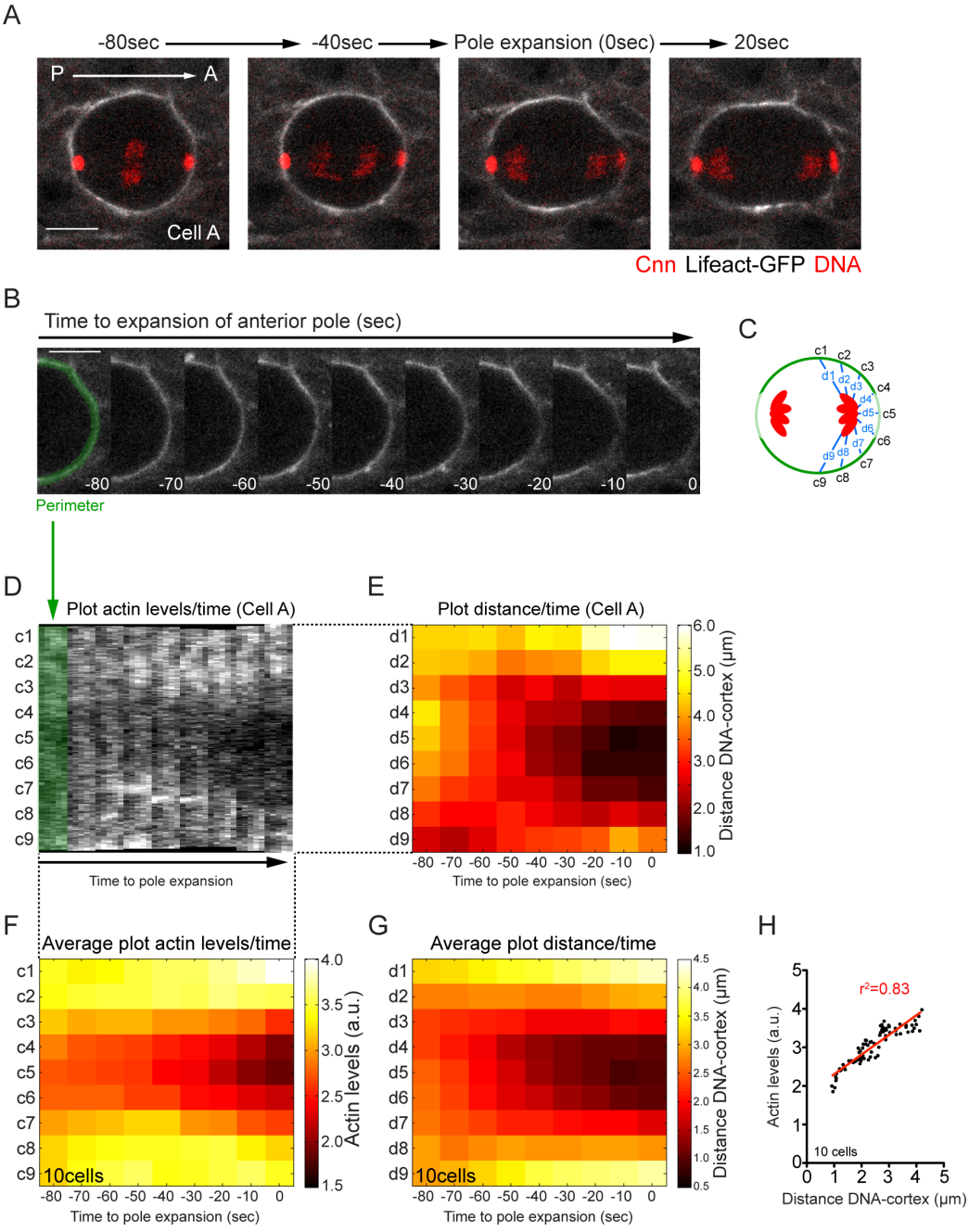
A
-80sec
-40sec
Pole expansion (0sec)
20sec
P
A
Cell A
Cnn Lifeact-GFP DNA
B
Time to expansion of anterior pole (sec)
-80 -70 -60 -50 -40 -30 -20 -10 0
Perimeter
C
c1 c2 c3 c4 c5 c6 c7 c8 c9
d1 d2 d3 d4 d5 d6 d7 d8 d9
D
Plot actin levels/time (Cell A)
Time to pole expansion
E
Plot distance/time (Cell A)
Distance DNA-cortex (µm)
Time to pole expansion (sec)
F
Average plot actin levels/time
Actin levels (a.u.)
10cells
Time to pole expansion (sec)
G
Average plot distance/time
Distance DNA-cortex (µm)
10cells
Time to pole expansion (sec)
H
r²=0.83
Actin levels (a.u.)
10 cells
Distance DNA-cortex (µm)

Figure 5.10

Figure 5.10 – Cortical actin is gradually lost over time as the chromosomes approach the cell poles.

A – SOP cell undergoing anaphase. Lifeact-GFP labels filamentous actin. *neur*-RFP labels the chromosomes. RFP-Cnn labels the centrosomes. Polar expansion initiates at 0sec. Scale bar = 5µm. Genotype:

w^-; *neur*-RFP/*ubi*-RFP-Cnn; *pnr*-GAL4, UAS-Lifeact-GFP/+;

Note: flies were grown at 25°C during early development and at 29°C during pupariation.

B – Montage depicting the anterior pole (of Cell A) monitored during early anaphase.

C – Scheme of cortical regions c1-9 and DNA-to-cortex distances d1-9.

D – Kymograph of the cortical perimeter of Cell A monitored over time (10sec resolution).

E – Plot of DNA-to-cortex distance over time for Cell A.

F – Average plot of cortical actin monitored in 10 cells during early anaphase.

G – Average plot of DNA-to-cortex distance over time (refers to **F**).

H – Correlation of actin levels and DNA-to-cortex distance (refers to **F** and **G**). Red line: linear regression (see chapter 2 for more details).

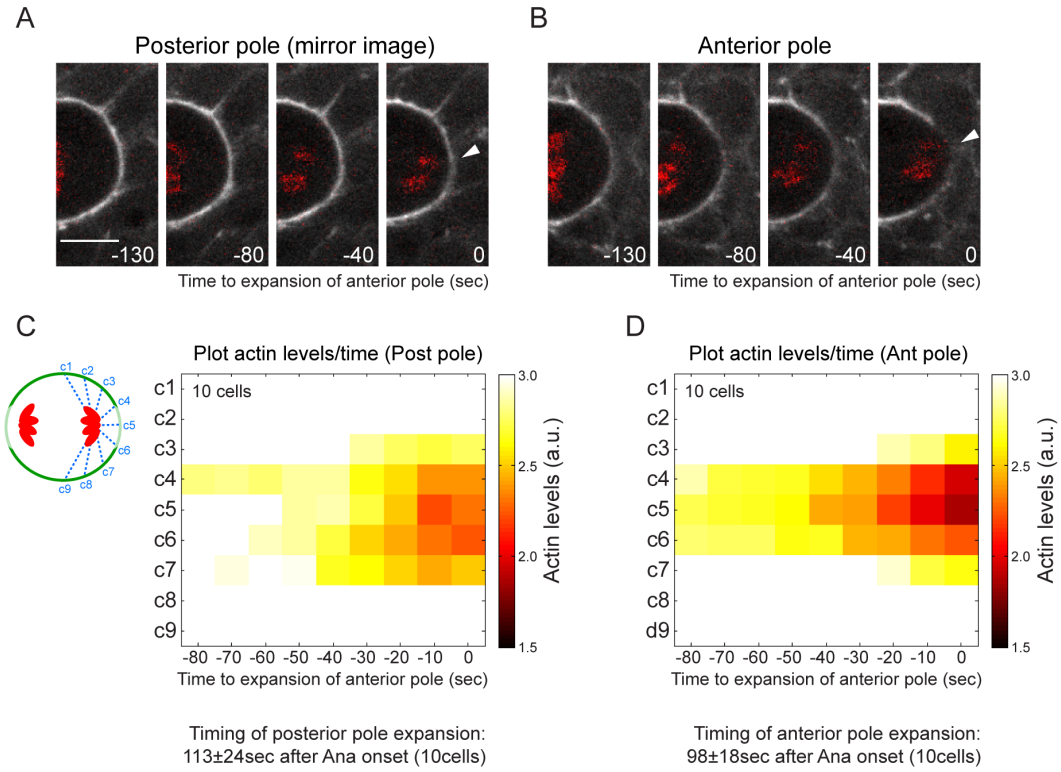

Figure 5.11 – Actin clearance from the anterior pole in SOP cells precedes clearance from the posterior pole.

A – Stills of the posterior pole of a representative SOP cell imaged in early anaphase. Arrowhead points to poor actin clearance. Lifeact-GFP labels filamentous actin (white). *neur*-RFP labels the chromosomes (red). Scale bar = 5µm. Genotype:

w$^-$; *neur*-RFP/+; *pnr*-GAL4, UAS-Lifeact-GFP/+;

Note: flies were grown at 25°C during early development and at 29°C during pupariation.

B – Stills of the anterior pole of the cell shown in **A**. Arrowhead points to strong actin clearance.

C – Average plot of cortical actin over time for the posterior pole.

D – Average plot of cortical actin over time for the anterior pole (same as in Figure **5.10F**. Threshold of actin levels set to 3.0).

5.6 Depletion of PP1-87B and Sds22 leads to aberrant relaxation of the anaphase cell poles

In Chapter 3 I demonstrated that the PP1-87B phosphatase and its regulatory subunit Sds22 dephosphorylate Moesin to trigger its inactivation at mitotic exit. It was therefore important to understand the molecular details of this regulatory mechanism in light of the recent observations that polar relaxation is sensitive to chromatin proximity.

I started my study by depleting PP1-87B or Sds22 in fly nota. Upon PP1-87B/Sds22 knockdown actin failed to clear from the poles as the DNA approached the cortex (Fig. 5.12 and 5.13A, B). Since actin clearance was impaired, the poles failed to expand in a bleb-like manner (Fig. 5.12) even though the chromatin mass was almost apposed to the cortex at this point in anaphase (Fig. 5.12 and 5.13A, C and D). Accordingly, cells depleted for PP1-87B or Sds22 elongated at a lower speed than the control cohort (Fig. 5.14).

In section 5.2 I showed that myosin-II and actin exhibited different patterns of polarisation along the anaphase cortex. These observations pointed that the accumulation of actin at the equatorial cortex cannot be exclusively propelled by myosin-II-generated contractility (Zhou and Wang, 2008). Furthermore, while depletion of RacGAP1 led to faulty polarisation of actin and myosin-II along the cell equator, it did not affect the clearance of actin filaments from the poles at mid-anaphase. This furthered the idea that sources other than the spindle are likely signalling to the cortex, instructing actin rearrangements therein. Knowing that clearance of polar actin in anaphase was impaired upon PP1 depletion, it was now essential to analyse the dynamics of myosin-II in this context. I observed that while the polarisation of actin was severely impaired in cells with lowered amounts of PP1 phosphatase, myosin-II was able to efficiently concentrate at the equatorial furrow (Fig. 5.15). My work points to a previously undocumented model, where PP1/Sds22 and the spindle microtubules are at the core of two distinct pathways driving cortical polarisation in early cytokinesis.

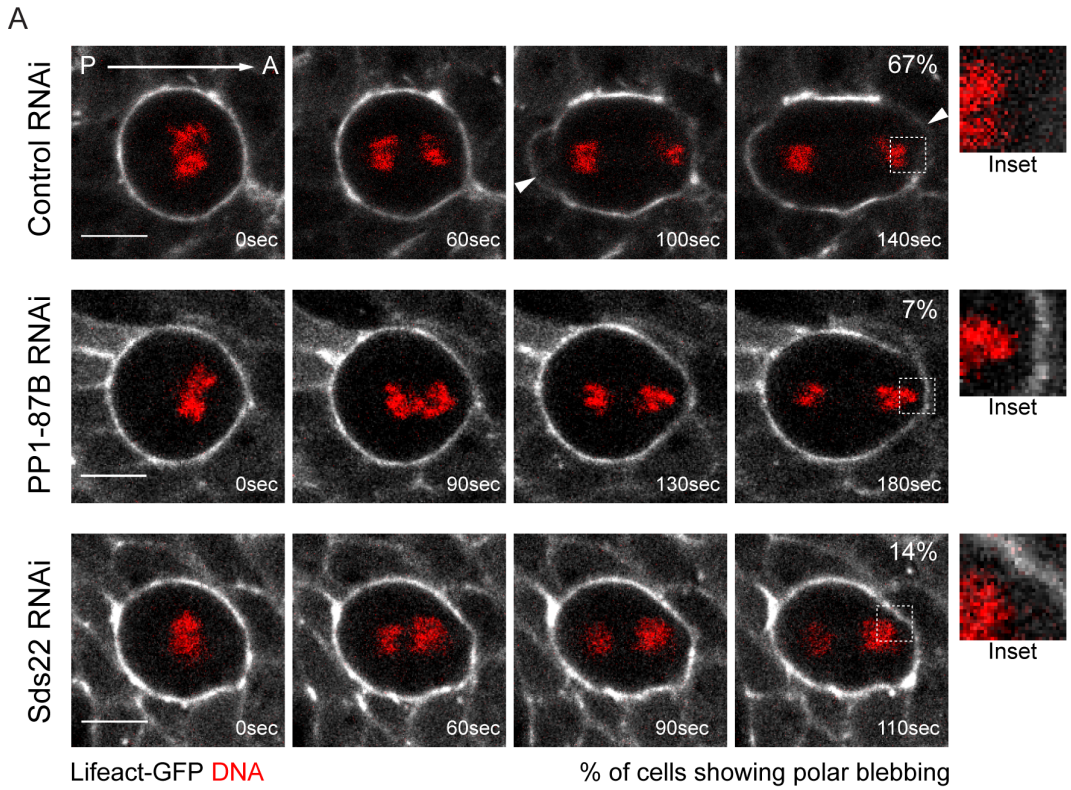

Figure 5.12 – PP1-87B and Sds22 phosphatase subunits are required for polar relaxation at mid-anaphase.

A – Time-lapse imaging of SOP cells in control RNAi, PP1-87B RNAi and Sds22 RNAi backgrounds. White arrowheads indicate actin clearance at the poles. Lifeact-GFP labels filamentous actin. *neur*-RFP labels the chromosomes. Anaphase onset = 0sec. Scale bar = 5µm. Control RNAi, 15 cells; PP1-87B RNAi, 15 cells; Sds22 RNAi, 14 cells. ≥ 3 animals analysed in each genetic background. Genotypes:

w^-; *neur*-RFP/+; *pnr*-GAL4, UAS-Lifeact-GFP/+;

w^-; *neur*-RFP/UAS-PP1-87B-IR; *pnr*-GAL4, UAS-Lifeact-GFP/tubP-GAL80^{ts};

w^-; *neur*-RFP/UAS-Sds22-IR; *pnr*-GAL4, UAS-Lifeact-GFP/+;

Note: flies were grown at 18°C during early development and at 29°C during pupariation.

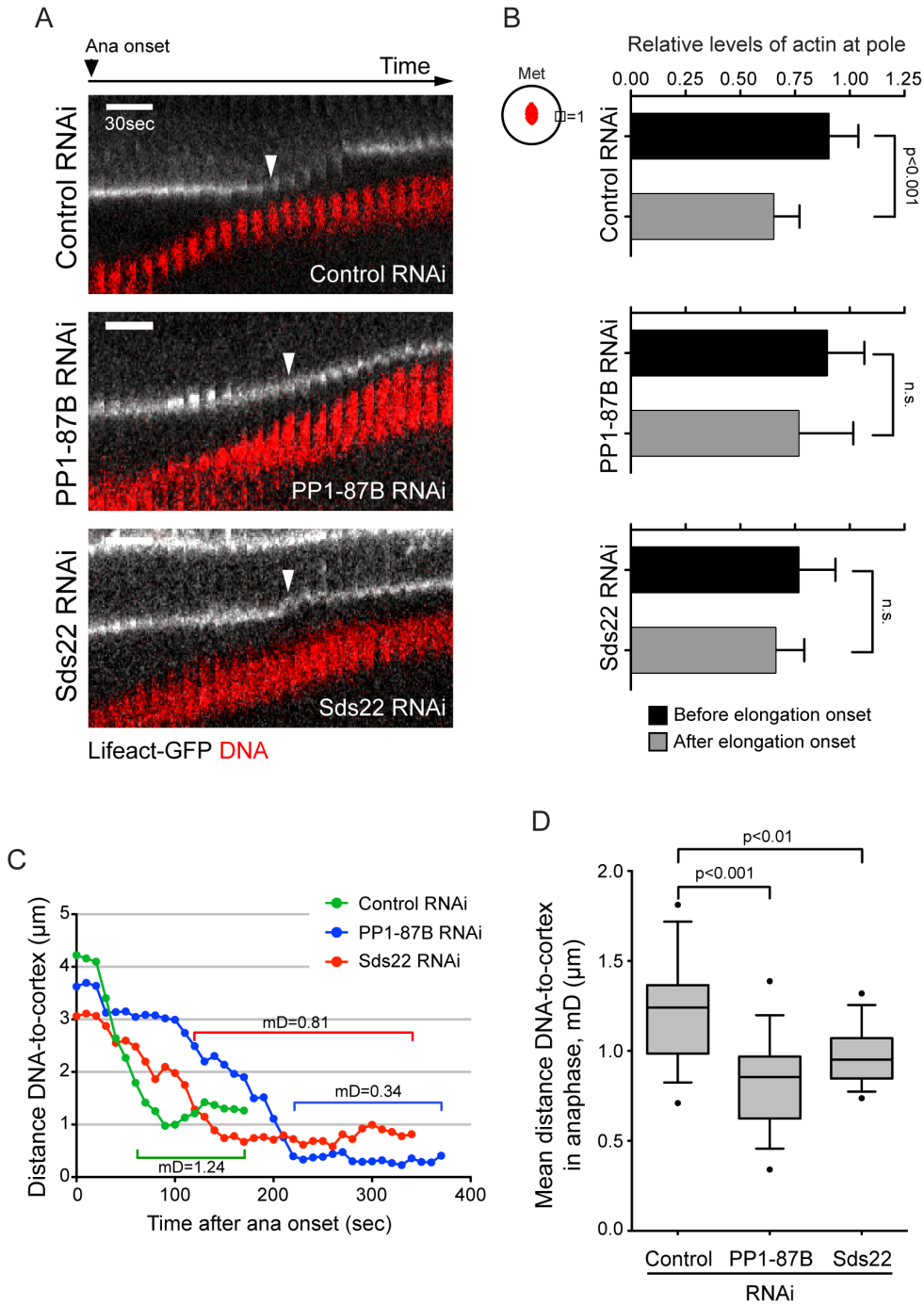
A
Ana onset
Time
30sec
Control RNAi
PP1-87B RNAi
Sds22 RNAi
Lifeact-GFP DNA
B
Relative levels of actin at pole
Met
=1
0.00 0.25 0.50 0.75 1.00 1.25
p<0.001
n.s.
n.s.
Before elongation onset
After elongation onset
C
Distance DNA-to-cortex (µm)
Time after ana onset (sec)
mD=0.81
mD=0.34
mD=1.24
D
Mean distance DNA-to-cortex in anaphase, mD (µm)
p<0.01
p<0.001
Control
PP1-87B
Sds22
RNAi

Figure 5.13

Figure 5.13 – Depletion of PP1-87B or Sds22 leads to impaired clearance of polar actin in SOP cells.

A – Kymographs of anaphase progression (refer to Figure **5.12A**). Arrowheads indicates elongation onset. Genotypes:

w^-; *neur*-RFP/+; *pnr*-GAL4, UAS-Lifeact-GFP/+;

w^-; *neur*-RFP/UAS-PP1-87B-IR; *pnr*-GAL4, UAS-Lifeact-GFP/tubP-GAL80^{ts};

w^-; *neur*-RFP/UAS-Sds22-IR; *pnr*-GAL4, UAS-Lifeact-GFP/+;

Note: flies were grown at 18°C during early development and at 29°C during pupariation.

B – Relative levels of polar actin in SOP cells.

C – Plotting of the distance DNA-to-cortex during anaphase in representative SOP cells in control, PP1-87B RNAi and Sds22 RNAi backgrounds. Anterior pole depicted.

D – Plot of the mean distance DNA-to-cortex in mid-anaphase.

Control RNAi, 15 cells; PP1-87B RNAi, 15 cells; Sds22 RNAi, 14 cells. ≥ 3 animals analysed in each genetic background (quantifications in **B** and **D**).

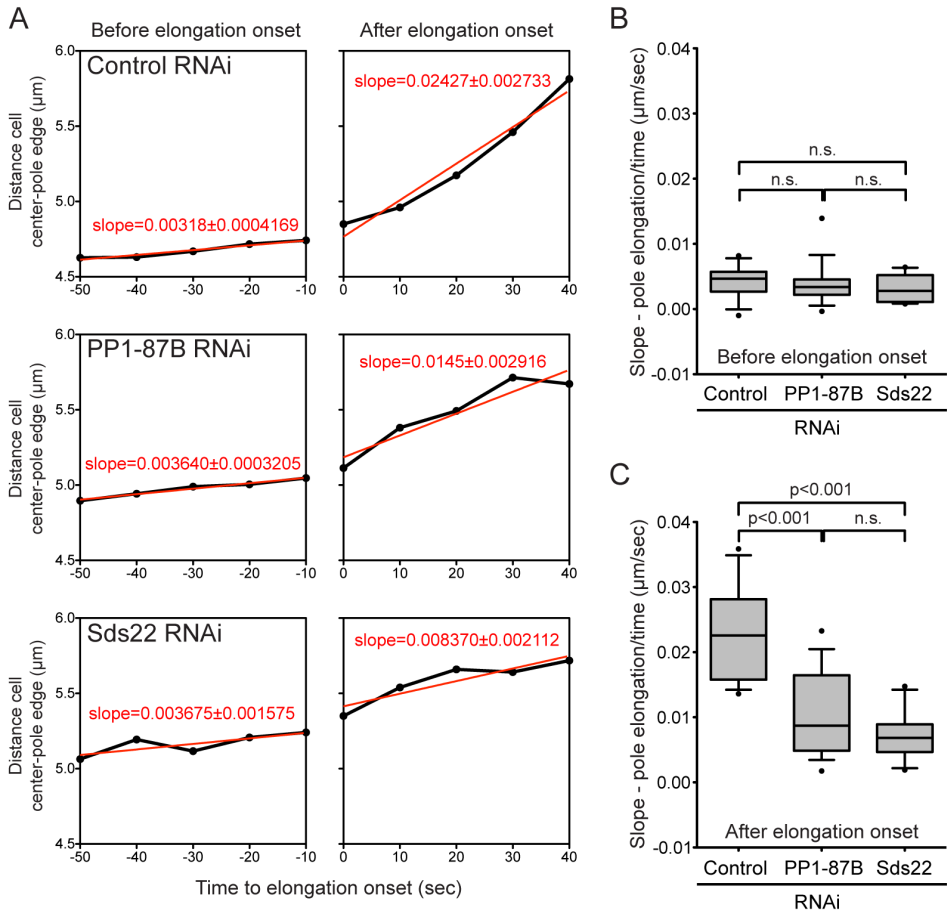

Figure 5.14 – Depletion of PP1-87B or Sds22 leads to impaired cell elongation in anaphase.

A – Plots of distance cell centre-cell pole monitored before and after the elongation onset in representative cells. Linear regression (red) and slopes are indicated. Genotypes:

w^{-}; *neur*-RFP/+; *pnr*-GAL4, UAS-Lifeact-GFP/+;

w^{-}; *neur*-RFP/UAS-PP1-87B-IR; *pnr*-GAL4, UAS-Lifeact-GFP/tubP-GAL80^{ts};

w^{-}; *neur*-RFP/UAS-Sds22-IR; *pnr*-GAL4, UAS-Lifeact-GFP/+;

Note: flies were grown at 18°C during early development and at 29°C during pupariation.

B – Boxplot of the slopes of linear regression (as seen in **A**) before the elongation onset.

C – Boxplot of the slopes of linear regression (as seen in **A**) after the elongation onset. Control RNAi, 12 cells; PP1-87B RNAi, 16 cells; Sds22 RNAi, 10 cells. ≥ 3 animals analysed in each genetic background.

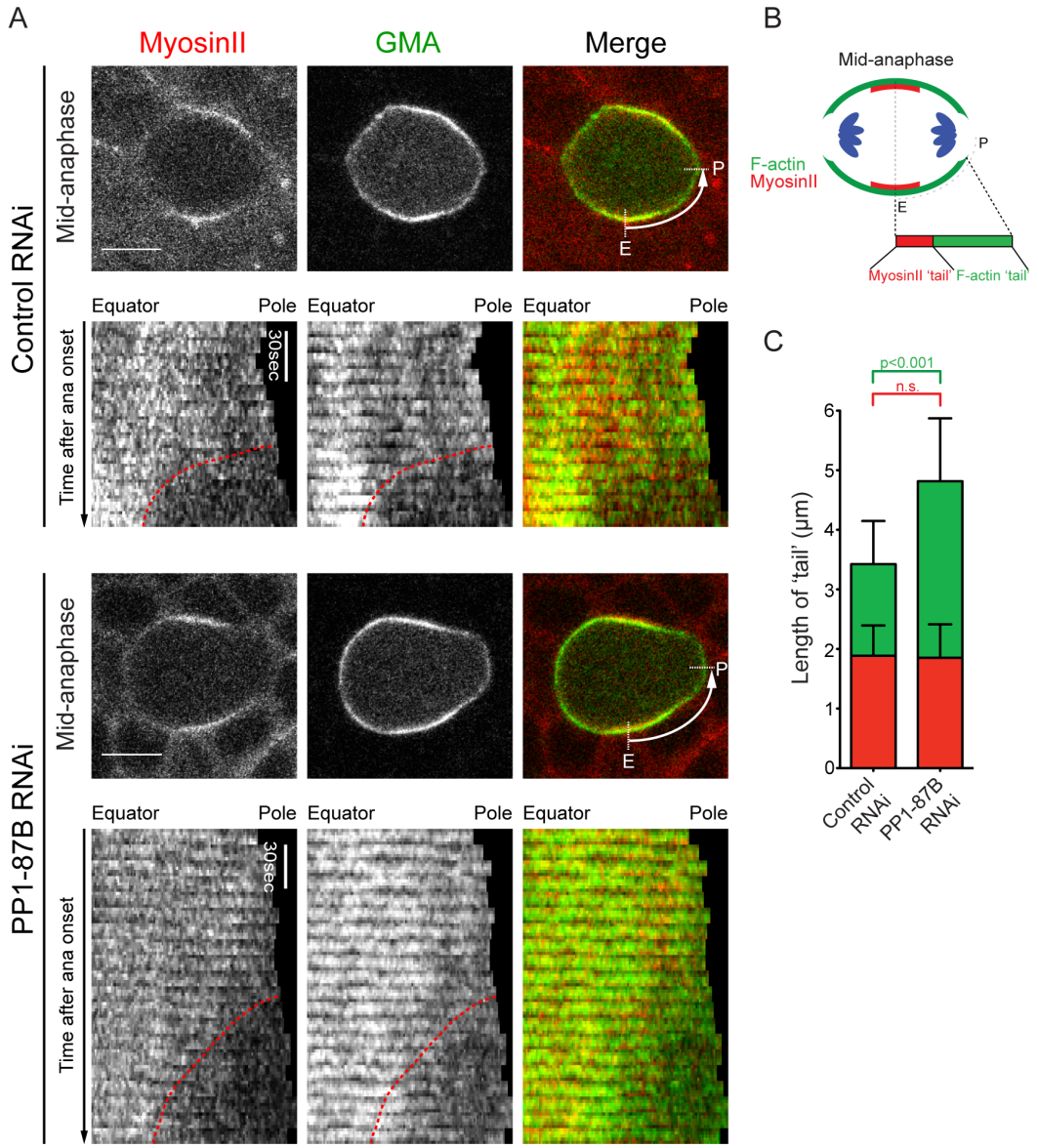

Figure 5.15 – Polarisation of cortical Myosin-II in anaphase does not depend on PP1 phosphatase.

A – Stills of control and PP1-87B-depleted SOP cells in anaphase labelled for myosin-II (Sqh-mCherry) and F-actin (GMA). Kymographs of the 'E-P' perimeter monitored over time. Red dotted lines delineate the redistribution pattern of myosin-II from the pole toward the equator. Genotypes:

w^-; *neur*-GMA/+; *pnr*-GAL4, *sqh*-Sqh-mCherry/+;

w^-; *neur*-GMA/UAS-PP1-87B-IR; *pnr*-GAL4, *sqh*-Sqh-mCherry/tubP-GAL80^{ts};

Note: flies were grown at 18°C during early development and at 29°C during pupariation.

B – Scheme illustrating cortical myosin-II and actin 'tails' in an anaphase cell.

C – Measurement of the length of myosin-II and actin 'tails' in anaphase cells. Control RNAi, 12 cells; PP1-87B RNAi, 16 cells. ≥ 3 animals analysed in each genetic background.

5.7 Kinetochore-localised PP1/Sds22 induces polar relaxation to propel anaphase cell elongation

Next it was important to identify the detailed molecular mechanism by which PP1/Sds22 is able to induce local dephosphorylation and inactivation of Moesin molecules crosslinking actin to the plasma membrane at the cell poles. Importantly, it has been demonstrated that PP1 and Sds22 can localise to the kinetochores, where they control Aurora B activity (Emanuele et al., 2008, Kim et al., 2010, Posch et al., 2010, Qian et al., 2011, Qian et al., 2013) and are involved in SAC silencing (Pinsky et al., 2009, Vanoosthuyse and Hardwick, 2009, Lesage et al., 2011). By imaging epithelial cells expressing GFP-tagged Sds22 (Grusche et al., 2009) and RFP-tagged Spc25, a component of the Ndc80 complex (Ciferri et al., 2007), I saw that a significant pool of Sds22 localised to the kinetochores during mitotic exit (Fig. 5.16 and 5.17A). Given the fluorescence signal in the cytoplasm, I could follow cell shape changes during mitosis. Polar blebbing occurred when the kinetochores were in close proximity to the cell boundary (Fig. 5.16B, C and 5.17A). This is consistent with the results shown in section 5.5. To determine if polar relaxation is specifically triggered by a kinetochore-localised pool of PP1/Sds22, I decided to impair its recruitment to the kinetochores. To do so, I depleted the levels of KNL1 in fly tissues. KNL1 is a conserved component of the KMN super-complex that controls the interaction between microtubules and the chromosomes (Schittenhelm et al., 2009, Feijao et al., 2013, Krenn et al., 2014) and it was shown to recruit PP1 to the outer kinetochore to allow SAC silencing (Liu et al., 2010, Meadows et al., 2011, Rosenberg et al., 2011).

Using Sds22-GFP localisation as readout for kinetochore localisation of the PP1/Sds22 complex, I observed that this is reduced upon KNL1 depletion (Fig. 5.17A), in line with previous findings (Liu et al., 2010). This led to a loss of polar blebbing as cells progressed through anaphase (Fig. 5.17A, B). This was accompanied by a decrease in cell elongation (Fig. 5.17C). These findings have not been reported before. Furthermore, the observed shape defects in KNL1 RNAi cells are likely contributing to cell division failure and tissue malformation (Fig. 5.17D).

While there seems to be a plausible link between lowered polar relaxation and the reduction in PP1/Sds22 kinetochore levels in KNL1-depleted cells, it is intriguing that these cells did not exhibit noticeable defects regarding mitotic timing, such that they exited mitosis in a relatively timely manner. Note that KNL1-dependent PP1 localisation at the kinetochores is thought to promote SAC silencing (Espeut et al., 2012, Meadows et al., 2011, Rosenberg et al., 2011). One mechanism that accounts for PP1-dependent SAC silencing is through the dephosphorylation of Aurora B-targeted kinetochore components (Liu et al., 2010, Posch et al., 2010, Rosenberg et al., 2011). On the other hand, PP1 can also dephosphorylate KNL1 itself (London et al., 2012), thereby releasing SAC proteins (such as Bub1 and Bub3) from KNL1 binding sites and driving cells toward anaphase (Krenn et al., 2014, London et al., 2012). This is countered by the Mps1 kinase, which promotes the retention of SAC proteins at the kinetochores until all chromosomes are bioriented (London et al., 2012, Shepperd et al., 2012, Yamagishi et al., 2012). Given my findings, it is possible that the accumulation of SAC proteins at the kinetochores of KNL1 RNAi cells is lowered, thereby leading to premature SAC silencing and allowing cells to perform anaphase (as was observed). Alternatively, one could have also expected that KNL1 RNAi cells would fail to exit mitosis, given that impairment of PP1 accumulation at the kinetochore could lead to endured SAC signalling. Lastly, it should be noted that, to do the experiments I describe in this section, the degree of KNL1 knockdown had to be tuned down in order to overcome animal lethality, and therefore, protein depletion was only partial. Hence, this could also account for the fact that KNL1-depleted cells were able to exit mitosis.

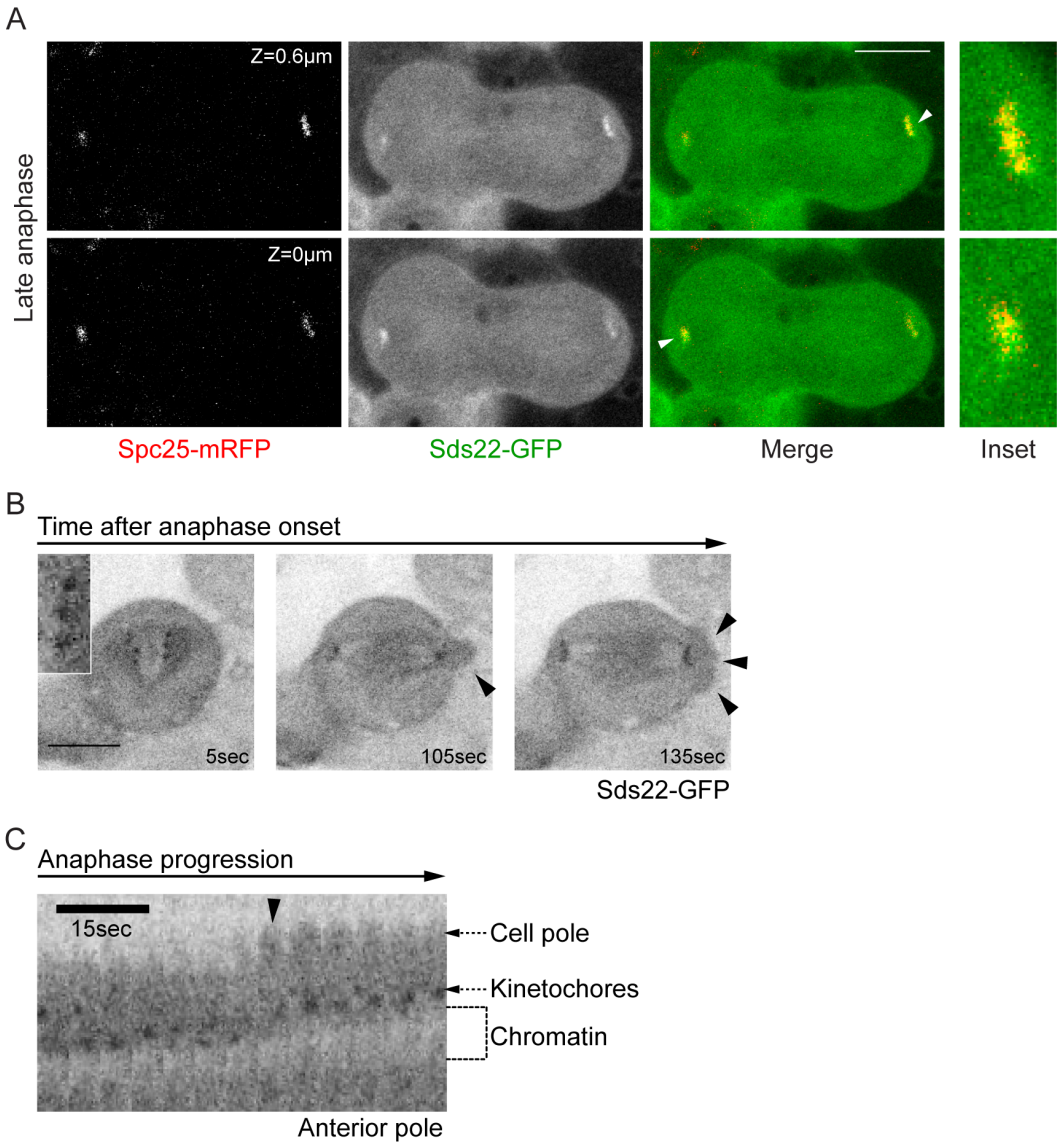

Figure 5.16 – Kinetochore-localised Sds22 triggers polar blebbing in anaphase.

A – Time-lapse stills of an anaphase epithelial cell showing co-localisation between Sds22 and the kinetochore protein Spc25. Insets of regions pointed by arrowheads.

B – Epithelial cell expressing Sds22-GFP imaged during anaphase. Scale bar = 5µm.

C – Kymograph of anaphase progression of the cell shown in **B**. Black arrowheads point to polar blebbing. Inverted lookup table in **B** and **C**. Genotypes:

w^-; EM462-GAL4/UAS-Sds22-GFP; gSpc25-mRFP/+;

w^-; EM462-GAL4/UAS-Sds22-GFP; TM2/+;

Note: flies were grown at 25°C through early development and pupariation.

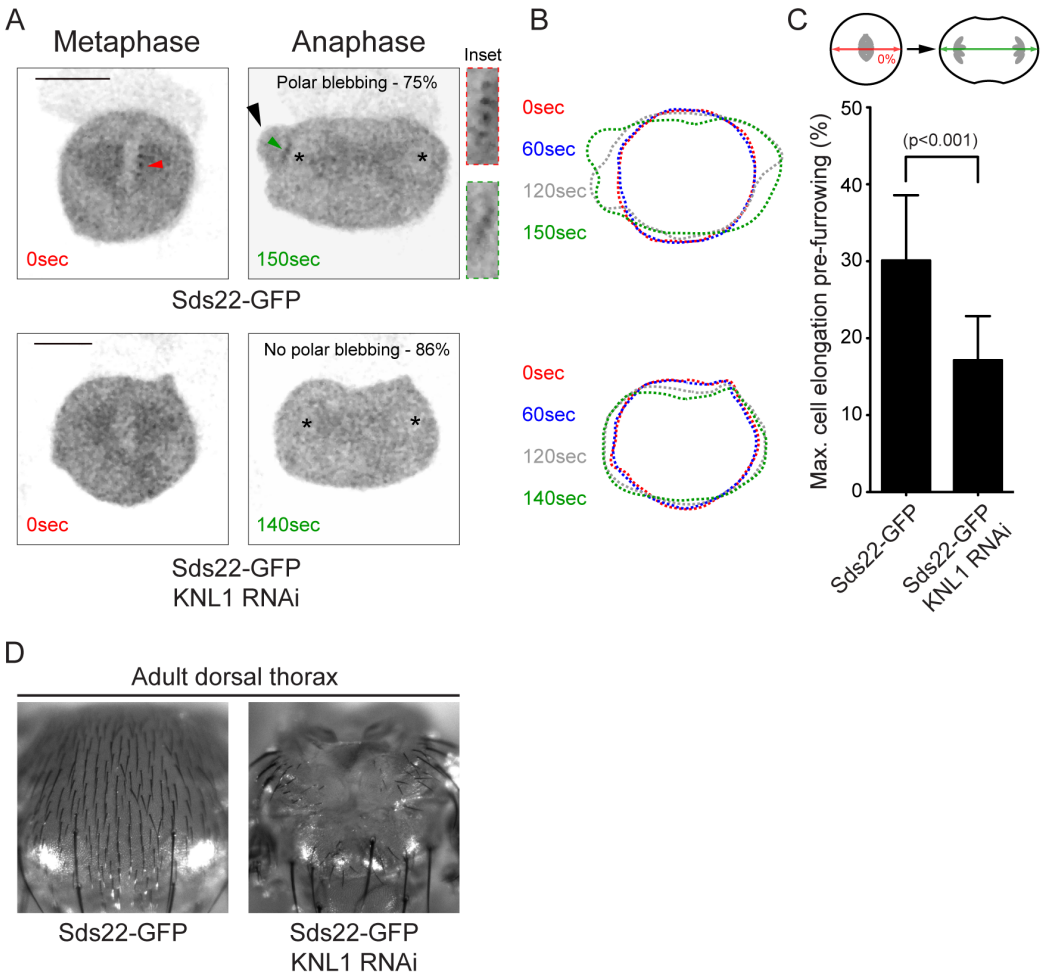

Figure 5.17 – Kinetochore-localised Sds22 induces cortical relaxation in a KNL1-dependent manner.

A – Sds22-GFP-expressing fly cells in control and KNL1-depleted backgrounds. Insets of regions pointed by red and green arrowheads. Black arrowhead points to polar blebbing. Asterisks mark the chromosomes. Scale bar = 5µm. Genotypes:

w^-; EM462-GAL4/UAS-Sds22-GFP; TM2/+;

w^-; EM462-GAL4/UAS-Sds22-GFP; UAS-Spc105-hairpin/+;

Note: flies were grown at 25°C through early development and pupariation.

B – Outlines of cell boundary at different time-points during anaphase.

C – Quantification of maximal cell elongation in Sds22-GFP-expressing cells in 'control' (13 cells) or KNL1-depleted backgrounds (14 cells). ≥ 3 animals analysed in each genetic background.

D – Representative adults thoraces of Sds22-GFP-expressing flies with normal or reduced levels of KNL1.

5.8 Misregulation of cortical Moesin leads to size and shape defects in cytokinesis

To confirm that the defects in polar relaxation caused by PP1/Sds22 depletion are due to Moesin misregulation at the anaphase cortex, I expressed a constitutively active form of Moesin in mitotic SOP cells. I made use of a Moesin transgene where the conserved C-terminus threonine residue was mutated into Aspartate, locking the protein in its active conformation (hereafter referred to as MoesinT559D). Expression of this transgene leads to excessive cortical rigidity in cells (Carreno et al., 2008, Kunda et al., 2008) and various defects in fly development (Polesello et al., 2002, Hipfner et al., 2004, Karagiosis and Ready, 2004, Cheng et al., 2011). When I expressed GFP-tagged MoesinT559D in SOP cells passing through anaphase, I observed that the cortex was rendered non-responsive to the anaphase chromosomes (Fig. 5.18A). Consequently, the majority of the cells failed to exhibit polar blebbing, thus allowing the chromosome mass to get into closer cortical apposition than in cells expressing 'wild-type' Moesin (Fig. 5.18A-D).

Next I studied the impact of aberrant polar relaxation in the overall cell shape at cytokinesis. I observed that depletion of PP1-87B or Sds22 as well as expression of MoesinT559D all led to identical shape defects at the end of mitosis. As seen in Figure 5.19, cells in all three of those conditions exhibited ectopic deformations, thus reflecting a low circularity index. Therefore, these data add further proof that misregulation of cortical Moesin compromises the shape stability of cells exiting mitosis.

In an additional experiment, I tested whether aberrant polar relaxation can affect the size of the nascent daughter cells at cytokinesis. To do so, I again expressed MoesinT559D-GFP in metaphase SOP cells. Additionally, I expressed a GFP-targeted nanobody (originally conceived by Rothbauer and colleagues (Rothbauer et al., 2008)) that is itself fused to a Pon localisation sequence (hereafter referred to as Pon-GBP; unpublished material from Emmanuel Derivery and Marcos Gonzalez-Gaitan). In doing so, I was able to exaggerate the accumulation of GFP-tagged MoesinT559D on the anterior metaphase cortex and consequently in the PIIb cell. In this scenario, PIIa cells appeared to be

considerably larger than those in tissues expressing either Moesin-GFP or MoesinT559D-GFP without Pon-GBP, while the size of PIIb was unaltered (Fig. 5.20A, B). This reflected in a significant drop in the cell size ratio PIIb/PIIa (Fig. 5.20C). This is interesting because one could have also expected that excessive accumulation of MoesinT559D in the PIIb cell would render it more rigid and therefore smaller. These preliminary data, although promising, require further experimental validation.

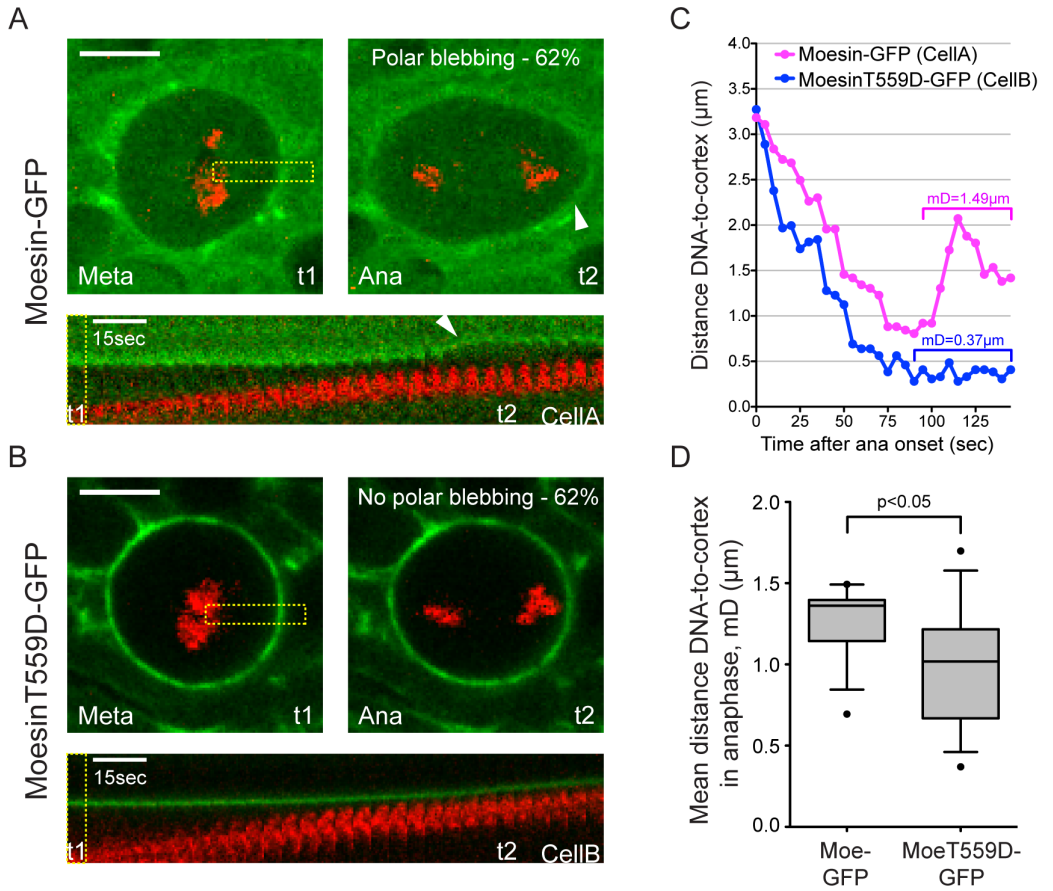

Figure 5.18 – Expression of a phosphomimetic form of Moesin impairs polar relaxation in SOP cells.

A, B – Imaging of SOP cells expressing Moesin-GFP (**A**) or MoesinT559D-GFP (**B**) during anaphase. The kymographs refer to the dotted section indicated. White arrowheads points to polar blebbing. Scale bar = 5µm. Genotypes:

w$^-$; *neur*-RFP/+; *pnr*-GAL4/UAS-Moesin-GFP;

w$^-$; *neur*-RFP/+; *pnr*-GAL4/UAS-MoesinT559D-GFP;

Note: flies were grown at 25°C during early development and at 29°C during pupariation.

C – Plotting of the distance DNA-to-cortex during anaphase in cells shown in **A** and **B**. 5sec resolution. mD indicates mean distance (during mid-anaphase).

D – Quantification of the mean distance DNA-to-cortex in mid-anaphase. Moesin-GFP, 13 cells; MoesinT559D-GFP, 13 cells. 4 animals analysed in each genetic background.

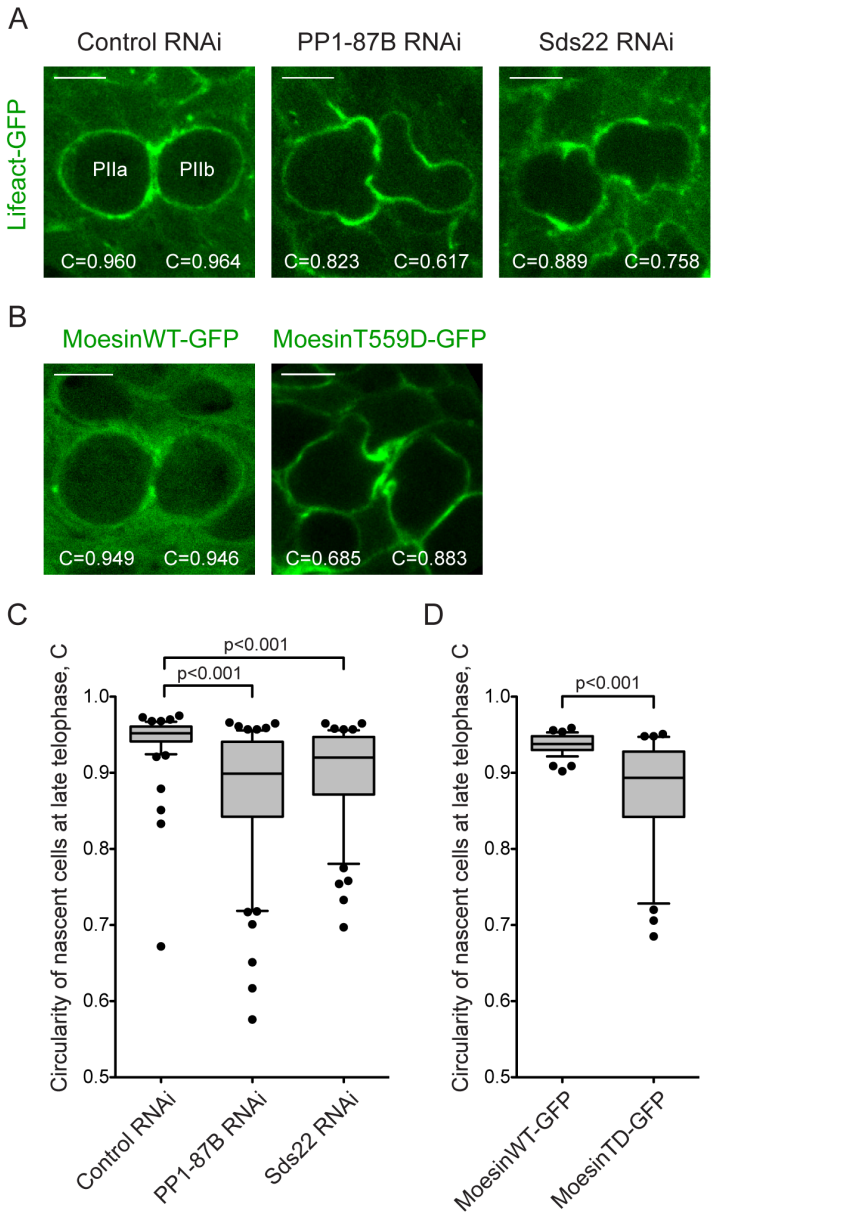
A
Control RNAi
PP1-87B RNAi
Sds22 RNAi
Lifeact-GFP
PIIa
PIIb
C=0.960
C=0.964
C=0.823
C=0.617
C=0.889
C=0.758
B
MoesinWT-GFP
MoesinT559D-GFP
C=0.949
C=0.946
C=0.685
C=0.883
C
D
p<0.001
p<0.001
Circularity of nascent cells at late telophase, C
1.0
0.9
0.8
0.7
0.6
0.5
Control RNAi
PP1-87B RNAi
Sds22 RNAi
p<0.001
MoesinWT-GFP
MoesinTD-GFP

Figure 5.19

Figure 5.19 – Depletion of PP1-87B and Sd22, or expression of MoesinT559D-GFP all lead to severe shape defects in telophase cells.

A – Stills of representative telophase cells in control RNAi, PP1-87B RNAi or Sds22 RNAi. Lifeact-GFP labels filamentous actin. Genotypes:

w^-; *neur*-RFP/+; *pnr*-GAL4, UAS-Lifeact-GFP/+;

w^-; *neur*-RFP/UAS-PP1-87B-IR; *pnr*-GAL4, UAS-Lifeact-GFP/tubP-GAL80^{ts};

w^-; *neur*-RFP/UAS-Sds22-IR; *pnr*-GAL4, UAS-Lifeact-GFP/+;

Note: flies were grown at 18°C during early development and at 29°C during pupariation.

B – Stills of representative telophase cells expressing Moesin-GFP or MoesinT559D-GFP. Values of cell circularity, C, are indicated in **A** and **B**. Genotypes:

w^-; *neur*-RFP/+; *pnr*-GAL4/UAS-Moesin-GFP;

w^-; *neur*-RFP/+; *pnr*-GAL4/UAS-MoesinT559D-GFP;

Note: flies were grown at 25°C during early development and at 29°C during pupariation.

C – Boxplot of the circularity of telophase cells in control RNAi (64 cells, 32 divisions), PP1-87B RNAi (62 cells, 31 divisions) and Sds22 RNAi (54 cells, 27 divisions) tissues.

D – Boxplot of the circularity of telophase cells in Moesin-GFP (38 cells, 19 divisions) and MoesinT559D-GFP (30 cells, 15 divisions) expressing tissues. ≥ 3 animals analysed in each genetic background. Scale bar = 5μm.

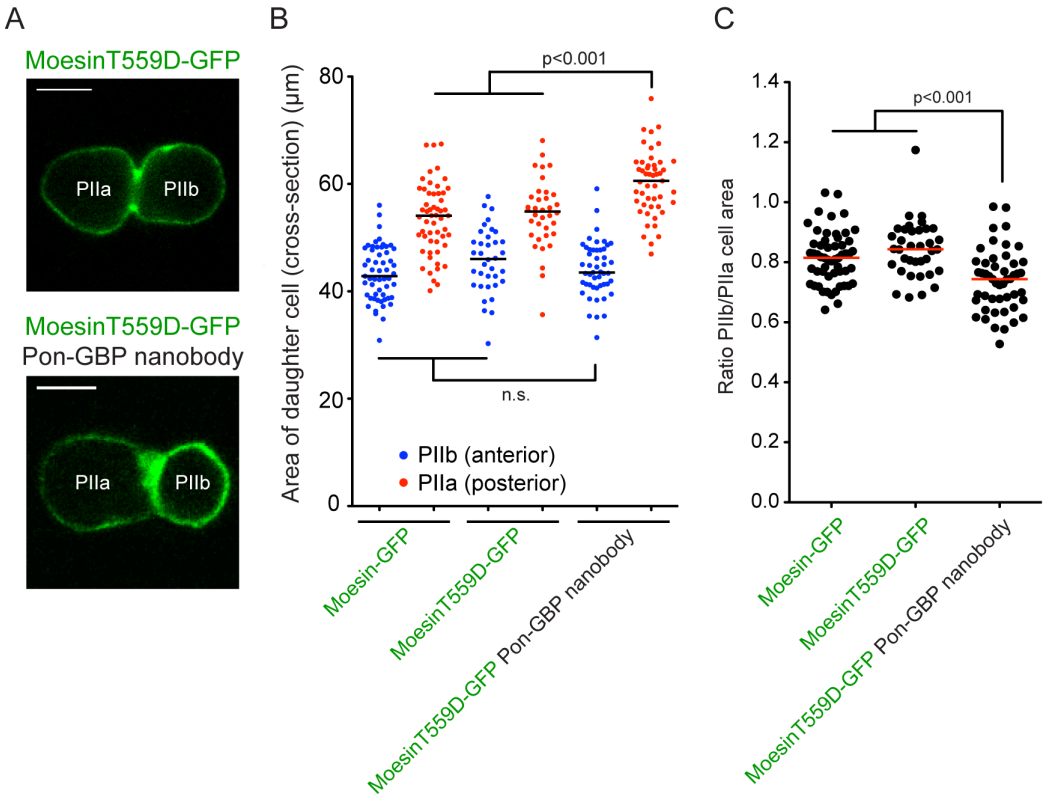

Figure 5.20 – Asymmetric distribution of cortical MoesinT559D in dividing SOPs leads to an enhanced discrepancy in size between PIIa and PIIb cells.

A – Stills of SOP cells expressing MoesinT559D-GFP with or without the Pon-GBP nanobody. Scale bar = 5µm.

B – Quantification of the area of PIIa and PIIb cells. Black lines indicate the median.

C – Quantification of the ratio PIIb/PIIa of cell area. Red lines indicated the median. Moesin-GFP (55 cells); MoesinT559D-GFP (36 cells); Moesin-GFP/Pon-GBP (49 cells). ≥ 3 animals analysed in each genetic background. Genotypes:

w^{-};; *neur*-GAL4/UAS-Moesin-GFP;

w^{-};; *neur*-GAL4/UAS-MoesinT559-GFP;

w^{-}; UAS-PON-GBP/+; *neur*-GAL4/UAS-MoesinT559D-GFP;

Note: flies were grown at 25°C during early development and at 29°C during pupariation.

5.9 Conclusions

Understanding the biochemistry and mechanics underlying the polarisation of the cortex at mitotic exit has been the focus of many studies. However, given the complexity of this mechanism, dissecting it has proved difficult. One of the quests in this thesis was to characterise the mechanism of polar relaxation in early cytokinesis. Indeed, I was able to show that this event, which is marked by the loss of Moesin and actin from the poles, allows cell elongation and is independent of furrow constriction. I demonstrated this by depleting the centralspindlin component RacGAP1 in SOPs, which led to a severe impairment or complete failure of furrow ingression. These cells were still able to clear polar actin and to elongate significantly during anaphase. Additionally, at this point of mitotic exit, myosin-II and actin exhibited different patterns of cortical polarisation, such that the latter moved from the poles toward the equator at a slower rate than the former. I also showed that polar relaxation is independent of centrosome- or astral microtubule-derived signals. My data appear to contrast with previous reports, in which the astral microtubules have been shown to have an active role in relaxing the cell poles by inhibiting myosin-II and by clearing actin from these cortical regions (Werner et al., 2007, Foe and von Dassow, 2008, Murthy and Wadsworth, 2008, Tseng et al., 2012). Subsequently, I demonstrated that polar clearance of Moesin and actin in anaphase occurs when the chromatin is in close proximity to the cell edge. I was able to show that this event of polar relaxation is dependent on the pool of kinetochore-localised PP1-87B/Sds22 complex. Remarkably, depletion of KNL1, a protein implicated in the recruitment of PP1 to the kinetochore (Liu et al., 2010), leads to impaired polar blebbing and faulty cell elongation during anaphase. Lastly, I demonstrated that, like PP1 or Sds22 depletion, overexpression of MoesinT559D leads to faulty polar relaxation and severe shape defects in cells completing cytokinesis.

Chapter 6

General Discussion

6.1 Coupling cell shape changes and actin reorganisation to cell cycle progression

Animal cells undergo extensive structural reorganisation during mitosis. Upon mitotic entry, the chromatin becomes condensed, the nuclear envelope breaks down and a bipolar spindle is formed, which gathers the chromosomes at the cell centre. At mitotic exit, the two sets of sister chromatids move toward opposite poles and the cell splits at the equator to generate two new cells. All these events depend on the activity of mitotic kinases and counteracting phosphatases, which act on local and global scales (Medema and Lindqvist, 2011). However, the coupling between cell cycle regulation and actin-driven shape changes in mitosis is poorly understood. While the connection between cell cycle machinery and cytokinetic furrowing is well understood (Green et al., 2012), the regulation of mitotic rounding and anaphase polar relaxation by cell cycle components has not been extensively studied.

Mitotic rounding in animal cells is accompanied by rearrangement of F-actin networks and by the formation of an actin-rich cortex (Fig. 6.1) (Fujibuchi et al., 2005, Kaji et al., 2008, Kunda and Baum, 2009, Zhuang et al., 2011, Matthews et al., 2012). These processes are orchestrated by myosin-II-driven contractility and by the activity of crosslinking proteins, such as ERMs (Fig. 6.1) (Maddox and Burridge, 2003, Carreno et al., 2008, Kunda et al., 2008, Luxenburg et al., 2011, Kondo and Hayashi, 2013). While the link between the mitotic kinase CDK1 and determinants of cell morphology in yeast is well established (Moseley and Nurse, 2009), evidence for cell cycle regulation of actin-driven shape changes in animals is limited. One study for example, has demonstrated that CDK1 directly phosphorylates Abi1, which in turn dampens the activity of the WAVE complex and subsequent F-actin assembly (Zhuang et al., 2011). In addition, CDK1 has been shown to target the RhoGEF Ect2 to promote cell rounding and the formation of a stiff actomyosin cortex (Matthews et al., 2012).

In this thesis I show that Moesin phosphorylation is subject to cell cycle control. Thus, at mitotic entry, levels of phosphorylated, active Moesin increased significantly both basally and laterally. Interestingly, using the Disphos software for phosphorylation site prediction, I noted that Slik contains ten consensus S/T-P

sequences, which are putatively CDK1 target sites (Enserink and Kolodner, 2010). Therefore, Slik may provide the biochemical coupling between Moesin activation and CDK1 regulation. This would be a good subject for future work.

In Chapters 3 and 5 I demonstrated that the beginning of anaphase cell elongation is marked by relaxation of cell poles. This is accompanied by the loss of cortical p-Moesin and F-actin. In contrast, Slik remains localised at the membrane throughout mitotic progression. Thus, either its activity near the poles is altered or is overridden by counteracting forces. My discovery that kinetochore-localised PP1-87B/Sds22 inactivates polar Moesin, may explain how this is achieved without the need for local changes in local Slik activity. Nevertheless, it is also conceivable that CDK-dependent phosphorylation of Slik is reversed by the local action of PP1 cell poles, leading to a loss of Slik activity that contributes to the sudden kinetochore-mediated change in cortical mechanics.

It should also be noted that isoforms of PP1 have been shown to localise to the cell cortex in mitosis (Bloecher and Tatchell, 2000, Trinkle-Mulcahy et al., 2003, Trinkle-Mulcahy et al., 2006). This may even be the case for a portion of the cellular pool of PP1-87B/Sds22, since cortical levels of active Moesin are increased in metaphase cells depleted for PP1-87B/Sds22. Nevertheless, my data suggest that while there may be two different pools of active PP1 that act on p-Moesin, anaphase polar relaxation is specifically triggered by kinetochore-bound phosphatase. This was most clearly established in experiments in which I studied the effects of KNL1 depletion in flies. This led to deficient PP1/Sds22 recruitment to the kinetochores and an almost complete absence of polar blebbing at anaphase.

Interestingly, polar relaxation may be a very transient process. Thus, in chapter 3 I showed that Moesin and F-actin become re-enriched at the cortex of newly formed cells at telophase. A possible explanation for this is the shielding of the polar cortex from PP1 after anaphase. This could be due to the bulk re-localisation of PP1 to chromosome arms in late anaphase (Trinkle-Mulcahy et al., 2006, Qian et al., 2013), where it promotes DNA decondensation and nuclear envelope reformation (Landsverk et al., 2005, Vagnarelli et al., 2011), or a result of the assembly of the nuclear envelope itself. To test these ideas, one could try and impair the relocalisation of PP1 to the chromatin, perturb nuclear reassembly at telophase or prevent breakdown of the anaphase spindle, and see how these treatments affect the telophase restoration of uniform p-Moesin.

6.2 The involvement of Moesin in cell rounding and stabilisation of the metaphase cortex

Mitotic cell rounding is accompanied by reorganisation of the actin cytoskeleton and formation of a stiff cortex. Some years ago our lab showed that Moesin is required for mitotic rounding of fly cells in culture (Kunda et al., 2008). We then proposed that ERM proteins are key players in the tethering of the actomyosin cortex to the plasma membrane, thereby increasing cortical rigidity (Fig. 6.1). In this thesis however, I demonstrated that Moesin appears to be dispensable for mitotic rounding of SOP cells in the notum. It was somewhat surprising to observe that cells depleted for Moesin or for its kinase Slik were able to attain a rounded shape at prophase since the cortical levels of active Moesin increase dramatically at this point of the cell cycle (Fig. 6.1). One possible explanation is that SOP cells are confined in a tissue that grants them a cuboidal architecture in interphase, which may facilitate cell rounding. Therefore, the cortex in SOPs may not have to perform as much work at the G2/M passage as it does in flat cells in culture, which have to undergo a drastic reduction is their adhesive area and an increase in cell height as they reach metaphase. In addition, it may be that rounding within a tissue context depends more or osmotic swelling than it does on a large increase in cortical actomyosin (Stewart et al., 2011). Nevertheless, SOP cells still need to retract medial and basal actin-rich protrusions toward the cell body. The reorganisation of these structures likely depends on a decrease in the activity of the actin nucleators underlying lamellipodial formation (Zhuang et al., 2011), although further investigation is required to test this hypothesis. Interestingly my findings are in agreement with a study on the role of Moesin in spindle positioning in *Drosophila* testes (Cheng et al., 2011), where the expression of dominant negative form of Moesin (in which the conserved threonine residue is mutated into an alanine, thereby making it non-phosphorylatable) or depletion of Moesin by RNAi in somatic cyst stem cells (CySCs) did not lead to any defects in shape changes as cells passed from interphase to mitosis. In addition, like SOPs, CyCSs are constrained by other cells in the gonad that likely support their three-dimensional geometry.

To experimentally validate whether Moesin is dispensable for early mitotic shape changes in SOP cells, it will be important to analyse mitotic cells expressing a null allele for the ERM gene. This could be achieved by using the FRT/FLP system, which allows the generation of mutant clones in an otherwise wildtype tissue (Theodosiou and Xu, 1998). However, since epithelial integrity is strongly impaired upon complete suppression of Moesin levels, it may be difficult to generate large Moesin null clones (Hipfner and Cohen, 2003, Hipfner et al., 2004, Hughes and Fehon, 2006).

While Moesin appears to not be required for the early changes in mitotic cell shape, my work shows that it is important in the stabilisation of the actomyosin cortex and cell shape once cells have rounded at late prophase and early prometaphase. Depletion of Moesin or Slik leads to strong cortical instabilities in mitotic SOP cells. In these cells, cortical oscillations are observed in which patches of actin moved from one spot of the cell to another in a periodic fashion. These actin oscillations are powered by actomyosin contractility, since they depend on myosin-II, and depend on the actin nucleator Diaphanous. However, the mechanism that sustains these cortical instabilities remains elusive. To better understand this phenomenon, it will be helpful to draw on our understanding of actin dynamics in cell spreading and migration. Indeed, studies on lamellipodial dynamics have proposed that actin oscillations depend on complex interactions and feedback between membrane-bound proteins, nucleation-promoting factors and myosin-II motors (Ryan et al., 2012b, Allard and Mogilner, 2013). Several coarse-grained models have been proposed to explain the propagation of actin waves. For instance, it was been suggested that actin oscillations at the cell's leading edge depend on curvature-sensing membrane proteins, such as BAR proteins, which in turn may control the local activity of actin nucleators (Shlomovitz and Gov, 2007). Other lines of evidence suggest that periodic instabilities underlying wave behaviour can result from mechanical stress (Wolgemuth, 2005). Whereas Hecht and colleagues proposed that wave propagation can also be explained by a model of excitable dynamics, in which activators and inhibitors of F-actin assembly diffuse along the membrane (Hecht et al., 2010). This model, based upon Turing models, proposes that this excitability is driven by stochastic variation in the levels of activator. In turn, the activator recruits an inhibitor that diffuses more quickly along the membrane. As

a consequence, the difference in protein diffusion rates leads to bursts of localised excitations (Bretschneider et al., 2009, Hecht et al., 2010, Ryan et al., 2012a).

The actin instabilities observed in Moesin-depleted cells can also be interpreted in light of previous work in biomimetic systems from the Sykes lab (Paluch et al., 2005). Using cell fragments, the authors demonstrated that actomyosin oscillations can be triggered by spontaneous breakages in an otherwise uniform cortex, leading to shape instabilities. They showed that after cortical rupture, a portion of the membrane is transiently devoid of actin and myosin-II. At the same time, molecules begin accumulating at the opposite side of the cell, initiating the next cycle of contractile oscillations. This is very similar to what I observed in the majority of cells depleted for Moesin or Slik.

Actin wave behaviour has also been observed in mitotic cells. Mitsushima and colleagues reported the existence of a cloud of actin filaments in the cytoplasm of HeLa cells in mitosis, which revolves around the cell in a periodic manner (Mitsushima et al., 2010). They demonstrated that assembly of this cloud depends on Arp2/3 activity and speculated that excessive amounts of cytoplasmic actin might be detrimental for successful cell division. This was indeed confirmed in other studies (Moulding et al., 2007, Moulding et al., 2012). While these are interesting findings, they highlight a phenomenon that occurs in the cytoplasm, while my thesis documents an event that occurs at the cortex. In fly cells *in vivo* I have never seen a cytoplasmic pool of cortical actin like that reported in HeLa cells. Moreover, as is being proposed by our lab, Arp2/3 is likely dispensable in F-actin assembly at the cortex of SOP cells (Rosa et al., in revision).

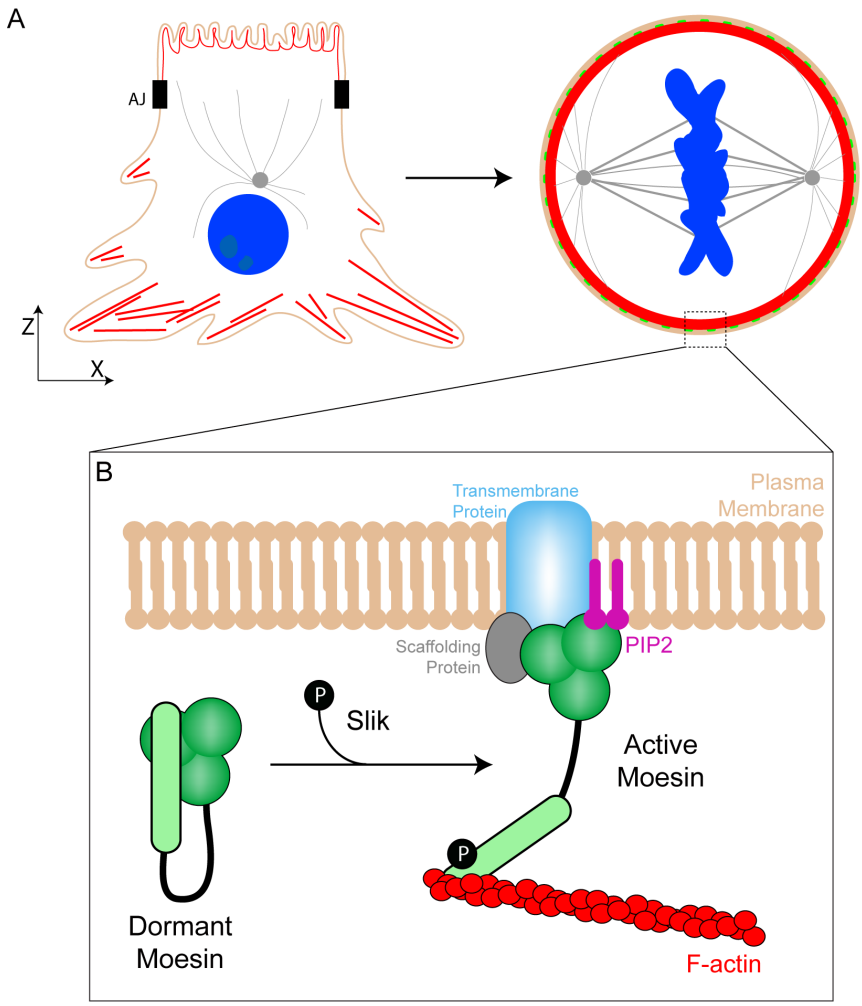

Figure 6.1 – Moesin orchestrates cortical and shape changes in mitosis in a Slik-dependent manner.

A – Scheme depicting an epithelial cell with an irregular shape in interphase (on the left) and with a rounded shape in metaphase (on the right). The actin cortex is dramatically reorganised in a Moesin-dependent manner as epithelial cells reach metaphase. F-actin in red, microtubules in grey, Moesin in green, DNA in blue and plasma membrane in beige. AJ – adherens junctions.

B – Inset of the dotted section shown in **A**. This scheme depicts the mechanism of Slik-dependent activation of Moesin in mitosis, which leads to accumulation of actin filaments at the cortex and stabilisation of cell shape.

6.3 Interplay between the actomyosin cortex and the mitotic spindle

Research on somatic and meiotic cell division has shown that the spindle microtubules communicate with actin structures both at cortical and subcortical levels (Schuh and Ellenberg, 2008, Woolner and Papalopulu, 2012, Chaigne et al., 2013). This communication is important in spindle orientation and positioning. One study in particular has shown that spindle orientation is biased by external forces exerted by retraction fibres (Fink et al., 2011). The authors observed that spindle movements were directly influenced by a subcortical population of actin filaments, which appeared to polarise along the axis of tension.

Several lines of evidence from our and other labs point that ERM proteins play a role in the spindle-cortex crosstalk (Carreno et al., 2008, Kunda et al., 2008, Hebert et al., 2012, Solinet et al., 2013, Machicoane et al., 2014). Indeed, work from our lab and Payre lab showed that depletion of fly Moesin led to dramatic defects in the formation and stability of the spindle, likely due to faulty cortex-microtubule anchoring. This was later supported by a study reporting that the fly Moesin can directly bind to microtubules and regulate spindle-cortex interactions (Solinet et al., 2013). The role of ERMs in cortex-spindle interplay has also been validated in mammalian systems. A recent report showed that ERMs play a significant role in guiding spindle orientation. This was seen in cultured cells and in neural progenitors of the mouse neocortex (Machicoane et al., 2014). It was therefore surprising that impairment of Moesin activity in SOPs did not lead to errors in spindle stability or orientation. This suggests that the spindle of SOP cells is insensitive to cortical instabilities. One possible interpretation is that division orientation in these cells is primarily guided by the PCP pathway, which regulates the polarisation of cortical determinants that control spindle alignment along the A-P axis (Gho and Schweisguth, 1998). Therefore, it is likely that PCP signals override the potential interplay between cortical actin and spindle. To validate this, it will be important to impair the activity of PCP components in the fly notum and assess whether the spindle will become more sensitive to cortical instabilities. It is also possible that ERM proteins only play a minor role in the process.

6.4 Kinetochore and chromosome-derived signals as triggers of polar relaxation in anaphase

Most studies on cytokinesis have focused on the role of the spindle apparatus in controlling furrow specification and ingression (Green et al., 2012). The predominant model is that microtubules of the midzone promote the equatorial accumulation of molecules that are required for furrow constriction (Fig. 6.2). Concurrently, the astral microtubules inactivate cortical contractility at the cell poles, while helping to specify the site of cleavage. My data however, point to a process of cortical polarisation that is independent of microtubules and is dependent on the chromosomes. In particular, I demonstrated that the kinetochores, the proteinaceous structures apposed to the centromeres, signal to the actomyosin cortex to trigger polar relaxation and cell elongation (Fig. 6.2). These findings highlight the existence of a novel mechanism that contributes to the cortical changes required in cytokinesis.

Literature reporting DNA-induced cortical polarisation is scarce. The first reports suggesting the potential involvement of mitotic chromosomes in surface relaxation date to the early twentieth century. Using sea urchin blastomeres to understand cell division, Ralph Lillie proposed that the chromosomes release a surface-tension-reducing substance once they are in close proximity to the cell membrane. He suggested that this mechanism was likely due to the difference in electric charge between the DNA and the cell surface (Lillie, 1903). Similarly, Chalkley postulated that fission of amoebae depended on an increase in cytoplasmic fluidity near the poles caused by a substrate released by the chromatin (Chalkley, 1951). The idea that the chromosomes might instruct rearrangements of the cell cortex gained solidity in a recent study by the Cheeseman lab (Kiyomitsu and Cheeseman, 2013). In this study, the authors have demonstrated that during anaphase chromosome-derived Ran-GFP signals act on the cell cortex by locally reducing the levels of Anillin (Fig. 6.2). The resulting asymmetric localisation of Anillin impinges on the polarisation of myosin-II distribution. They argued that this mechanism is particularly relevant in cells where the spindle and the separating chromosomes are off-centre in early anaphase, such that asymmetric polar relaxation may help correct spindle

positioning and ensure successful cell division. While this constitutes a novel mechanism underlying anaphase polar relaxation, Ran-GTP signals have also been implicated in the polarisation of cortical proteins in metaphase. Indeed, the same lab had previously shown that this cellular gradient restricts the localisation of NuMA-LGN to the lateral cell cortex of HeLa cells to maintain the axis of spindle orientation (Kiyomitsu and Cheeseman, 2012). Furthermore, Ran signalling has also been shown to induce cortical polarisation in mouse oocytes. In particular, several studies have demonstrated that Ran-GTP signals deriving from the metaphase chromatin promote cdc42-dependent F-actin assembly and myosin-II accumulation to form a thick cortical cap overlying the spindle (Deng et al., 2007, Dehapiot et al., 2013). Interestingly, another study has shown that Ran GTPase promotes the polarisation of ERM proteins along the meiotic cortex by clearing these proteins from the cortical cap aforementioned (Dehapiot and Halet, 2013). The work presented in this thesis highlights a novel mechanism of polar relaxation that depends on kinetochore-localised PP1/Sds22. While it is possible that both Ran GTPase and PP1 signals act together to elicit cortical changes (Fig. 6.2), the latter is likely exclusive to anaphase. This is supported by studies that showed that PP1, as well as other mitotic phosphatases, is largely inactive during prometaphase and metaphase, during which the activity of Aurora B is dominant (Kim et al., 2010, Liu et al., 2010, Lesage et al., 2011). Once all chromosomes are bioriented, PP1 phosphatase promotes SAC silencing and stabilises chromosome segregation during anaphase, and it does so by counteracting Aurora B activity (Lesage et al., 2011). It has been shown that activation of Aurora B at the spindle midzone during anaphase and telophase generates an intracellular phosphorylation gradient (Fuller et al., 2008). Therefore, it is feasible that while Aurora B is mostly active at the cell centre, chromosome- and kinetochore-localised PP1 becomes increasingly active as the DNA masses move toward the cell poles (Wurzenberger et al., 2012, Afonso et al., 2014). To confirm that PP1/Sds22 signals to the cortex specifically in anaphase, Sergey Lekomtsev and I have assessed the extent of cortical actin clearance near the DNA in cells that remain flat throughout mitosis (Lancaster et al., 2013). We observed that the levels of actin in the cortical regions constraining the metaphase chromatin (above and below) are unchanged in comparison to other regions of the cortex. In mitotic exit however, the amount of cortical actin near the chromosomes drops significantly,

something that is impaired upon depletion of Sds22. Taken together, the findings documented in this thesis point to a novel mechanism of polar relaxation dependent on kinetochore-localised PP1/Sds22, and reveal a strong link between cell cycle progression, cortical rearrangements and timely changes in cell morphology.

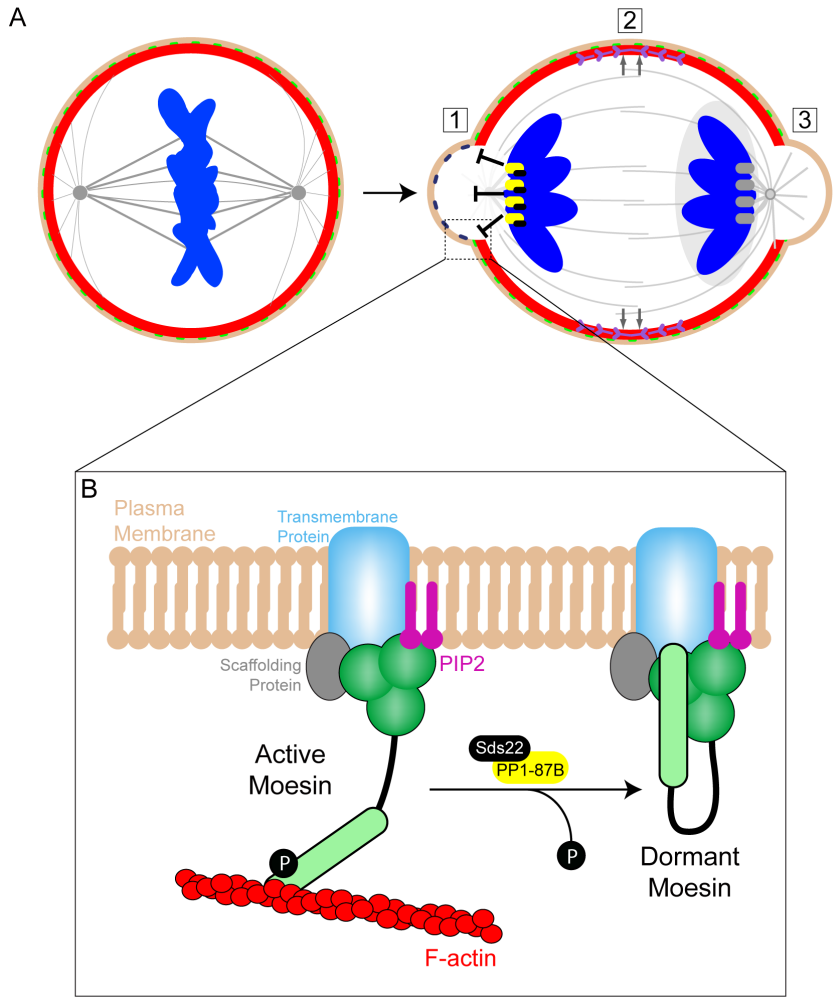

Figure 6.2 – The actomyosin cortex is polarised in cells exiting mitosis.

A – Scheme depicting a cell with a round shape and homogenous actin cortex in metaphase (on the left) and with an elongated shape and polarised cortex in anaphase (on the right). Several anaphase signals induce symmetry breaking of the cortex: 1 – Kinetochore-localised PP1/Sds22 inactivate Moesin and trigger polar relaxation (demonstrated in this thesis); 2 – Spindle midzone signals promote the equatorial accumulation of myosin-II and furrowing (studied in Chapter 5); 3 – Chromatin-derived RanGTP signal promotes cortical repolarisation and polar expansion (Kiyomitsu and Cheeseman, 2013). F-actin in red, microtubules in grey, plasma membrane in beige, Moesin in green (or in dark blue – see dashed line on the membrane), DNA in blue, myosin-II in purple, PP1-87B/Sds22 in yellow/black and Ran signal in light grey.

B – Inset of the dotted section shown in **A**. This scheme depicts the mechanism of PP1-87B/Sds22-dependent inactivation of Moesin at the cell poles in anaphase, which leads to polar relaxation (through the detachment of F-actin from the membrane) and initiation of cell elongation (demonstrated in this thesis).

Chapter 7

Bibliography

AFONSO, O., MATOS, I., PEREIRA, A. J., AGUIAR, P., LAMPSON, M. A. & MAIATO, H. 2014. Feedback control of chromosome separation by a midzone Aurora B gradient. *Science,* 345**,** 332-6.

ALLARD, J. & MOGILNER, A. 2013. Traveling waves in actin dynamics and cell motility. *Curr Opin Cell Biol,* 25**,** 107-15.

ASANO, Y., JIMENEZ-DALMARONI, A., LIVERPOOL, T. B., MARCHETTI, M. C., GIOMI, L., KIGER, A., DUKE, T. & BAUM, B. 2009. Pak3 inhibits local actin filament formation to regulate global cell polarity. *HFSP J,* 3**,** 194-203.

BARR, F. A., ELLIOTT, P. R. & GRUNEBERG, U. 2011. Protein phosphatases and the regulation of mitosis. *J Cell Sci,* 124**,** 2323-34.

BARR, F. A., SILLJE, H. H. & NIGG, E. A. 2004. Polo-like kinases and the orchestration of cell division. *Nat Rev Mol Cell Biol,* 5**,** 429-40.

BARROS, C. S., PHELPS, C. B. & BRAND, A. H. 2003. Drosophila nonmuscle myosin II promotes the asymmetric segregation of cell fate determinants by cortical exclusion rather than active transport. *Dev Cell,* 5**,** 829-40.

BARROS, T. P., KINOSHITA, K., HYMAN, A. A. & RAFF, J. W. 2005. Aurora A activates D-TACC-Msps complexes exclusively at centrosomes to stabilize centrosomal microtubules. *J Cell Biol,* 170**,** 1039-46.

BASTO, R., LAU, J., VINOGRADOVA, T., GARDIOL, A., WOODS, C. G., KHODJAKOV, A. & RAFF, J. W. 2006. Flies without centrioles. *Cell,* 125**,** 1375-86.

BASTOS, R. N., PENATE, X., BATES, M., HAMMOND, D. & BARR, F. A. 2012. CYK4 inhibits Rac1-dependent PAK1 and ARHGEF7 effector pathways during cytokinesis. *J Cell Biol,* 198**,** 865-80.

BAUMGARTNER, M., SILLMAN, A. L., BLACKWOOD, E. M., SRIVASTAVA, J., MADSON, N., SCHILLING, J. W., WRIGHT, J. H. & BARBER, D. L. 2006. The Nck-interacting kinase phosphorylates ERM

proteins for formation of lamellipodium by growth factors. *Proc Natl Acad Sci U S A,* 103**,** 13391-6.

BELKINA, N. V., LIU, Y., HAO, J. J., KARASUYAMA, H. & SHAW, S. 2009. LOK is a major ERM kinase in resting lymphocytes and regulates cytoskeletal rearrangement through ERM phosphorylation. *Proc Natl Acad Sci U S A,* 106**,** 4707-12.

BELLAICHE, Y., BEAUDOIN-MASSIANI, O., STUTTEM, I. & SCHWEISGUTH, F. 2004. The planar cell polarity protein Strabismus promotes Pins anterior localization during asymmetric division of sensory organ precursor cells in Drosophila. *Development,* 131**,** 469-78.

BELLAICHE, Y., GHO, M., KALTSCHMIDT, J. A., BRAND, A. H. & SCHWEISGUTH, F. 2001. Frizzled regulates localization of cell-fate determinants and mitotic spindle rotation during asymmetric cell division. *Nat Cell Biol,* 3**,** 50-7.

BEN-AISSA, K., PATINO-LOPEZ, G., BELKINA, N. V., MANITI, O., ROSALES, T., HAO, J. J., KRUHLAK, M. J., KNUTSON, J. R., PICART, C. & SHAW, S. 2012. Activation of moesin, a protein that links actin cytoskeleton to the plasma membrane, occurs by phosphatidylinositol 4,5-bisphosphate (PIP2) binding sequentially to two sites and releasing an autoinhibitory linker. *J Biol Chem,* 287**,** 16311-23.

BENNETT, D., LYULCHEVA, E., ALPHEY, L. & HAWCROFT, G. 2006. Towards a comprehensive analysis of the protein phosphatase 1 interactome in Drosophila. *J Mol Biol,* 364**,** 196-212.

BERDNIK, D. & KNOBLICH, J. A. 2002. Drosophila Aurora-A is required for centrosome maturation and actin-dependent asymmetric protein localization during mitosis. *Curr Biol,* 12**,** 640-7.

BETTENCOURT-DIAS, M., RODRIGUES-MARTINS, A., CARPENTER, L., RIPARBELLI, M., LEHMANN, L., GATT, M. K., CARMO, N., BALLOUX, F., CALLAINI, G. & GLOVER, D. M. 2005. SAK/PLK4 is required for centriole duplication and flagella development. *Curr Biol,* 15**,** 2199-207.

BEZANILLA, M. & WADSWORTH, P. 2009. Spindle positioning: actin mediates pushing and pulling. *Curr Biol,* 19**,** R168-9.

BIELING, P., TELLEY, I. A. & SURREY, T. 2010. A minimal midzone protein module controls formation and length of antiparallel microtubule overlaps. *Cell,* 142**,** 420-32.

BLACHON, S., GOPALAKRISHNAN, J., OMORI, Y., POLYANOVSKY, A., CHURCH, A., NICASTRO, D., MALICKI, J. & AVIDOR-REISS, T. 2008. Drosophila asterless and vertebrate Cep152 Are orthologs essential for centriole duplication. *Genetics,* 180**,** 2081-94.

BLIN, G., MARGEAT, E., CARVALHO, K., ROYER, C. A., ROY, C. & PICART, C. 2008. Quantitative analysis of the binding of ezrin to large unilamellar vesicles containing phosphatidylinositol 4,5 bisphosphate. *Biophys J,* 94**,** 1021-33.

BLOECHER, A. & TATCHELL, K. 2000. Dynamic localization of protein phosphatase type 1 in the mitotic cell cycle of Saccharomyces cerevisiae. *J Cell Biol,* 149**,** 125-40.

BOHNERT, K. A., WILLET, A. H., KOVAR, D. R. & GOULD, K. L. 2013. Formin-based control of the actin cytoskeleton during cytokinesis. *Biochem Soc Trans,* 41**,** 1750-4.

BOLLEN, M., GERLICH, D. W. & LESAGE, B. 2009. Mitotic phosphatases: from entry guards to exit guides. *Trends Cell Biol,* 19**,** 531-41.

BOLLEN, M., PETI, W., RAGUSA, M. J. & BEULLENS, M. 2010. The extended PP1 toolkit: designed to create specificity. *Trends Biochem Sci,* 35**,** 450-8.

BONACCORSI, S., GIANSANTI, M. G. & GATTI, M. 1998. Spindle self-organization and cytokinesis during male meiosis in asterless mutants of Drosophila melanogaster. *J Cell Biol,* 142**,** 751-61.

BOSVELD, F., BONNET, I., GUIRAO, B., TLILI, S., WANG, Z., PETITALOT, A., MARCHAND, R., BARDET, P. L., MARCQ, P., GRANER, F. & BELLAICHE, Y. 2012. Mechanical control of morphogenesis by Fat/Dachsous/Four-jointed planar cell polarity pathway. *Science,* 336**,** 724-7.

BOUCROT, E. & KIRCHHAUSEN, T. 2007. Endosomal recycling controls plasma membrane area during mitosis. *Proc Natl Acad Sci U S A,* 104**,** 7939-44.

BOUCROT, E. & KIRCHHAUSEN, T. 2008. Mammalian cells change volume during mitosis. *PLoS One,* 3**,** e1477.

BOURBON, H. M., GONZY-TREBOUL, G., PERONNET, F., ALIN, M. F., ARDOUREL, C., BENASSAYAG, C., CRIBBS, D., DEUTSCH, J., FERRER, P., HAENLIN, M., LEPESANT, J. A., NOSELLI, S. & VINCENT, A. 2002. A P-insertion screen identifying novel X-linked essential genes in Drosophila. *Mech Dev,* 110**,** 71-83.

BOVELLAN, M., ROMEO, Y., BIRO, M., BODEN, A., CHUGH, P., YONIS, A., VAGHELA, M., FRITZSCHE, M., MOULDING, D., THOROGATE, R., JEGOU, A., THRASHER, A. J., ROMET-LEMONNE, G., ROUX, P. P., PALUCH, E. K. & CHARRAS, G. 2014. Cellular control of cortical actin nucleation. *Curr Biol,* 24**,** 1628-35.

BRAND, A. H. & PERRIMON, N. 1993. Targeted gene expression as a means of altering cell fates and generating dominant phenotypes. *Development,* 118**,** 401-15.

BRAY, D. & WHITE, J. G. 1988. Cortical flow in animal cells. *Science,* 239**,** 883-8.

BRETSCHER, A., EDWARDS, K. & FEHON, R. G. 2002. ERM proteins and merlin: integrators at the cell cortex. *Nat Rev Mol Cell Biol,* 3**,** 586-99.

BRETSCHER, A., GARY, R. & BERRYMAN, M. 1995. Soluble ezrin purified from placenta exists as stable monomers and elongated dimers with masked C-terminal ezrin-radixin-moesin association domains. *Biochemistry,* 34**,** 16830-7.

BRETSCHNEIDER, T., ANDERSON, K., ECKE, M., MULLER-TAUBENBERGER, A., SCHROTH-DIEZ, B., ISHIKAWA-ANKERHOLD, H. C. & GERISCH, G. 2009. The three-dimensional dynamics of actin waves, a model of cytoskeletal self-organization. *Biophys J,* 96**,** 2888-900.

BRINGMANN, H. & HYMAN, A. A. 2005. A cytokinesis furrow is positioned by two consecutive signals. *Nature,* 436**,** 731-4.

BUSINO, L., CHIESA, M., DRAETTA, G. F. & DONZELLI, M. 2004. Cdc25A phosphatase: combinatorial phosphorylation, ubiquitylation and proteolysis. *Oncogene,* 23**,** 2050-6.

BUSSON, D. & PRET, A. M. 2007. GAL4/UAS targeted gene expression for studying Drosophila Hedgehog signaling. *Methods Mol Biol,* 397**,** 161-201.

CABERNARD, C., PREHODA, K. E. & DOE, C. Q. 2010. A spindle-independent cleavage furrow positioning pathway. *Nature,* 467**,** 91-4.

CADART, C., ZLOTEK-ZLOTKIEWICZ, E., LE BERRE, M., PIEL, M. & MATTHEWS, H. K. 2014. Exploring the function of cell shape and size during mitosis. *Dev Cell,* 29**,** 159-69.

CALLEJA, M., HERRANZ, H., ESTELLA, C., CASAL, J., LAWRENCE, P., SIMPSON, P. & MORATA, G. 2000. Generation of medial and lateral dorsal body domains by the pannier gene of Drosophila. *Development,* 127**,** 3971-80.

CALLEJA, M., RENAUD, O., USUI, K., PISTILLO, D., MORATA, G. & SIMPSON, P. 2002. How to pattern an epithelium: lessons from achaete-scute regulation on the notum of Drosophila. *Gene,* 292**,** 1-12.

CANMAN, J. C., LEWELLYN, L., LABAND, K., SMERDON, S. J., DESAI, A., BOWERMAN, B. & OEGEMA, K. 2008. Inhibition of Rac by the GAP activity of centralspindlin is essential for cytokinesis. *Science,* 322**,** 1543-6.

CAO, J., CREST, J., FASULO, B. & SULLIVAN, W. 2010. Cortical actin dynamics facilitate early-stage centrosome separation. *Curr Biol,* 20**,** 770-6.

CARLSSON, A. E. 2010. Actin dynamics: from nanoscale to microscale. *Annu Rev Biophys,* 39**,** 91-110.

CARMENA, M., RUCHAUD, S. & EARNSHAW, W. C. 2009. Making the Auroras glow: regulation of Aurora A and B kinase function by interacting proteins. *Curr Opin Cell Biol,* 21**,** 796-805.

CARMENA, M., WHEELOCK, M., FUNABIKI, H. & EARNSHAW, W. C. 2012. The chromosomal passenger complex (CPC): from easy rider to the godfather of mitosis. *Nat Rev Mol Cell Biol,* 13**,** 789-803.

CARRENO, S., KOURANTI, I., GLUSMAN, E. S., FULLER, M. T., ECHARD, A. & PAYRE, F. 2008. Moesin and its activating kinase Slik are required for cortical stability and microtubule organization in mitotic cells. *J Cell Biol,* 180**,** 739-46.

CASALETTO, J. B., SAOTOME, I., CURTO, M. & MCCLATCHEY, A. I. 2011. Ezrin-mediated apical integrity is required for intestinal homeostasis. *Proc Natl Acad Sci U S A,* 108**,** 11924-9.

CASTANON, I., ABRAMI, L., HOLTZER, L., HEISENBERG, C. P., VAN DER GOOT, F. G. & GONZALEZ-GAITAN, M. 2013. Anthrax toxin receptor 2a controls mitotic spindle positioning. *Nat Cell Biol,* 15**,** 28-39.

CASTRO, B., BAROLO, S., BAILEY, A. M. & POSAKONY, J. W. 2005. Lateral inhibition in proneural clusters: cis-regulatory logic and default repression by Suppressor of Hairless. *Development,* 132**,** 3333-44.

CHAIGNE, A., CAMPILLO, C., GOV, N. S., VOITURIEZ, R., AZOURY, J., UMANA-DIAZ, C., ALMONACID, M., QUEGUINER, I., NASSOY, P., SYKES, C., VERLHAC, M. H. & TERRET, M. E. 2013. A soft cortex is essential for asymmetric spindle positioning in mouse oocytes. *Nat Cell Biol,* 15**,** 958-66.

CHALKLEY, H. W. 1951. Control of fission in Amoeba proteus as related to the mechanism of cell division. *Ann N Y Acad Sci,* 51**,** 1303-10.

CHARRAS, G. & PALUCH, E. 2008. Blebs lead the way: how to migrate without lamellipodia. *Nat Rev Mol Cell Biol,* 9**,** 730-6.

CHARRAS, G. T., COUGHLIN, M., MITCHISON, T. J. & MAHADEVAN, L. 2008. Life and times of a cellular bleb. *Biophys J,* 94**,** 1836-53.

CHARRAS, G. T., HU, C. K., COUGHLIN, M. & MITCHISON, T. J. 2006. Reassembly of contractile actin cortex in cell blebs. *J Cell Biol,* 175**,** 477-90.

CHEN, F., ARCHAMBAULT, V., KAR, A., LIO, P., D'AVINO, P. P., SINKA, R., LILLEY, K., LAUE, E. D., DEAK, P., CAPALBO, L. & GLOVER, D. M. 2007. Multiple protein phosphatases are required for mitosis in Drosophila. *Curr Biol,* 17**,** 293-303.

CHEN, W., FOSS, M., TSENG, K. F. & ZHANG, D. 2008. Redundant mechanisms recruit actin into the contractile ring in silkworm spermatocytes. *PLoS Biol,* 6**,** e209.

CHENG, J., TIYABOONCHAI, A., YAMASHITA, Y. M. & HUNT, A. J. 2011. Asymmetric division of cyst stem cells in Drosophila testis is ensured by anaphase spindle repositioning. *Development,* 138**,** 831-7.

CHISHTI, A. H., KIM, A. C., MARFATIA, S. M., LUTCHMAN, M., HANSPAL, M., JINDAL, H., LIU, S. C., LOW, P. S., ROULEAU, G. A., MOHANDAS, N., CHASIS, J. A., CONBOY, J. G., GASCARD, P., TAKAKUWA, Y., HUANG, S. C., BENZ, E. J., JR., BRETSCHER, A., FEHON, R. G., GUSELLA, J. F., RAMESH, V., SOLOMON, F., MARCHESI, V. T., TSUKITA, S., HOOVER, K. B. & ET AL. 1998. The FERM domain: a unique module involved in the linkage of cytoplasmic proteins to the membrane. *Trends Biochem Sci,* 23**,** 281-2.

CIFERRI, C., MUSACCHIO, A. & PETROVIC, A. 2007. The Ndc80 complex: hub of kinetochore activity. *FEBS Lett,* 581**,** 2862-9.

CLARK, A. G., DIERKES, K. & PALUCH, E. K. 2013. Monitoring actin cortex thickness in live cells. *Biophys J,* 105**,** 570-80.

CLARKE, A. S., TANG, T. T., OOI, D. L. & ORR-WEAVER, T. L. 2005. POLO kinase regulates the Drosophila centromere cohesion protein MEI-S332. *Dev Cell,* 8**,** 53-64.

COHEN, M., GEORGIOU, M., STEVENSON, N. L., MIODOWNIK, M. & BAUM, B. 2010. Dynamic filopodia transmit intermittent Delta-Notch signaling to drive pattern refinement during lateral inhibition. *Dev Cell,* 19**,** 78-89.

COUDREUSE, D. & NURSE, P. 2010. Driving the cell cycle with a minimal CDK control network. *Nature,* 468**,** 1074-9.

COWAN, C. R. & HYMAN, A. A. 2004. Centrosomes direct cell polarity independently of microtubule assembly in C. elegans embryos. *Nature,* 431**,** 92-6.

CRAMER, L. P. & MITCHISON, T. J. 1997. Investigation of the mechanism of retraction of the cell margin and rearward flow of nodules during mitotic cell rounding. *Mol Biol Cell,* 8**,** 109-19.

CUBADDA, Y., HEITZLER, P., RAY, R. P., BOUROUIS, M., RAMAIN, P., GELBART, W., SIMPSON, P. & HAENLIN, M. 1997. u-shaped encodes a zinc finger protein that regulates the proneural genes achaete and scute during the formation of bristles in Drosophila. *Genes Dev,* 11**,** 3083-95.

CUNDELL, M. J., BASTOS, R. N., ZHANG, T., HOLDER, J., GRUNEBERG, U., NOVAK, B. & BARR, F. A. 2013. The BEG (PP2A-

B55/ENSA/Greatwall) pathway ensures cytokinesis follows chromosome separation. *Mol Cell,* 52**,** 393-405.

D'AVINO, P. P., ARCHAMBAULT, V., PRZEWLOKA, M. R., ZHANG, W., LILLEY, K. S., LAUE, E. & GLOVER, D. M. 2007. Recruitment of Polo kinase to the spindle midzone during cytokinesis requires the Feo/Klp3A complex. *PLoS One,* 2**,** e572.

D'AVINO, P. P., SAVOIAN, M. S., CAPALBO, L. & GLOVER, D. M. 2006. RacGAP50C is sufficient to signal cleavage furrow formation during cytokinesis. *J Cell Sci,* 119**,** 4402-8.

DAI, J., SULLIVAN, B. A. & HIGGINS, J. M. 2006. Regulation of mitotic chromosome cohesion by Haspin and Aurora B. *Dev Cell,* 11**,** 741-50.

DAO, V. T., DUPUY, A. G., GAVET, O., CARON, E. & DE GUNZBURG, J. 2009. Dynamic changes in Rap1 activity are required for cell retraction and spreading during mitosis. *J Cell Sci,* 122**,** 2996-3004.

DE CELIS, J. F., BARRIO, R. & KAFATOS, F. C. 1999. Regulation of the spalt/spalt-related gene complex and its function during sensory organ development in the Drosophila thorax. *Development,* 126**,** 2653-62.

DEAN, S. O., ROGERS, S. L., STUURMAN, N., VALE, R. D. & SPUDICH, J. A. 2005. Distinct pathways control recruitment and maintenance of myosin II at the cleavage furrow during cytokinesis. *Proc Natl Acad Sci U S A,* 102**,** 13473-8.

DEBIASIO, R. L., LAROCCA, G. M., POST, P. L. & TAYLOR, D. L. 1996. Myosin II transport, organization, and phosphorylation: evidence for cortical flow/solation-contraction coupling during cytokinesis and cell locomotion. *Mol Biol Cell,* 7**,** 1259-82.

DEHAPIOT, B., CARRIERE, V., CARROLL, J. & HALET, G. 2013. Polarized Cdc42 activation promotes polar body protrusion and asymmetric division in mouse oocytes. *Dev Biol,* 377**,** 202-12.

DEHAPIOT, B. & HALET, G. 2013. Ran GTPase promotes oocyte polarization by regulating ERM (Ezrin/Radixin/Moesin) inactivation. *Cell Cycle,* 12**,** 1672-8.

DENG, M., SURANENI, P., SCHULTZ, R. M. & LI, R. 2007. The Ran GTPase mediates chromatin signaling to control cortical polarity during polar body extrusion in mouse oocytes. *Dev Cell,* 12**,** 301-8.

DIETZL, G., CHEN, D., SCHNORRER, F., SU, K. C., BARINOVA, Y., FELLNER, M., GASSER, B., KINSEY, K., OPPEL, S., SCHEIBLAUER, S., COUTO, A., MARRA, V., KELEMAN, K. & DICKSON, B. J. 2007. A genome-wide transgenic RNAi library for conditional gene inactivation in Drosophila. *Nature,* 448**,** 151-6.

DOI, Y., ITOH, M., YONEMURA, S., ISHIHARA, S., TAKANO, H., NODA, T. & TSUKITA, S. 1999. Normal development of mice and unimpaired cell adhesion/cell motility/actin-based cytoskeleton without compensatory up-regulation of ezrin or radixin in moesin gene knockout. *J Biol Chem,* 274**,** 2315-21.

DOUGLAS, M. E., DAVIES, T., JOSEPH, N. & MISHIMA, M. 2010. Aurora B and 14-3-3 coordinately regulate clustering of centralspindlin during cytokinesis. *Curr Biol,* 20**,** 927-33.

DUNSCH, A. K., LINNANE, E., BARR, F. A. & GRUNEBERG, U. 2011. The astrin-kinastrin/SKAP complex localizes to microtubule plus ends and facilitates chromosome alignment. *J Cell Biol,* 192**,** 959-68.

EISENMANN, K. M., HARRIS, E. S., KITCHEN, S. M., HOLMAN, H. A., HIGGS, H. N. & ALBERTS, A. S. 2007. Dia-interacting protein modulates formin-mediated actin assembly at the cell cortex. *Curr Biol,* 17**,** 579-91.

ELLIOTT, D. A. & BRAND, A. H. 2008. The GAL4 system : a versatile system for the expression of genes. *Methods Mol Biol,* 420**,** 79-95.

EMANUELE, M. J., LAN, W., JWA, M., MILLER, S. A., CHAN, C. S. & STUKENBERG, P. T. 2008. Aurora B kinase and protein phosphatase 1 have opposing roles in modulating kinetochore assembly. *J Cell Biol,* 181**,** 241-54.

EMERY, G., HUTTERER, A., BERDNIK, D., MAYER, B., WIRTZ-PEITZ, F., GAITAN, M. G. & KNOBLICH, J. A. 2005. Asymmetric Rab 11 endosomes regulate delta recycling and specify cell fate in the Drosophila nervous system. *Cell,* 122**,** 763-73.

ENSERINK, J. M. & KOLODNER, R. D. 2010. An overview of Cdk1-controlled targets and processes. *Cell Div,* 5**,** 11.

ERBEN, V., WALDHUBER, M., LANGER, D., FETKA, I., JANSEN, R. P. & PETRITSCH, C. 2008. Asymmetric localization of the adaptor protein

Miranda in neuroblasts is achieved by diffusion and sequential interaction of Myosin II and VI. *J Cell Sci,* 121**,** 1403-14.

ESPEUT, J., CHEERAMBATHUR, D. K., KRENNING, L., OEGEMA, K. & DESAI, A. 2012. Microtubule binding by KNL-1 contributes to spindle checkpoint silencing at the kinetochore. *J Cell Biol,* 196**,** 469-82.

ETO, M., KIRKBRIDE, J. A. & BRAUTIGAN, D. L. 2005. Assembly of MYPT1 with protein phosphatase-1 in fibroblasts redirects localization and reorganizes the actin cytoskeleton. *Cell Motil Cytoskeleton,* 62**,** 100-9.

EUTENEUER, U. & MCINTOSH, J. R. 1980. Polarity of midbody and phragmoplast microtubules. *J Cell Biol,* 87**,** 509-15.

FANG, G., YU, H. & KIRSCHNER, M. W. 1998. The checkpoint protein MAD2 and the mitotic regulator CDC20 form a ternary complex with the anaphase-promoting complex to control anaphase initiation. *Genes Dev,* 12**,** 1871-83.

FEHON, R. G., MCCLATCHEY, A. I. & BRETSCHER, A. 2010. Organizing the cell cortex: the role of ERM proteins. *Nat Rev Mol Cell Biol,* 11**,** 276-87.

FEIJAO, T., AFONSO, O., MAIA, A. F. & SUNKEL, C. E. 2013. Stability of kinetochore-microtubule attachment and the role of different KMN network components in Drosophila. *Cytoskeleton (Hoboken),* 70**,** 661-75.

FICHELSON, P. & GHO, M. 2003. The glial cell undergoes apoptosis in the microchaete lineage of Drosophila. *Development,* 130**,** 123-33.

FIELD, C. M., COUGHLIN, M., DOBERSTEIN, S., MARTY, T. & SULLIVAN, W. 2005. Characterization of anillin mutants reveals essential roles in septin localization and plasma membrane integrity. *Development,* 132**,** 2849-60.

FIEVET, B., LOUVARD, D. & ARPIN, M. 2007. ERM proteins in epithelial cell organization and functions. *Biochim Biophys Acta,* 1773**,** 653-60.

FIEVET, B. T., GAUTREAU, A., ROY, C., DEL MAESTRO, L., MANGEAT, P., LOUVARD, D. & ARPIN, M. 2004. Phosphoinositide binding and phosphorylation act sequentially in the activation mechanism of ezrin. *J Cell Biol,* 164**,** 653-9.

FINK, J., CARPI, N., BETZ, T., BETARD, A., CHEBAH, M., AZIOUNE, A., BORNENS, M., SYKES, C., FETLER, L., CUVELIER, D. & PIEL, M.

2011. External forces control mitotic spindle positioning. *Nat Cell Biol,* 13**,** 771-8.

FISCHER-FRIEDRICH, E., HYMAN, A. A., JULICHER, F., MULLER, D. J. & HELENIUS, J. 2014. Quantification of surface tension and internal pressure generated by single mitotic cells. *Sci Rep,* 4**,** 6213.

FLETCHER, D. A. & MULLINS, R. D. 2010. Cell mechanics and the cytoskeleton. *Nature,* 463**,** 485-92.

FOE, V. E., FIELD, C. M. & ODELL, G. M. 2000. Microtubules and mitotic cycle phase modulate spatiotemporal distributions of F-actin and myosin II in Drosophila syncytial blastoderm embryos. *Development,* 127**,** 1767-87.

FOE, V. E. & VON DASSOW, G. 2008. Stable and dynamic microtubules coordinately shape the myosin activation zone during cytokinetic furrow formation. *J Cell Biol,* 183**,** 457-70.

FOUNOUNOU, N., LOYER, N. & LE BORGNE, R. 2013. Septins regulate the contractility of the actomyosin ring to enable adherens junction remodeling during cytokinesis of epithelial cells. *Dev Cell,* 24**,** 242-55.

FROMENTAL-RAMAIN, C., VANOLST, L., DELAPORTE, C. & RAMAIN, P. 2008. pannier encodes two structurally related isoforms that are differentially expressed during Drosophila development and display distinct functions during thorax patterning. *Mech Dev,* 125**,** 43-57.

FUJIBUCHI, T., ABE, Y., TAKEUCHI, T., IMAI, Y., KAMEI, Y., MURASE, R., UEDA, N., SHIGEMOTO, K., YAMAMOTO, H. & KITO, K. 2005. AIP1/WDR1 supports mitotic cell rounding. *Biochem Biophys Res Commun,* 327**,** 268-75.

FUKATA, Y., KIMURA, K., OSHIRO, N., SAYA, H., MATSUURA, Y. & KAIBUCHI, K. 1998. Association of the myosin-binding subunit of myosin phosphatase and moesin: dual regulation of moesin phosphorylation by Rho-associated kinase and myosin phosphatase. *J Cell Biol,* 141**,** 409-18.

FULLER, B. G., LAMPSON, M. A., FOLEY, E. A., ROSASCO-NITCHER, S., LE, K. V., TOBELMANN, P., BRAUTIGAN, D. L., STUKENBERG, P. T. & KAPOOR, T. M. 2008. Midzone activation of aurora B in anaphase produces an intracellular phosphorylation gradient. *Nature,* 453**,** 1132-6.

FUNG, T. K. & POON, R. Y. 2005. A roller coaster ride with the mitotic cyclins. *Semin Cell Dev Biol,* 16**,** 335-42.

GAILLARD, J., NEUMANN, E., VAN DAMME, D., STOPPIN-MELLET, V., EBEL, C., BARBIER, E., GEELEN, D. & VANTARD, M. 2008. Two microtubule-associated proteins of Arabidopsis MAP65s promote antiparallel microtubule bundling. *Mol Biol Cell,* 19**,** 4534-44.

GARCIA-GARCIA, M. J., RAMAIN, P., SIMPSON, P. & MODOLELL, J. 1999. Different contributions of pannier and wingless to the patterning of the dorsal mesothorax of Drosophila. *Development,* 126**,** 3523-32.

GARY, R. & BRETSCHER, A. 1993. Heterotypic and homotypic associations between ezrin and moesin, two putative membrane-cytoskeletal linking proteins. *Proc Natl Acad Sci U S A,* 90**,** 10846-50.

GARY, R. & BRETSCHER, A. 1995. Ezrin self-association involves binding of an N-terminal domain to a normally masked C-terminal domain that includes the F-actin binding site. *Mol Biol Cell,* 6**,** 1061-75.

GEORGIOU, M. & BAUM, B. 2010. Polarity proteins and Rho GTPases cooperate to spatially organise epithelial actin-based protrusions. *J Cell Sci,* 123**,** 1089-98.

GHARBI-AYACHI, A., LABBE, J. C., BURGESS, A., VIGNERON, S., STRUB, J. M., BRIOUDES, E., VAN-DORSSELAER, A., CASTRO, A. & LORCA, T. 2010. The substrate of Greatwall kinase, Arpp19, controls mitosis by inhibiting protein phosphatase 2A. *Science,* 330**,** 1673-7.

GHO, M., BELLAICHE, Y. & SCHWEISGUTH, F. 1999. Revisiting the Drosophila microchaete lineage: a novel intrinsically asymmetric cell division generates a glial cell. *Development,* 126**,** 3573-84.

GHO, M. & SCHWEISGUTH, F. 1998. Frizzled signalling controls orientation of asymmetric sense organ precursor cell divisions in Drosophila. *Nature,* 393**,** 178-81.

GLOTZER, M. 2005. The molecular requirements for cytokinesis. *Science,* 307**,** 1735-9.

GLOTZER, M. 2009. The 3Ms of central spindle assembly: microtubules, motors and MAPs. *Nat Rev Mol Cell Biol,* 10**,** 9-20.

GOEHRING, N. W., TRONG, P. K., BOIS, J. S., CHOWDHURY, D., NICOLA, E. M., HYMAN, A. A. & GRILL, S. W. 2011. Polarization of PAR

proteins by advective triggering of a pattern-forming system. *Science,* 334**,** 1137-41.

GOSHIMA, G., NEDELEC, F. & VALE, R. D. 2005. Mechanisms for focusing mitotic spindle poles by minus end-directed motor proteins. *J Cell Biol,* 171**,** 229-40.

GRAY, R. S., ROSZKO, I. & SOLNICA-KREZEL, L. 2011. Planar cell polarity: coordinating morphogenetic cell behaviors with embryonic polarity. *Dev Cell,* 21**,** 120-33.

GREEN, R. A., PALUCH, E. & OEGEMA, K. 2012. Cytokinesis in animal cells. *Annu Rev Cell Dev Biol,* 28**,** 29-58.

GRIEDER, N. C., MORATA, G., AFFOLTER, M. & GEHRING, W. J. 2009. Spalt major controls the development of the notum and of wing hinge primordia of the Drosophila melanogaster wing imaginal disc. *Dev Biol,* 329**,** 315-26.

GRUNEBERG, U., NEEF, R., LI, X., CHAN, E. H., CHALAMALASETTY, R. B., NIGG, E. A. & BARR, F. A. 2006. KIF14 and citron kinase act together to promote efficient cytokinesis. *J Cell Biol,* 172**,** 363-72.

GRUSCHE, F. A., HIDALGO, C., FLETCHER, G., SUNG, H. H., SAHAI, E. & THOMPSON, B. J. 2009. Sds22, a PP1 phosphatase regulatory subunit, regulates epithelial cell polarity and shape [Sds22 in epithelial morphology]. *BMC Dev Biol,* 9**,** 14.

GUCK, J., ANANTHAKRISHNAN, R., MAHMOOD, H., MOON, T. J., CUNNINGHAM, C. C. & KAS, J. 2001. The optical stretcher: a novel laser tool to micromanipulate cells. *Biophys J,* 81**,** 767-84.

GUILLOT, C. & LECUIT, T. 2013. Adhesion disengagement uncouples intrinsic and extrinsic forces to drive cytokinesis in epithelial tissues. *Dev Cell,* 24**,** 227-41.

GUSE, A., MISHIMA, M. & GLOTZER, M. 2005. Phosphorylation of ZEN-4/MKLP1 by aurora B regulates completion of cytokinesis. *Curr Biol,* 15**,** 778-86.

HAGA, H., NAGAYAMA, M., KAWABATA, K., ITO, E., USHIKI, T. & SAMBONGI, T. 2000. Time-lapse viscoelastic imaging of living fibroblasts using force modulation mode in AFM. *J Electron Microsc (Tokyo),* 49**,** 473-81.

HANAKAM, F., ALBRECHT, R., ECKERSKORN, C., MATZNER, M. & GERISCH, G. 1996. Myristoylated and non-myristoylated forms of the pH sensor protein hisactophilin II: intracellular shuttling to plasma membrane and nucleus monitored in real time by a fusion with green fluorescent protein. *EMBO J,* 15**,** 2935-43.

HANNAK, E., KIRKHAM, M., HYMAN, A. A. & OEGEMA, K. 2001. Aurora-A kinase is required for centrosome maturation in Caenorhabditis elegans. *J Cell Biol,* 155**,** 1109-16.

HANNEMANN, S., MADRID, R., STASTNA, J., KITZING, T., GASTEIER, J., SCHONICHEN, A., BOUCHET, J., JIMENEZ, A., GEYER, M., GROSSE, R., BENICHOU, S. & FACKLER, O. T. 2008. The Diaphanous-related Formin FHOD1 associates with ROCK1 and promotes Src-dependent plasma membrane blebbing. *J Biol Chem,* 283**,** 27891-903.

HANZEL, D., REGGIO, H., BRETSCHER, A., FORTE, J. G. & MANGEAT, P. 1991. The secretion-stimulated 80K phosphoprotein of parietal cells is ezrin, and has properties of a membrane cytoskeletal linker in the induced apical microvilli. *EMBO J,* 10**,** 2363-73.

HARRIS, A. 1973. Location of cellular adhesions to solid substrata. *Dev Biol,* 35**,** 97-114.

HARTENSTEIN, V. & POSAKONY, J. W. 1989. Development of adult sensilla on the wing and notum of Drosophila melanogaster. *Development,* 107**,** 389-405.

HARTMANN, C. & JACKLE, H. 1995. Spatiotemporal relationships between a novel Drosophila stripe expressing gene and known segmentation genes by simultaneous visualization of transcript patterns. *Chromosoma,* 104**,** 84-91.

HARVEY, S. L., CHARLET, A., HAAS, W., GYGI, S. P. & KELLOGG, D. R. 2005. Cdk1-dependent regulation of the mitotic inhibitor Wee1. *Cell,* 122**,** 407-20.

HEBERT, A. M., DUBOFF, B., CASALETTO, J. B., GLADDEN, A. B. & MCCLATCHEY, A. I. 2012. Merlin/ERM proteins establish cortical asymmetry and centrosome position. *Genes Dev,* 26**,** 2709-23.

HEBERT, M., POTIN, S., SEBBAGH, M., BERTOGLIO, J., BREARD, J. & HAMELIN, J. 2008. Rho-ROCK-dependent ezrin-radixin-moesin

phosphorylation regulates Fas-mediated apoptosis in Jurkat cells. *J Immunol,* 181**,** 5963-73.

HECHT, I., KESSLER, D. A. & LEVINE, H. 2010. Transient localized patterns in noise-driven reaction-diffusion systems. *Phys Rev Lett,* 104**,** 158301.

HEGARAT, N., SMITH, E., NAYAK, G., TAKEDA, S., EYERS, P. A. & HOCHEGGER, H. 2011. Aurora A and Aurora B jointly coordinate chromosome segregation and anaphase microtubule dynamics. *J Cell Biol,* 195**,** 1103-13.

HEITZLER, P., BOUROUIS, M., RUEL, L., CARTERET, C. & SIMPSON, P. 1996. Genes of the Enhancer of split and achaete-scute complexes are required for a regulatory loop between Notch and Delta during lateral signalling in Drosophila. *Development,* 122**,** 161-71.

HERSZTERG, S., LEIBFRIED, A., BOSVELD, F., MARTIN, C. & BELLAICHE, Y. 2013. Interplay between the dividing cell and its neighbors regulates adherens junction formation during cytokinesis in epithelial tissue. *Dev Cell,* 24**,** 256-70.

HICKSON, G. R., ECHARD, A. & O'FARRELL, P. H. 2006. Rho-kinase controls cell shape changes during cytokinesis. *Curr Biol,* 16**,** 359-70.

HIPFNER, D. R. & COHEN, S. M. 2003. The Drosophila sterile-20 kinase slik controls cell proliferation and apoptosis during imaginal disc development. *PLoS Biol,* 1**,** E35.

HIPFNER, D. R., KELLER, N. & COHEN, S. M. 2004. Slik Sterile-20 kinase regulates Moesin activity to promote epithelial integrity during tissue growth. *Genes Dev,* 18**,** 2243-8.

HIRATA, T., NOMACHI, A., TOHYA, K., MIYASAKA, M., TSUKITA, S., WATANABE, T. & NARUMIYA, S. 2012. Moesin-deficient mice reveal a non-redundant role for moesin in lymphocyte homeostasis. *Int Immunol,* 24**,** 705-17.

HOCHEGGER, H., HEGARAT, N. & PEREIRA-LEAL, J. B. 2013. Aurora at the pole and equator: overlapping functions of Aurora kinases in the mitotic spindle. *Open Biol,* 3**,** 120185.

HUGHES, S. C. & FEHON, R. G. 2006. Phosphorylation and activity of the tumor suppressor Merlin and the ERM protein Moesin are coordinately regulated by the Slik kinase. *J Cell Biol,* 175**,** 305-13.

HUGHES, S. C., FORMSTECHER, E. & FEHON, R. G. 2010. Sip1, the Drosophila orthologue of EBP50/NHERF1, functions with the sterile 20 family kinase Slik to regulate Moesin activity. *J Cell Sci,* 123**,** 1099-107.

HUXLEY, A. F. 2000. Mechanics and models of the myosin motor. *Philos Trans R Soc Lond B Biol Sci,* 355**,** 433-40.

IKEBE, M. 2008. Regulation of the function of mammalian myosin and its conformational change. *Biochem Biophys Res Commun,* 369**,** 157-64.

JANKOVICS, F., SINKA, R., LUKACSOVICH, T. & ERDELYI, M. 2002. MOESIN crosslinks actin and cell membrane in Drosophila oocytes and is required for OSKAR anchoring. *Curr Biol,* 12**,** 2060-5.

JANSSENS, V., LONGIN, S. & GORIS, J. 2008. PP2A holoenzyme assembly: in cauda venenum (the sting is in the tail). *Trends Biochem Sci,* 33**,** 113-21.

JEON, S., KIM, S., PARK, J. B., SUH, P. G., KIM, Y. S., BAE, C. D. & PARK, J. 2002. RhoA and Rho kinase-dependent phosphorylation of moesin at Thr-558 in hippocampal neuronal cells by glutamate. *J Biol Chem,* 277**,** 16576-84.

JIANG, Y., SCOTT, K. L., KWAK, S. J., CHEN, R. & MARDON, G. 2011. Sds22/PP1 links epithelial integrity and tumor suppression via regulation of myosin II and JNK signaling. *Oncogene,* 30**,** 3248-60.

KAJI, N., MURAMOTO, A. & MIZUNO, K. 2008. LIM kinase-mediated cofilin phosphorylation during mitosis is required for precise spindle positioning. *J Biol Chem,* 283**,** 4983-92.

KARAGIOSIS, S. A. & READY, D. F. 2004. Moesin contributes an essential structural role in Drosophila photoreceptor morphogenesis. *Development,* 131**,** 725-32.

KAUR, S., FIELDING, A. B., GASSNER, G., CARTER, N. J. & ROYLE, S. J. 2014. An unmet actin requirement explains the mitotic inhibition of clathrin-mediated endocytosis. *Elife,* 3**,** e00829.

KIKUCHI, S., HATA, M., FUKUMOTO, K., YAMANE, Y., MATSUI, T., TAMURA, A., YONEMURA, S., YAMAGISHI, H., KEPPLER, D. & TSUKITA, S. 2002. Radixin deficiency causes conjugated hyperbilirubinemia with loss of Mrp2 from bile canalicular membranes. *Nat Genet,* 31**,** 320-5.

KIM, Y., HOLLAND, A. J., LAN, W. & CLEVELAND, D. W. 2010. Aurora kinases and protein phosphatase 1 mediate chromosome congression through regulation of CENP-E. *Cell,* 142**,** 444-55.

KINOSHITA, K., NOETZEL, T. L., PELLETIER, L., MECHTLER, K., DRECHSEL, D. N., SCHWAGER, A., LEE, M., RAFF, J. W. & HYMAN, A. A. 2005. Aurora A phosphorylation of TACC3/maskin is required for centrosome-dependent microtubule assembly in mitosis. *J Cell Biol,* 170**,** 1047-55.

KIRCHNER, J., GROSS, S., BENNETT, D. & ALPHEY, L. 2007. Essential, overlapping and redundant roles of the Drosophila protein phosphatase 1 alpha and 1 beta genes. *Genetics,* 176**,** 273-81.

KITAJIMA, T. S., SAKUNO, T., ISHIGURO, K., IEMURA, S., NATSUME, T., KAWASHIMA, S. A. & WATANABE, Y. 2006. Shugoshin collaborates with protein phosphatase 2A to protect cohesin. *Nature,* 441**,** 46-52.

KITAJIRI, S., FUKUMOTO, K., HATA, M., SASAKI, H., KATSUNO, T., NAKAGAWA, T., ITO, J. & TSUKITA, S. 2004. Radixin deficiency causes deafness associated with progressive degeneration of cochlear stereocilia. *J Cell Biol,* 166**,** 559-70.

KIYOMITSU, T. & CHEESEMAN, I. M. 2012. Chromosome- and spindle-pole-derived signals generate an intrinsic code for spindle position and orientation. *Nat Cell Biol,* 14**,** 311-7.

KIYOMITSU, T. & CHEESEMAN, I. M. 2013. Cortical dynein and asymmetric membrane elongation coordinately position the spindle in anaphase. *Cell,* 154**,** 391-402.

KNOBLICH, J. A. 2010. Asymmetric cell division: recent developments and their implications for tumour biology. *Nat Rev Mol Cell Biol,* 11**,** 849-60.

KNOBLICH, J. A., JAN, L. Y. & JAN, Y. N. 1997. The N terminus of the Drosophila Numb protein directs membrane association and actin-dependent asymmetric localization. *Proc Natl Acad Sci U S A,* 94**,** 13005-10.

KOCH, A. L. 1984. Shrinkage of growing Escherichia coli cells by osmotic challenge. *J Bacteriol,* 159**,** 919-24.

KONDO, T. & HAYASHI, S. 2013. Mitotic cell rounding accelerates epithelial invagination. *Nature,* 494**,** 125-9.

KOSAKO, H., YOSHIDA, T., MATSUMURA, F., ISHIZAKI, T., NARUMIYA, S. & INAGAKI, M. 2000. Rho-kinase/ROCK is involved in cytokinesis through the phosphorylation of myosin light chain and not ezrin/radixin/moesin proteins at the cleavage furrow. *Oncogene,* 19**,** 6059-64.

KOSODO, Y., TOIDA, K., DUBREUIL, V., ALEXANDRE, P., SCHENK, J., KIYOKAGE, E., ATTARDO, A., MORA-BERMUDEZ, F., ARII, T., CLARKE, J. D. & HUTTNER, W. B. 2008. Cytokinesis of neuroepithelial cells can divide their basal process before anaphase. *EMBO J,* 27**,** 3151-63.

KOTAK, S. & GONCZY, P. 2013. Mechanisms of spindle positioning: cortical force generators in the limelight. *Curr Opin Cell Biol,* 25**,** 741-8.

KOTO, A., KURANAGA, E. & MIURA, M. 2011. Apoptosis ensures spacing pattern formation of Drosophila sensory organs. *Curr Biol,* 21**,** 278-87.

KRENN, V., OVERLACK, K., PRIMORAC, I., VAN GERWEN, S. & MUSACCHIO, A. 2014. KI motifs of human Knl1 enhance assembly of comprehensive spindle checkpoint complexes around MELT repeats. *Curr Biol,* 24**,** 29-39.

KRIEG, J. & HUNTER, T. 1992. Identification of the two major epidermal growth factor-induced tyrosine phosphorylation sites in the microvillar core protein ezrin. *J Biol Chem,* 267**,** 19258-65.

KULL, F. J. & ENDOW, S. A. 2013. Force generation by kinesin and myosin cytoskeletal motor proteins. *J Cell Sci,* 126**,** 9-19.

KUNDA, P. & BAUM, B. 2009. The actin cytoskeleton in spindle assembly and positioning. *Trends Cell Biol,* 19**,** 174-9.

KUNDA, P., PELLING, A. E., LIU, T. & BAUM, B. 2008. Moesin controls cortical rigidity, cell rounding, and spindle morphogenesis during mitosis. *Curr Biol,* 18**,** 91-101.

KUNDA, P., RODRIGUES, N. T., MOEENDARBARY, E., LIU, T., IVETIC, A., CHARRAS, G. & BAUM, B. 2012. PP1-mediated moesin dephosphorylation couples polar relaxation to mitotic exit. *Curr Biol,* 22**,** 231-6.

LANCASTER, O. M., LE BERRE, M., DIMITRACOPOULOS, A., BONAZZI, D., ZLOTEK-ZLOTKIEWICZ, E., PICONE, R., DUKE, T., PIEL, M. &

BAUM, B. 2013. Mitotic rounding alters cell geometry to ensure efficient bipolar spindle formation. *Dev Cell,* 25**,** 270-83.

LANDSVERK, H. B., KIRKHUS, M., BOLLEN, M., KUNTZIGER, T. & COLLAS, P. 2005. PNUTS enhances in vitro chromosome decondensation in a PP1-dependent manner. *Biochem J,* 390**,** 709-17.

LANKES, W., GRIESMACHER, A., GRUNWALD, J., SCHWARTZ-ALBIEZ, R. & KELLER, R. 1988. A heparin-binding protein involved in inhibition of smooth-muscle cell proliferation. *Biochem J,* 251**,** 831-42.

LE BORGNE, R. & SCHWEISGUTH, F. 2003. Unequal segregation of Neuralized biases Notch activation during asymmetric cell division. *Dev Cell,* 5**,** 139-48.

LECUIT, T. & LENNE, P. F. 2007. Cell surface mechanics and the control of cell shape, tissue patterns and morphogenesis. *Nat Rev Mol Cell Biol,* 8**,** 633-44.

LEE, K. & RHEE, K. 2011. PLK1 phosphorylation of pericentrin initiates centrosome maturation at the onset of mitosis. *J Cell Biol,* 195**,** 1093-101.

LEKOMTSEV, S., SU, K. C., PYE, V. E., BLIGHT, K., SUNDARAMOORTHY, S., TAKAKI, T., COLLINSON, L. M., CHEREPANOV, P., DIVECHA, N. & PETRONCZKI, M. 2012. Centralspindlin links the mitotic spindle to the plasma membrane during cytokinesis. *Nature,* 492**,** 276-9.

LESAGE, B., QIAN, J. & BOLLEN, M. 2011. Spindle checkpoint silencing: PP1 tips the balance. *Curr Biol,* 21**,** R898-903.

LEVAYER, R. & LECUIT, T. 2012. Biomechanical regulation of contractility: spatial control and dynamics. *Trends Cell Biol,* 22**,** 61-81.

LI, K. & KAUFMAN, T. C. 1996. The homeotic target gene centrosomin encodes an essential centrosomal component. *Cell,* 85**,** 585-96.

LI, Q., NANCE, M. R., KULIKAUSKAS, R., NYBERG, K., FEHON, R., KARPLUS, P. A., BRETSCHER, A. & TESMER, J. J. 2007. Self-masking in an intact ERM-merlin protein: an active role for the central alpha-helical domain. *J Mol Biol,* 365**,** 1446-59.

LILLIE, R. S. 1903. Fusion of Blastomeres and Nuclear Division without Cell-Division in Solutions of Non-Electrolytes. *The Biological Bulletin,* 4**,** 164-178.

LIU, D., VLEUGEL, M., BACKER, C. B., HORI, T., FUKAGAWA, T., CHEESEMAN, I. M. & LAMPSON, M. A. 2010. Regulated targeting of protein phosphatase 1 to the outer kinetochore by KNL1 opposes Aurora B kinase. *J Cell Biol,* 188**,** 809-20.

LONDON, N., CETO, S., RANISH, J. A. & BIGGINS, S. 2012. Phosphoregulation of Spc105 by Mps1 and PP1 regulates Bub1 localization to kinetochores. *Curr Biol,* 22**,** 900-6.

LORIA, A., LONGHINI, K. M. & GLOTZER, M. 2012. The RhoGAP domain of CYK-4 has an essential role in RhoA activation. *Curr Biol,* 22**,** 213-9.

LOUVET-VALLEE, S. 2000. ERM proteins: from cellular architecture to cell signaling. *Biol Cell,* 92**,** 305-16.

LU, B., ACKERMAN, L., JAN, L. Y. & JAN, Y. N. 1999. Modes of protein movement that lead to the asymmetric localization of partner of Numb during Drosophila neuroblast division. *Mol Cell,* 4**,** 883-91.

LUXENBURG, C., PASOLLI, H. A., WILLIAMS, S. E. & FUCHS, E. 2011. Developmental roles for Srf, cortical cytoskeleton and cell shape in epidermal spindle orientation. *Nat Cell Biol,* 13**,** 203-14.

MACHICOANE, M., DE FRUTOS, C. A., FINK, J., ROCANCOURT, M., LOMBARDI, Y., GAREL, S., PIEL, M. & ECHARD, A. 2014. SLK-dependent activation of ERMs controls LGN-NuMA localization and spindle orientation. *J Cell Biol,* 205**,** 791-9.

MACKELVIE, S. H., ANDREWS, P. D. & STARK, M. J. 1995. The Saccharomyces cerevisiae gene SDS22 encodes a potential regulator of the mitotic function of yeast type 1 protein phosphatase. *Mol Cell Biol,* 15**,** 3777-85.

MADDOX, A. S. & BURRIDGE, K. 2003. RhoA is required for cortical retraction and rigidity during mitotic cell rounding. *J Cell Biol,* 160**,** 255-65.

MARINARI, E., MEHONIC, A., CURRAN, S., GALE, J., DUKE, T. & BAUM, B. 2012. Live-cell delamination counterbalances epithelial growth to limit tissue overcrowding. *Nature,* 484**,** 542-5.

MARTIN, A. C., KASCHUBE, M. & WIESCHAUS, E. F. 2009. Pulsed contractions of an actin-myosin network drive apical constriction. *Nature,* 457**,** 495-9.

MARUMOTO, T., HONDA, S., HARA, T., NITTA, M., HIROTA, T., KOHMURA, E. & SAYA, H. 2003. Aurora-A kinase maintains the fidelity of early and late mitotic events in HeLa cells. *J Biol Chem,* 278**,** 51786-95.

MATSUI, T., MAEDA, M., DOI, Y., YONEMURA, S., AMANO, M., KAIBUCHI, K. & TSUKITA, S. 1998. Rho-kinase phosphorylates COOH-terminal threonines of ezrin/radixin/moesin (ERM) proteins and regulates their head-to-tail association. *J Cell Biol,* 140**,** 647-57.

MATSUMOTO, K., TOH-E, A. & OSHIMA, Y. 1978. Genetic control of galactokinase synthesis in Saccharomyces cerevisiae: evidence for constitutive expression of the positive regulatory gene gal4. *J Bacteriol,* 134**,** 446-457

MATSUMURA, F. 2005. Regulation of myosin II during cytokinesis in higher eukaryotes. *Trends Cell Biol,* 15**,** 371-7.

MATTHEWS, H. K., DELABRE, U., ROHN, J. L., GUCK, J., KUNDA, P. & BAUM, B. 2012. Changes in Ect2 localization couple actomyosin-dependent cell shape changes to mitotic progression. *Dev Cell,* 23**,** 371-83.

MAYER, B., EMERY, G., BERDNIK, D., WIRTZ-PEITZ, F. & KNOBLICH, J. A. 2005. Quantitative analysis of protein dynamics during asymmetric cell division. *Curr Biol,* 15**,** 1847-54.

MCCLATCHEY, A. I. & FEHON, R. G. 2009. Merlin and the ERM proteins--regulators of receptor distribution and signaling at the cell cortex. *Trends Cell Biol,* 19**,** 198-206.

MCGUIRE, S. E., LE, P. T., OSBORN, A. J., MATSUMOTO, K. & DAVIS, R. L. 2003. Spatiotemporal rescue of memory dysfunction in Drosophila. *Science,* 302**,** 1765-8.

MEADOWS, J. C., SHEPPERD, L. A., VANOOSTHUYSE, V., LANCASTER, T. C., SOCHAJ, A. M., BUTTRICK, G. J., HARDWICK, K. G. & MILLAR, J. B. 2011. Spindle checkpoint silencing requires association of PP1 to both Spc7 and kinesin-8 motors. *Dev Cell,* 20**,** 739-50.

MEDEMA, R. H. & LINDQVIST, A. 2011. Boosting and suppressing mitotic phosphorylation. *Trends Biochem Sci,* 36**,** 578-84.

MEUNIER, S. & VERNOS, I. 2012. Microtubule assembly during mitosis - from distinct origins to distinct functions? *J Cell Sci,* 125**,** 2805-14.

MEYER, E. J., IKMI, A. & GIBSON, M. C. 2011. Interkinetic nuclear migration is a broadly conserved feature of cell division in pseudostratified epithelia. *Curr Biol,* 21**,** 485-91.

MISHIMA, M., KAITNA, S. & GLOTZER, M. 2002. Central spindle assembly and cytokinesis require a kinesin-like protein/RhoGAP complex with microtubule bundling activity. *Dev Cell,* 2**,** 41-54.

MITSUSHIMA, M., AOKI, K., EBISUYA, M., MATSUMURA, S., YAMAMOTO, T., MATSUDA, M., TOYOSHIMA, F. & NISHIDA, E. 2010. Revolving movement of a dynamic cluster of actin filaments during mitosis. *J Cell Biol,* 191**,** 453-62.

MOCHIDA, S., MASLEN, S. L., SKEHEL, M. & HUNT, T. 2010. Greatwall phosphorylates an inhibitor of protein phosphatase 2A that is essential for mitosis. *Science,* 330**,** 1670-3.

MORGAN, D. O. 1997. Cyclin-dependent kinases: engines, clocks, and microprocessors. *Annu Rev Cell Dev Biol,* 13**,** 261-91.

MORIN, X. & BELLAICHE, Y. 2011. Mitotic spindle orientation in asymmetric and symmetric cell divisions during animal development. *Dev Cell,* 21**,** 102-19.

MORONE, N., FUJIWARA, T., MURASE, K., KASAI, R. S., IKE, H., YUASA, S., USUKURA, J. & KUSUMI, A. 2006. Three-dimensional reconstruction of the membrane skeleton at the plasma membrane interface by electron tomography. *J Cell Biol,* 174**,** 851-62.

MOSELEY, J. B. & NURSE, P. 2009. Cdk1 and cell morphology: connections and directions. *Curr Opin Cell Biol,* 21**,** 82-8.

MOULDING, D. A., BLUNDELL, M. P., SPILLER, D. G., WHITE, M. R., CORY, G. O., CALLE, Y., KEMPSKI, H., SINCLAIR, J., ANCLIFF, P. J., KINNON, C., JONES, G. E. & THRASHER, A. J. 2007. Unregulated actin polymerization by WASp causes defects of mitosis and cytokinesis in X-linked neutropenia. *J Exp Med,* 204**,** 2213-24.

MOULDING, D. A., MOEENDARBARY, E., VALON, L., RECORD, J., CHARRAS, G. T. & THRASHER, A. J. 2012. Excess F-actin mechanically impedes mitosis leading to cytokinesis failure in X-linked neutropenia by exceeding Aurora B kinase error correction capacity. *Blood,* 120**,** 3803-11.

MOUTINHO-PEREIRA, S., DEBEC, A. & MAIATO, H. 2009. Microtubule cytoskeleton remodeling by acentriolar microtubule-organizing centers at the entry and exit from mitosis in Drosophila somatic cells. *Mol Biol Cell,* 20**,** 2796-808.

MUMMERY-WIDMER, J. L., YAMAZAKI, M., STOEGER, T., NOVATCHKOVA, M., BHALERAO, S., CHEN, D., DIETZL, G., DICKSON, B. J. & KNOBLICH, J. A. 2009. Genome-wide analysis of Notch signalling in Drosophila by transgenic RNAi. *Nature,* 458**,** 987-92.

MUNRO, E., NANCE, J. & PRIESS, J. R. 2004. Cortical flows powered by asymmetrical contraction transport PAR proteins to establish and maintain anterior-posterior polarity in the early C. elegans embryo. *Dev Cell,* 7**,** 413-24.

MURTHY, K. & WADSWORTH, P. 2005. Myosin-II-dependent localization and dynamics of F-actin during cytokinesis. *Curr Biol,* 15**,** 724-31.

MURTHY, K. & WADSWORTH, P. 2008. Dual role for microtubules in regulating cortical contractility during cytokinesis. *J Cell Sci,* 121**,** 2350-9.

MUSACCHIO, A. 2011. Spindle assembly checkpoint: the third decade. *Philos Trans R Soc Lond B Biol Sci,* 366**,** 3595-604.

NAKAJIMA, Y., MEYER, E. J., KROESEN, A., MCKINNEY, S. A. & GIBSON, M. C. 2013. Epithelial junctions maintain tissue architecture by directing planar spindle orientation. *Nature,* 500**,** 359-62.

NAKAMURA, F., AMIEVA, M. R. & FURTHMAYR, H. 1995. Phosphorylation of threonine 558 in the carboxyl-terminal actin-binding domain of moesin by thrombin activation of human platelets. *J Biol Chem,* 270**,** 31377-85.

NAKAMURA, N., OSHIRO, N., FUKATA, Y., AMANO, M., FUKATA, M., KURODA, S., MATSUURA, Y., LEUNG, T., LIM, L. & KAIBUCHI, K. 2000. Phosphorylation of ERM proteins at filopodia induced by Cdc42. *Genes Cells,* 5**,** 571-81.

NIGGLI, V., ANDREOLI, C., ROY, C. & MANGEAT, P. 1995. Identification of a phosphatidylinositol-4,5-bisphosphate-binding domain in the N-terminal region of ezrin. *FEBS Lett,* 376**,** 172-6.

NISHIMURA, Y. & YONEMURA, S. 2006. Centralspindlin regulates ECT2 and RhoA accumulation at the equatorial cortex during cytokinesis. *J Cell Sci,* 119**,** 104-14.

NOMACHI, A., YOSHINAGA, M., LIU, J., KANCHANAWONG, P., TOHYAMA, K., THUMKEO, D., WATANABE, T., NARUMIYA, S. & HIRATA, T. 2013. Moesin controls clathrin-mediated S1PR1 internalization in T cells. *PLoS One,* 8**,** e82590.

NORDEN, C., YOUNG, S., LINK, B. A. & HARRIS, W. A. 2009. Actomyosin is the main driver of interkinetic nuclear migration in the retina. *Cell,* 138**,** 1195-208.

NUNES BASTOS, R., GANDHI, S. R., BARON, R. D., GRUNEBERG, U., NIGG, E. A. & BARR, F. A. 2013. Aurora B suppresses microtubule dynamics and limits central spindle size by locally activating KIF4A. *J Cell Biol,* 202**,** 605-21.

O'CONNELL, K. F., MAXWELL, K. N. & WHITE, J. G. 2000. The spd-2 gene is required for polarization of the anteroposterior axis and formation of the sperm asters in the Caenorhabditis elegans zygote. *Dev Biol,* 222**,** 55-70.

O'FARRELL, P. H. 2001. Triggering the all-or-nothing switch into mitosis. *Trends Cell Biol,* 11**,** 512-9.

ODELL, G. M. & FOE, V. E. 2008. An agent-based model contrasts opposite effects of dynamic and stable microtubules on cleavage furrow positioning. *J Cell Biol,* 183**,** 471-83.

OEGEMA, K. & MITCHISON, T. J. 1997. Rappaport rules: cleavage furrow induction in animal cells. *Proc Natl Acad Sci U S A,* 94**,** 4817-20.

OHKURA, H. & YANAGIDA, M. 1991. S. pombe gene sds22+ essential for a midmitotic transition encodes a leucine-rich repeat protein that positively modulates protein phosphatase-1. *Cell,* 64**,** 149-57.

OKUMURA, E., MORITA, A., WAKAI, M., MOCHIDA, S., HARA, M. & KISHIMOTO, T. 2014. Cyclin B-Cdk1 inhibits protein phosphatase PP2A-B55 via a Greatwall kinase-independent mechanism. *J Cell Biol,* 204**,** 881-9.

OLGUIN, P., GLAVIC, A. & MLODZIK, M. 2011. Intertissue mechanical stress affects Frizzled-mediated planar cell polarity in the Drosophila notum epidermis. *Curr Biol,* 21**,** 236-42.

OLIFERENKO, S., CHEW, T. G. & BALASUBRAMANIAN, M. K. 2009. Positioning cytokinesis. *Genes Dev,* 23**,** 660-74.

PALUCH, E., PIEL, M., PROST, J., BORNENS, M. & SYKES, C. 2005. Cortical actomyosin breakage triggers shape oscillations in cells and cell fragments. *Biophys J,* 89**,** 724-33.

PAN, Y. R., TSENG, W. S., CHANG, P. W. & CHEN, H. C. 2013. Phosphorylation of moesin by Jun N-terminal kinase is important for podosome rosette formation in Src-transformed fibroblasts. *J Cell Sci,* 126**,** 5670-80.

PANOUSOPOULOU, E. & GREEN, J. B. 2014. Spindle orientation processes in epithelial growth and organisation. *Semin Cell Dev Biol,* 34C**,** 124-132.

PETER, A., SCHOTTLER, P., WERNER, M., BEINERT, N., DOWE, G., BURKERT, P., MOURKIOTI, F., DENTZER, L., HE, Y., DEAK, P., BENOS, P. V., GATT, M. K., MURPHY, L., HARRIS, D., BARRELL, B., FERRAZ, C., VIDAL, S., BRUN, C., DEMAILLE, J., CADIEU, E., DREANO, S., GLOUX, S., LELAURE, V., MOTTIER, S., GALIBERT, F., BORKOVA, D., MINANA, B., KAFATOS, F. C., BOLSHAKOV, S., SIDEN-KIAMOS, I., PAPAGIANNAKIS, G., SPANOS, L., LOUIS, C., MADUENO, E., DE PABLOS, B., MODOLELL, J., BUCHETON, A., CALLISTER, D., CAMPBELL, L., HENDERSON, N. S., MCMILLAN, P. J., SALLES, C., TAIT, E., VALENTI, P., SAUNDERS, R. D., BILLAUD, A., PACHTER, L., KLAPPER, R., JANNING, W., GLOVER, D. M., ASHBURNER, M., BELLEN, H. J., JACKLE, H. & SCHAFER, U. 2002. Mapping and identification of essential gene functions on the X chromosome of Drosophila. *EMBO Rep,* 3**,** 34-8.

PETERS, J. M. 2002. The anaphase-promoting complex: proteolysis in mitosis and beyond. *Mol Cell,* 9**,** 931-43.

PETRONCZKI, M., GLOTZER, M., KRAUT, N. & PETERS, J. M. 2007. Polo-like kinase 1 triggers the initiation of cytokinesis in human cells by promoting recruitment of the RhoGEF Ect2 to the central spindle. *Dev Cell,* 12**,** 713-25.

PI, H., HUANG, S. K., TANG, C. Y., SUN, Y. H. & CHIEN, C. T. 2004. phyllopod is a target gene of proneural proteins in Drosophila external sensory organ development. *Proc Natl Acad Sci U S A,* 101**,** 8378-83.

PIEKNY, A. J. & GLOTZER, M. 2008. Anillin is a scaffold protein that links RhoA, actin, and myosin during cytokinesis. *Curr Biol,* 18**,** 30-6.

PINES, J. 2006. Mitosis: a matter of getting rid of the right protein at the right time. *Trends Cell Biol,* 16**,** 55-63.

PINSKY, B. A., NELSON, C. R. & BIGGINS, S. 2009. Protein phosphatase 1 regulates exit from the spindle checkpoint in budding yeast. *Curr Biol,* 19**,** 1182-7.

PISTILLO, D., SKAER, N. & SIMPSON, P. 2002. scute expression in Calliphora vicina reveals an ancestral pattern of longitudinal stripes on the thorax of higher Diptera. *Development,* 129**,** 563-72.

POLESELLO, C., DELON, I., VALENTI, P., FERRER, P. & PAYRE, F. 2002. Dmoesin controls actin-based cell shape and polarity during Drosophila melanogaster oogenesis. *Nat Cell Biol,* 4**,** 782-9.

POLESELLO, C. & PAYRE, F. 2004. Small is beautiful: what flies tell us about ERM protein function in development. *Trends Cell Biol,* 14**,** 294-302.

POLLARD, T. D. 2010. Mechanics of cytokinesis in eukaryotes. *Curr Opin Cell Biol,* 22**,** 50-6.

PORTER, K., PRESCOTT, D. & FRYE, J. 1973. Changes in surface morphology of Chinese hamster ovary cells during the cell cycle. *J Cell Biol,* 57**,** 815-36.

POSCH, M., KHOUDOLI, G. A., SWIFT, S., KING, E. M., DELUCA, J. G. & SWEDLOW, J. R. 2010. Sds22 regulates aurora B activity and microtubule-kinetochore interactions at mitosis. *J Cell Biol,* 191**,** 61-74.

QIAN, J., BEULLENS, M., LESAGE, B. & BOLLEN, M. 2013. Aurora B defines its own chromosomal targeting by opposing the recruitment of the phosphatase scaffold Repo-Man. *Curr Biol,* 23**,** 1136-43.

QIAN, J., LESAGE, B., BEULLENS, M., VAN EYNDE, A. & BOLLEN, M. 2011. PP1/Repo-man dephosphorylates mitotic histone H3 at T3 and regulates chromosomal aurora B targeting. *Curr Biol,* 21**,** 766-73.

RANKIN, K. E. & WORDEMAN, L. 2010. Long astral microtubules uncouple mitotic spindles from the cytokinetic furrow. *J Cell Biol,* 190**,** 35-43.

RAPPAPORT, R. 1996. Cytokinesis in animal cells. *Cambridge University Press, New York*.

RAUCHER, D. & SHEETZ, M. P. 1999. Membrane expansion increases endocytosis rate during mitosis. *J Cell Biol,* 144**,** 497-506.

RECZEK, D. & BRETSCHER, A. 1998. The carboxyl-terminal region of EBP50 binds to a site in the amino-terminal domain of ezrin that is masked in the dormant molecule. *J Biol Chem,* 273**,** 18452-8.

REICHL, E. M., REN, Y., MORPHEW, M. K., DELANNOY, M., EFFLER, J. C., GIRARD, K. D., DIVI, S., IGLESIAS, P. A., KUO, S. C. & ROBINSON, D. N. 2008. Interactions between myosin and actin crosslinkers control cytokinesis contractility dynamics and mechanics. *Curr Biol,* 18**,** 471-80.

REN, L., HONG, S. H., CASSAVAUGH, J., OSBORNE, T., CHOU, A. J., KIM, S. Y., GORLICK, R., HEWITT, S. M. & KHANNA, C. 2009a. The actin-cytoskeleton linker protein ezrin is regulated during osteosarcoma metastasis by PKC. *Oncogene,* 28**,** 792-802.

REN, Y., EFFLER, J. C., NORSTROM, M., LUO, T., FIRTEL, R. A., IGLESIAS, P. A., ROCK, R. S. & ROBINSON, D. N. 2009b. Mechanosensing through cooperative interactions between myosin II and the actin crosslinker cortexillin I. *Curr Biol,* 19**,** 1421-8.

RENZI, L., GERSCH, M. S., CAMPBELL, M. S., WU, L., OSMANI, S. A. & GORBSKY, G. J. 1997. MPM-2 antibody-reactive phosphorylations can be created in detergent-extracted cells by kinetochore-bound and soluble kinases. *J Cell Sci,* 110 (Pt 17)**,** 2013-25.

RHYU, M. S., JAN, L. Y. & JAN, Y. N. 1994. Asymmetric distribution of numb protein during division of the sensory organ precursor cell confers distinct fates to daughter cells. *Cell,* 76**,** 477-91.

RIEDL, J., CREVENNA, A. H., KESSENBROCK, K., YU, J. H., NEUKIRCHEN, D., BISTA, M., BRADKE, F., JENNE, D., HOLAK, T. A., WERB, Z., SIXT, M. & WEDLICH-SOLDNER, R. 2008. Lifeact: a versatile marker to visualize F-actin. *Nat Methods,* 5**,** 605-7.

ROCH, F., POLESELLO, C., ROUBINET, C., MARTIN, M., ROY, C., VALENTI, P., CARRENO, S., MANGEAT, P. & PAYRE, F. 2010. Differential roles of PtdIns(4,5)P2 and phosphorylation in moesin activation during Drosophila development. *J Cell Sci,* 123**,** 2058-67.

ROEGIERS, F., YOUNGER-SHEPHERD, S., JAN, L. Y. & JAN, Y. N. 2001. Two types of asymmetric divisions in the Drosophila sensory organ precursor cell lineage. *Nat Cell Biol,* 3**,** 58-67.

ROH-JOHNSON, M., SHEMER, G., HIGGINS, C. D., MCCLELLAN, J. H., WERTS, A. D., TULU, U. S., GAO, L., BETZIG, E., KIEHART, D. P. & GOLDSTEIN, B. 2012. Triggering a cell shape change by exploiting preexisting actomyosin contractions. *Science,* 335**,** 1232-5.

ROSENBERG, J. S., CROSS, F. R. & FUNABIKI, H. 2011. KNL1/Spc105 recruits PP1 to silence the spindle assembly checkpoint. *Curr Biol,* 21**,** 942-7.

ROSENBLATT, J., CRAMER, L. P., BAUM, B. & MCGEE, K. M. 2004. Myosin II-dependent cortical movement is required for centrosome separation and positioning during mitotic spindle assembly. *Cell,* 117**,** 361-72.

ROTHBAUER, U., ZOLGHADR, K., MUYLDERMANS, S., SCHEPERS, A., CARDOSO, M. C. & LEONHARDT, H. 2008. A versatile nanotrap for biochemical and functional studies with fluorescent fusion proteins. *Mol Cell Proteomics,* 7**,** 282-9.

ROUBINET, C., DECELLE, B., CHICANNE, G., DORN, J. F., PAYRASTRE, B., PAYRE, F. & CARRENO, S. 2011. Molecular networks linked by Moesin drive remodeling of the cell cortex during mitosis. *J Cell Biol,* 195**,** 99-112.

ROULEAU, G. A., MEREL, P., LUTCHMAN, M., SANSON, M., ZUCMAN, J., MARINEAU, C., HOANG-XUAN, K., DEMCZUK, S., DESMAZE, C., PLOUGASTEL, B. & ET AL. 1993. Alteration in a new gene encoding a putative membrane-organizing protein causes neuro-fibromatosis type 2. *Nature,* 363**,** 515-21.

RYAN, G. L., PETROCCIA, H. M., WATANABE, N. & VAVYLONIS, D. 2012a. Excitable actin dynamics in lamellipodial protrusion and retraction. *Biophys J,* 102**,** 1493-502.

RYAN, G. L., WATANABE, N. & VAVYLONIS, D. 2012b. A review of models of fluctuating protrusion and retraction patterns at the leading edge of motile cells. *Cytoskeleton (Hoboken),* 69**,** 195-206.

SALBREUX, G., CHARRAS, G. & PALUCH, E. 2012. Actin cortex mechanics and cellular morphogenesis. *Trends Cell Biol,* 22**,** 536-45.

SANGER, J. M., REINGOLD, A. M. & SANGER, J. W. 1984. Cell surface changes during mitosis and cytokinesis of epithelial cells. *Cell Tissue Res,* 237**,** 409-17.

SANGER, J. W. & SANGER, J. M. 1980. Surface and shape changes during cell division. *Cell Tissue Res,* 209**,** 177-86.

SANTOS, S. D., WOLLMAN, R., MEYER, T. & FERRELL, J. E., JR. 2012. Spatial positive feedback at the onset of mitosis. *Cell,* 149**,** 1500-13.

SAOTOME, I., CURTO, M. & MCCLATCHEY, A. I. 2004. Ezrin is essential for epithelial organization and villus morphogenesis in the developing intestine. *Dev Cell,* 6**,** 855-64.

SATO, N., YONEMURA, S., OBINATA, T. & TSUKITA, S. 1991. Radixin, a barbed end-capping actin-modulating protein, is concentrated at the cleavage furrow during cytokinesis. *J Cell Biol,* 113**,** 321-30.

SCHITTENHELM, R. B., CHALECKIS, R. & LEHNER, C. F. 2009. Intrakinetochore localization and essential functional domains of Drosophila Spc105. *EMBO J,* 28**,** 2374-86.

SCHMIDT, J. C., KIYOMITSU, T., HORI, T., BACKER, C. B., FUKAGAWA, T. & CHEESEMAN, I. M. 2010. Aurora B kinase controls the targeting of the Astrin-SKAP complex to bioriented kinetochores. *J Cell Biol,* 191**,** 269-80.

SCHUH, M. & ELLENBERG, J. 2008. A new model for asymmetric spindle positioning in mouse oocytes. *Curr Biol,* 18**,** 1986-92.

SEDZINSKI, J., BIRO, M., OSWALD, A., TINEVEZ, J. Y., SALBREUX, G. & PALUCH, E. 2011. Polar actomyosin contractility destabilizes the position of the cytokinetic furrow. *Nature,* 476**,** 462-6.

SEGALEN, M., JOHNSTON, C. A., MARTIN, C. A., DUMORTIER, J. G., PREHODA, K. E., DAVID, N. B., DOE, C. Q. & BELLAICHE, Y. 2010. The Fz-Dsh planar cell polarity pathway induces oriented cell division via Mud/NuMA in Drosophila and zebrafish. *Dev Cell,* 19**,** 740-52.

SHEPPERD, L. A., MEADOWS, J. C., SOCHAJ, A. M., LANCASTER, T. C., ZOU, J., BUTTRICK, G. J., RAPPSILBER, J., HARDWICK, K. G. & MILLAR, J. B. 2012. Phosphodependent recruitment of Bub1 and Bub3 to Spc7/KNL1 by Mph1 kinase maintains the spindle checkpoint. *Curr Biol,* 22**,** 891-9.

SHLOMOVITZ, R. & GOV, N. S. 2007. Membrane waves driven by actin and Myosin. *Phys Rev Lett,* 98**,** 168103.

SIMONS, P. C., PIETROMONACO, S. F., RECZEK, D., BRETSCHER, A. & ELIAS, L. 1998. C-terminal threonine phosphorylation activates ERM proteins to link the cell's cortical lipid bilayer to the cytoskeleton. *Biochem Biophys Res Commun,* 253**,** 561-5.

SIMPSON, P., WOEHL, R. & USUI, K. 1999. The development and evolution of bristle patterns in Diptera. *Development,* 126**,** 1349-64.

SIT, K. H., BAY, B. H. & WONG, K. P. 1993. Reduced surface area in mitotic rounding of human Chang liver cells. *Anat Rec,* 235**,** 183-90.

SIT, K. H., PARAMANANTHAM, R., BAY, B. H. & WONG, K. P. 1994. Reduced surface area in apoptotic rounding of human Chang liver cells from serum deprivation. *Anat Rec,* 240**,** 456-68.

SOLINET, S., MAHMUD, K., STEWMAN, S. F., BEN EL KADHI, K., DECELLE, B., TALJE, L., MA, A., KWOK, B. H. & CARRENO, S. 2013. The actin-binding ERM protein Moesin binds to and stabilizes microtubules at the cell cortex. *J Cell Biol,* 202**,** 251-60.

SOLOMON, M. J., GLOTZER, M., LEE, T. H., PHILIPPE, M. & KIRSCHNER, M. W. 1990. Cyclin activation of p34cdc2. *Cell,* 63**,** 1013-24.

SPEAR, P. C. & ERICKSON, C. A. 2012. Apical movement during interkinetic nuclear migration is a two-step process. *Dev Biol,* 370**,** 33-41.

SPECK, O., HUGHES, S. C., NOREN, N. K., KULIKAUSKAS, R. M. & FEHON, R. G. 2003. Moesin functions antagonistically to the Rho pathway to maintain epithelial integrity. *Nature,* 421**,** 83-7.

SPIRO, Z., THYAGARAJAN, K., DE SIMONE, A., TRAGER, S., AFSHAR, K. & GONCZY, P. 2014. Clathrin regulates centrosome positioning by promoting acto-myosin cortical tension in C. elegans embryos. *Development,* 141**,** 2712-23.

STEWART, M. P., HELENIUS, J., TOYODA, Y., RAMANATHAN, S. P., MULLER, D. J. & HYMAN, A. A. 2011. Hydrostatic pressure and the actomyosin cortex drive mitotic cell rounding. *Nature,* 469**,** 226-30.

SU, K. C., TAKAKI, T. & PETRONCZKI, M. 2011. Targeting of the RhoGEF Ect2 to the equatorial membrane controls cleavage furrow formation during cytokinesis. *Dev Cell,* 21**,** 1104-15.

SUSTER, M. L., SEUGNET, L., BATE, M. & SOKOLOWSKI, M. B. 2004. Refining GAL4-driven transgene expression in Drosophila with a GAL80 enhancer-trap. *Genesis,* 39**,** 240-5.

TAKAINE, M., NUMATA, O. & NAKANO, K. 2014. Fission yeast IQGAP maintains F-actin-independent localization of myosin-II in the contractile ring. *Genes Cells,* 19**,** 161-76.

TERADA, Y. 2001. Role of chromosomal passenger complex in chromosome segregation and cytokinesis. *Cell Struct Funct,* 26**,** 653-7.

TERAWAKI, S., MAESAKI, R. & HAKOSHIMA, T. 2006. Structural basis for NHERF recognition by ERM proteins. *Structure,* 14**,** 777-89.

THEODOSIOU, N. A. & XU, T. 1998. Use of FLP/FRT system to study Drosophila development. *Methods,* 14**,** 355-65.

THERY, M. & BORNENS, M. 2006. Cell shape and cell division. *Curr Opin Cell Biol,* 18**,** 648-57.

TOMINAGA, T., SAHAI, E., CHARDIN, P., MCCORMICK, F., COURTNEIDGE, S. A. & ALBERTS, A. S. 2000. Diaphanous-related formins bridge Rho GTPase and Src tyrosine kinase signaling. *Mol Cell,* 5**,** 13-25.

TRINKLE-MULCAHY, L., ANDERSEN, J., LAM, Y. W., MOORHEAD, G., MANN, M. & LAMOND, A. I. 2006. Repo-Man recruits PP1 gamma to chromatin and is essential for cell viability. *J Cell Biol,* 172**,** 679-92.

TRINKLE-MULCAHY, L., ANDREWS, P. D., WICKRAMASINGHE, S., SLEEMAN, J., PRESCOTT, A., LAM, Y. W., LYON, C., SWEDLOW, J. R. & LAMOND, A. I. 2003. Time-lapse imaging reveals dynamic relocalization of PP1gamma throughout the mammalian cell cycle. *Mol Biol Cell,* 14**,** 107-17.

TROFATTER, J. A., MACCOLLIN, M. M., RUTTER, J. L., MURRELL, J. R., DUYAO, M. P., PARRY, D. M., ELDRIDGE, R., KLEY, N., MENON, A. G., PULASKI, K. & ET AL. 1993. A novel moesin-, ezrin-, radixin-like gene is a candidate for the neurofibromatosis 2 tumor suppressor. *Cell,* 75**,** 826.

TSE, Y. C., PIEKNY, A. & GLOTZER, M. 2011. Anillin promotes astral microtubule-directed cortical myosin polarization. *Mol Biol Cell,* 22**,** 3165-75.

TSENG, K. F., FOSS, M. & ZHANG, D. 2012. Astral microtubules physically redistribute cortical actin filaments to the incipient contractile ring. *Cytoskeleton (Hoboken),* 69**,** 983-91.

TSUKITA, S. & HIEDA, Y. 1989. A new 82-kD barbed end-capping protein (radixin) localized in the cell-to-cell adherens junction: purification and characterization. *J Cell Biol,* 108**,** 2369-82.

TURUNEN, O., WAHLSTROM, T. & VAHERI, A. 1994. Ezrin has a COOH-terminal actin-binding site that is conserved in the ezrin protein family. *J Cell Biol,* 126**,** 1445-53.

UEHARA, R., GOSHIMA, G., MABUCHI, I., VALE, R. D., SPUDICH, J. A. & GRIFFIS, E. R. 2010. Determinants of myosin II cortical localization during cytokinesis. *Curr Biol,* 20**,** 1080-5.

UYEDA, T. Q. & NAGASAKI, A. 2004. Variations on a theme: the many modes of cytokinesis. *Curr Opin Cell Biol,* 16**,** 55-60.

VAGNARELLI, P., RIBEIRO, S., SENNELS, L., SANCHEZ-PULIDO, L., DE LIMA ALVES, F., VERHEYEN, T., KELLY, D. A., PONTING, C. P., RAPPSILBER, J. & EARNSHAW, W. C. 2011. Repo-Man coordinates chromosomal reorganization with nuclear envelope reassembly during mitotic exit. *Dev Cell,* 21**,** 328-42.

VALE, R. D., SPUDICH, J. A. & GRIFFIS, E. R. 2009. Dynamics of myosin, microtubules, and Kinesin-6 at the cortex during cytokinesis in Drosophila S2 cells. *J Cell Biol,* 186**,** 727-38.

VANOOSTHUYSE, V. & HARDWICK, K. G. 2009. A novel protein phosphatase 1-dependent spindle checkpoint silencing mechanism. *Curr Biol,* 19**,** 1176-81.

VARMARK, H., LLAMAZARES, S., REBOLLO, E., LANGE, B., REINA, J., SCHWARZ, H. & GONZALEZ, C. 2007. Asterless is a centriolar protein required for centrosome function and embryo development in Drosophila. *Curr Biol,* 17**,** 1735-45.

VERHERTBRUGGEN, Y., MARCUS, S. E., CHEN, J. & KNOX, J. P. 2013. Cell wall pectic arabinans influence the mechanical properties of Arabidopsis thaliana inflorescence stems and their response to mechanical stress. *Plant Cell Physiol,* 54**,** 1278-88.

VIGNERON, S., BRIOUDES, E., BURGESS, A., LABBE, J. C., LORCA, T. & CASTRO, A. 2009. Greatwall maintains mitosis through regulation of PP2A. *EMBO J,* 28**,** 2786-93.

VON DASSOW, G., VERBRUGGHE, K. J., MILLER, A. L., SIDER, J. R. & BEMENT, W. M. 2009. Action at a distance during cytokinesis. *J Cell Biol,* 187**,** 831-45.

WAKULA, P., BEULLENS, M., CEULEMANS, H., STALMANS, W. & BOLLEN, M. 2003. Degeneracy and function of the ubiquitous RVXF motif that mediates binding to protein phosphatase-1. *J Biol Chem,* 278**,** 18817-23.

WANG, W., CHEN, L., DING, Y., JIN, J. & LIAO, K. 2008. Centrosome separation driven by actin-microfilaments during mitosis is mediated by centrosome-associated tyrosine-phosphorylated cortactin. *J Cell Sci,* 121**,** 1334-43.

WELBURN, J. P., VLEUGEL, M., LIU, D., YATES, J. R., 3RD, LAMPSON, M. A., FUKAGAWA, T. & CHEESEMAN, I. M. 2010. Aurora B phosphorylates spatially distinct targets to differentially regulate the kinetochore-microtubule interface. *Mol Cell,* 38**,** 383-92.

WERNER, M., MUNRO, E. & GLOTZER, M. 2007. Astral signals spatially bias cortical myosin recruitment to break symmetry and promote cytokinesis. *Curr Biol,* 17**,** 1286-97.

WEST-FOYLE, H. & ROBINSON, D. N. 2012. Cytokinesis mechanics and mechanosensing. *Cytoskeleton (Hoboken),* 69**,** 700-9.

WHITE, E. A. & GLOTZER, M. 2012. Centralspindlin: at the heart of cytokinesis. *Cytoskeleton (Hoboken),* 69**,** 882-92.

WHITE, J. G. & BORISY, G. G. 1983. On the mechanisms of cytokinesis in animal cells. *J Theor Biol,* 101**,** 289-316.

WIRTZ-PEITZ, F., NISHIMURA, T. & KNOBLICH, J. A. 2008. Linking cell cycle to asymmetric division: Aurora-A phosphorylates the Par complex to regulate Numb localization. *Cell,* 135**,** 161-73.

WOLFE, B. A., TAKAKI, T., PETRONCZKI, M. & GLOTZER, M. 2009. Polo-like kinase 1 directs assembly of the HsCyk-4 RhoGAP/Ect2 RhoGEF complex to initiate cleavage furrow formation. *PLoS Biol,* 7**,** e1000110.

WOLGEMUTH, C. W. 2005. Lamellipodial contractions during crawling and spreading. *Biophys J,* 89**,** 1643-9.

WOLPERT, L. 1966. The mechanical properties of the membrane of the sea urchin egg during cleavage. *Exp Cell Res,* 41**,** 385-96.

WOOLNER, S., O'BRIEN, L. L., WIESE, C. & BEMENT, W. M. 2008. Myosin-10 and actin filaments are essential for mitotic spindle function. *J Cell Biol,* 182**,** 77-88.

WOOLNER, S. & PAPALOPULU, N. 2012. Spindle position in symmetric cell divisions during epiboly is controlled by opposing and dynamic apicobasal forces. *Dev Cell,* 22**,** 775-87.

WU, C. F., WANG, R., LIANG, Q., LIANG, J., LI, W., JUNG, S. Y., QIN, J., LIN, S. H. & KUANG, J. 2010. Dissecting the M phase-specific phosphorylation of serine-proline or threonine-proline motifs. *Mol Biol Cell,* 21**,** 1470-81.

WULBECK, C. & SIMPSON, P. 2000. Expression of achaete-scute homologues in discrete proneural clusters on the developing notum of the medfly Ceratitis capitata, suggests a common origin for the stereotyped bristle patterns of higher Diptera. *Development,* 127**,** 1411-20.

WURZENBERGER, C. & GERLICH, D. W. 2011. Phosphatases: providing safe passage through mitotic exit. *Nat Rev Mol Cell Biol,* 12**,** 469-82.

WURZENBERGER, C., HELD, M., LAMPSON, M. A., POSER, I., HYMAN, A. A. & GERLICH, D. W. 2012. Sds22 and Repo-Man stabilize chromosome segregation by counteracting Aurora B on anaphase kinetochores. *J Cell Biol,* 198**,** 173-83.

YAMAGISHI, Y., YANG, C. H., TANNO, Y. & WATANABE, Y. 2012. MPS1/Mph1 phosphorylates the kinetochore protein KNL1/Spc7 to recruit SAC components. *Nat Cell Biol,* 14**,** 746-52.

YANG, H. S. & HINDS, P. W. 2003. Increased ezrin expression and activation by CDK5 coincident with acquisition of the senescent phenotype. *Mol Cell,* 11**,** 1163-76.

YONEMURA, S., HIRAO, M., DOI, Y., TAKAHASHI, N., KONDO, T. & TSUKITA, S. 1998. Ezrin/radixin/moesin (ERM) proteins bind to a positively charged amino acid cluster in the juxta-membrane cytoplasmic domain of CD44, CD43, and ICAM-2. *J Cell Biol,* 140**,** 885-95.

YUMURA, S., UEDA, M., SAKO, Y., KITANISHI-YUMURA, T. & YANAGIDA, T. 2008. Multiple mechanisms for accumulation of myosin II filaments at the equator during cytokinesis. *Traffic,* 9**,** 2089-99.

YUN, C. H., LAMPRECHT, G., FORSTER, D. V. & SIDOR, A. 1998. NHE3 kinase A regulatory protein E3KARP binds the epithelial brush border Na+/H+ exchanger NHE3 and the cytoskeletal protein ezrin. *J Biol Chem,* 273**,** 25856-63.

ZAVORTINK, M., CONTRERAS, N., ADDY, T., BEJSOVEC, A. & SAINT, R. 2005. Tum/RacGAP50C provides a critical link between anaphase microtubules and the assembly of the contractile ring in Drosophila melanogaster. *J Cell Sci,* 118**,** 5381-92.

ZEITLINGER, J. & BOHMANN, D. 1999. Thorax closure in Drosophila: involvement of Fos and the JNK pathway. *Development,* 126**,** 3947-56.

ZENG, K., BASTOS, R. N., BARR, F. A. & GRUNEBERG, U. 2010. Protein phosphatase 6 regulates mitotic spindle formation by controlling the T-loop phosphorylation state of Aurora A bound to its activator TPX2. *J Cell Biol,* 191**,** 1315-32.

ZHAO, W. M. & FANG, G. 2005. MgcRacGAP controls the assembly of the contractile ring and the initiation of cytokinesis. *Proc Natl Acad Sci U S A,* 102**,** 13158-63.

ZHOU, M. & WANG, Y. L. 2008. Distinct pathways for the early recruitment of myosin II and actin to the cytokinetic furrow. *Mol Biol Cell,* 19**,** 318-26.

ZHUANG, C., TANG, H., DISSANAIKE, S., COBOS, E., TAO, Y. & DAI, Z. 2011. CDK1-mediated phosphorylation of Abi1 attenuates Bcr-Abl-induced F-actin assembly and tyrosine phosphorylation of WAVE complex during mitosis. *J Biol Chem,* 286**,** 38614-26.

ZIMMERMANN, U., HUSKEN, D. & SCHULZE, E. D. 1980. Direct turgor pressure measurements in individual leaf cells of Tradescantia virginiana. *Planta,* 149**,** 445-53.

ZITSERMAN, D. & ROEGIERS, F. 2011. Live-cell imaging of sensory organ precursor cells in intact Drosophila pupae. *J Vis Exp*.